Università degli Studi di Padova

DIPARTIMENTO DI SCIENZE CHIMICHE

Corso di Dottorato di Ricerca in Scienza e Ingegneria dei Materiali e delle Nanostrutture - Ciclo XXX

Tesi di Dottorato

Electro-assisted deposition of sol-gel thin films: study of the process and its applications

Coordinatore:
Ch.mo Prof. Giovanni Mattei

Supervisore:
Ch.mo Prof. Massimo Guglielmi

Dottorando:
Gianmarco Giordano
Matricola 1108481

Anno Accademico 2017-2018

To my brother

[...] demonstrationem mirabilem sane detexi.
Hanc marginis exiguitas non caperet.
(Pierre de Fermat)

Abstract

The aim of this thesis is the study of sol-gel thin films obtained via electrochemical-assisted deposition process, trying to identify the limits of the technique and, on the other hand, suggesting its versatility.

After a careful analysis of the literature, a first systematic study of the main variables governing the process was carried out, implementing the method using the pulsed potential technique.

For the first time in the literature, chronoamperometric curves were analyzed by varying the precursor concentration and the applied potential, finding a strong analogy with the 3D growth of electrochemically deposited metals. The curves were fitted using 3D progressive nucleation equations with diffusive-controlled growth.

It has been shown that with electro-assisted deposition it is possible to create multilayer structures using silica-based organic-inorganic materials. In addition, this technique can be used to increase the thickness of thin mesoporous films with nano-channels vertically-aligned to the substrate and well-ordered hexagonal structure. Finally, thin silica and titania films were intercalated in order to increase the substrate reflection and the respective refractive indexes were measured and compared on different substrates.

The NIP (nanoparticles imprinted polymers) process has been implemented using a silica matrix rather than a polymer matrix. A PDDA monolayer was deposited on an ITO substrate and, by means of electrostatic attraction, citrate-stabilized gold nanoparticles were deposited above it. Thus, a thin layer of silica with tunable thickness was used to partially incorporate the nanoparticles. After oxidation of gold, the re-uptake of nanoparticles on the imprinted matrix was monitored .

Sommario

Lo scopo del lavoro di tesi è lo studio del processo di deposizione di film sottili con il metodo sol-gel per via elettrochimica, cercando di individuare i limiti della tecnica e, dall'altro lato, suggerendone la versalità.

Dopo un'attenta analisi della letteratura, è stato effettuato un primo studio sistematico delle variabili principali che governano il processo, implementando il metodo con la tecnica del potenziale pulsato.

Per la prima volta in letteratura, le curve cronoamperometriche sono state analizzate al variare della concentrazione di precursore e del potenziale applicato, trovando una forte analogia con la crescita 3D di metalli depositati elettrochimicamente. Le curve sono state simulate usando le equazioni di nucleazione 3D progressiva con crescita a controllo diffusivo.

È stato dimostrato che con l'elettrodeposizione assistita è possibile costruire strutture multilayer con materiali ibridi organici-inorganici a base di silice. Inoltre, questa tecnica può essere usata per aumentare lo spessore di film sottili mesoporosi con nano-canali orientati verticalmente rispetto al substrato e ben ordinati con struttura esagonale. Infine, film sottili di silice e titania sono stati intercalati al fine di aumentare la riflessione del substrato e i rispettivi indici di rifrazione sono stati misurati e confrontati su diversi substrati.

Il processo NIP (*nanoparticles imprinted polymers*) è stato implementato usando una matrice di silice anziché polimerica. Un monolayer di PDDA è stato depositato su un substrato di ITO e, per mezzo dell'attrazione elettrostatica, delle nanoparticelle di oro stabilizate con citrato sono state depositate al di sopra di esso. Quindi, un sottile strato di silice a spessore controllato è stato usato per incorporare parzialmente le nanoparticelle. Dopo l'ossidazione dell'oro per via elettrochimica, è stato monitorato il riaccalappiamento delle nanoparticelle da parte della matrice impressa.

Acknowledgements

The PhD is a high-level training course. For me, the training is partly due to all the people who worked with me.

Heretofore I had never felt so grateful to a teacher. So, first of all, it is necessary to thank my supervisor Massimo Guglielmi, because the thesis would not be born without the help of his foresight.

A thank also to Christian Durante and Armando Gennaro for their helpful collaboration. A grateful acknowlefgement goes to Alessandro Martucci and David Avnir for answering my questions and for interesting scientific discussions.

Nancy, Jan. 2016. During my visit to LCPME - CNRS, I met many scientists I would like to thank: Mathieu Etienne, Grégoire Herzog, Grégory Francius, Liang Liu, Alonso Gamero, Cheryl Karman, Maciej Mierzwa, Tauquir Nasir, Lin Zhang, Martha Collins. In particular, an acknowledgement goes to Alain Walcarius and Neus Vilá to give me the possibility to develop multilayer of mesoporous silica.

Kindly, when I went in Jerusalem, to The Hebrew University, I found a friendly atmosphere and I also found many scientific ideas thanks to: Andrea Buffa, Lijie He, Sujoy Sarkar, Tehila Shachar Levian, Tamar Danieli, Noah Metoki, Eitan Katz. Also in this case, a particular acknowledgement goes to Daniel Mandler and Netta Bruchiel-Spanier for their advantageous collaboration.

Since my first sol-gel conference, I can not forget about my japanese friends Kazumasa Suzuki, Naoki Tarutani and Kenji Okada: you are genuine and youthful.

Above all, I am grateful to all my colleagues in Italy.

Last, but not least, a sincere thanks to my research group (NanoEng Group), composed by Elena Colusso, Marco Angiola, Marco Sturaro, Andrea Paduano, Prof. Massimo Guglielmi and Prof. Alessandro Martucci.

Logically, for those who know me, I left at least one hidden message in these thanks: go back and find out.

Contents

List of Figures

List of Tables

List of Symbols

i (or I)	Current	A
n	Number of moles	mol
F	Faraday constant	C/mol
A	Electrode surface	mm^2
C_0	Initial concentration	M
D	Diffusion coefficient	$mm/s^{1/2}$
t	Time	s
E_{app}	Applied potential	V
I_m	Maximum deposition current	A
t_m	Maximum deposition time	s
I_{dep}	Deposition current	A
I_{over}	Overlap current	A
ν	Scan rate	mV/s
n	Refractive index	$a.u.$
λ	Wavelength	nm
k	Wave vector	nm^{-1}

Introduction

Since 1939, the sol-gel process is a method that allows the formation of ceramic and organic-inorganic hybrids. The major precursors are metal or metalloid alkoxide which are split into two or more parts in relation to the amount of water and catalysts present, thanks to the hydrolysis reactions. Consequently they give rise to polymeric chains by means of condensation reactions.

One of the functional applications of the sol-gel process is the formation of thin films (from about ten nanometers to a few micrometers). Dip coating and spin coatings represent two of the major technological processes for making such films. The first method involves immersing the substrate in the solution, followed by removal at controlled speed and drying. The second method involves rotating the substrate in order to spread the coating material by centrifugal force. Although the method is, in principle, simple, there are still limitations to the extensive use of sol-gel, such as to cover substrates with complex surfaces.

In 1999, Shacham et al. developed a new deposition method that might solve this problem for electrical conductive surfaces. It is based on the local electrochemical generation of catalysts (hydroxide ions or protons) to increase the rate of sol-gel reactions. In the case of basic catalysis, and following the idea of the two-step method, the hydrolysis is carried out initially in acidic medium and the polycondensation is favored at the solution-substrate interface by a local increase in pH induced by the application of a sufficiently negative constant potential, which promotes the reduction reactions of oxygen and water.

The purpose of the thesis is to highlight the eclecticness of the method deepening some fundamental aspects of the theory and expanding future applications.

In chapter 1, a review of the state of the art was given. In these years, only few papers were dedicated to the understanding of the fundamental parameters governing the process. Several papers regards the possibility to create hybrid organic-inorganic materials, to codeposit nanoparticles and sol-gel films or to create nanocomposites.

In chapter 2, the main techniques and characterizations used during this work were explained, giving technical details on the instrumentation.

Using Design of Experiment (DOE), the effect of potential and time on the thickness was studied using simple TEOS-based acidic solutions to coat planar stainless steel samples in the chapter 3. Different starting solutions, The role of working temperature, oxygen concentration and the presence of KNO_3 until saturation were also tested. Moreover, the pulsed potential method was developed.

Aim of the chapter 4 is to highlight the strong relationship between standard galvanic deposition of metals and electrochemically assisted deposition of sol-gel. In order to analyze the current transients, the applied potential and the concentration of precursor were changed, keeping starting solution and potential constant, respectively. Furthermore, the thickness in function of time was evaluated by using an ellipsometer.

A particularly important point is the difficulty to obtain thick layers and, somehow related to it, the difficulty to coat objects with complex or hidden surfaces. The thickness is limited by the shrinkage of the gel and the resulting mechanical stresses arising when the deposited gel film dries under the constrain of the substrate. This is a well-known phenomenon, described at the beginning of the nineties by Brinker and Scherer shown that the maximum thickness obtainable by a single step dip-coating deposition does not exceed 1 μm. The experience is that it is very difficult to obtain silica layers exceeding 0.5 μm if a simple TEOS solution is used. Starting from this observation it was decided to deepen the comprehension on the experimental findings. In chapter 5, it was reported a new technique that avoid this problem: the deposition of multiple layers by repeated extraction and re-immersion of the sample from the batch after electrochemical assisted deposition. In the same chapter, it was developed a sequential Electro-Assisted Self-Assembly (EASA) method in order to increase the thickness of vertically-aligned hexagonally-packed silica-based mesochannels. The obtained coatings have been characterized by transmission electron microscopy and grazing incidence X-ray diffraction, and their permeability properties were investigated by cyclic voltammetry. It was also demonstrated that such film can be functionalized with redox moieties (ferrocene) being electrochemically accessible over the whole multilayer thickness. In the last section of chapter 5, silica and titania were intercalated on stainless steel and Indium Tin Oxide (ITO) substrates, creating a multillayer, in which two different materials can be intercalated each other, tuning the thickness. Morphological characterizations was carried out using Field Emission Gun (FEG-SEM). The images show that silica and titania layers were successfully deposited. Otherwise, optical characterization were obtained using ellipsometer. In particular, for the first time in literature, it was studied the refractive index on stainless steel and ITO both for silica and titania single layer, trying to collect the reflection of p-polarized light and, consequently, to compare

the real trend with the fitted theoretical curves.

In chapter 6, nanoparticles imprinted matrices (NAIMs) approach was used in order to create functional nanocomposites. The approach derives from the molecularly imprinted polymer (MIP) approach, in which nanoparticles are imprinted instead of molecules. NAIMs require the preparation of thin films onto which nanoparticles are deposited, followed by the triggered release of the nanoparticles template. The matrix imprinted with voids is subsequently used for selective reuptake of nanoparticles similar to those used in the imprinting procedure. We used a silica matrix for embedding gold nanoparticles stabilized with citrate (AuNPs-cit). The AuNPs-cit were first deposited onto ITO electrode, which was treated with positively charged polymer, which caused negatively charged AuNPs-cit to be adsorbed onto the electrode surface. Then, different silica films with different thicknesses were electrodeposited onto the electrode. Electrochemical oxidation dissolved the AuNPs-cit and formed cavities in the sol-gel films, which fit both the size and shape of the AuNPs-cit. Reuptake of these nanoparticles from an aqueous solution was successfully obtained using the imprinted films, whereas the control non imprinted films did not reuptake the AuNPs-cit.

Finally, in chapter 7, the conlusions had been taken, giving some future perspectives for further research.

Chapter 1

Electrochemical Assisted Deposition: a New Technique for Sol-Gel Deposition

1.1 General Concepts

The formation of thin films on various type of substrates is among the most important and successful technological applications of the sol-gel process. Dip coating, spin coating and spray coating are the principal coating methods. Each of them has, of course, advantages and disadvantages, but a common problem they have is that it is diffcult to coat object with complex or hidden surfaces, at least in a controlled way.

In 1999, Shacham, Avnir and Mandler [1] developed a new deposition method that might, in principle, solve this problem for electrical conductive surfaces. It is based on the local electrochemical generation of catalysts (hydroxide ions or protons) to increase the rate of sol-gel reactions.

Following the idea of the two steps method, the hydrolysis is carried out initially in acid medium and the application of a constant negative potential gives rise to the increase of pH at the electrode surfaces, due to reduction reactions of oxygen and water, which in acidic environment involve the consumption of protons:

$$O_2 + 4H^+ + 4e^- \rightarrow 2H_2O \tag{1.1}$$

$$2H^+ + 2e^- \rightarrow H_2 \tag{1.2}$$

reaching neutral or basic medium, where the production of hydroxide ions takes place:

$$O_2 + 2H_2O + 4e^- \rightarrow 4OH^- \tag{1.3}$$

$$2H_2O + 2e^- \rightarrow H_2 + 2OH^- \tag{1.4}$$

$$O_2 + 2H_2O + 2e^- \rightarrow H_2O_2 + 2OH^- \tag{1.5}$$

Depending on the initial acidity the solution may become basic, promoting hydrolysis and condensation under this regime with all known consequences on surface, but immediately, due to the concentration gradient (diffusion) and the electric field (migration), unreacted hydroxyl ions move away from the surface region generating a complex pH gradient in the solution. If the batch is mechanically stirred the situation becomes even more complex, with the addition of a convective term. The increase of the pH in the solution changes the kinetics of the reactions involved in the sol-to-gel transition. How all these phenomena affect the layer deposited on the samples surface (thickness, morphology, density, etc.) is hard to predict, and the experimental approach seems the most convenient one, taking the general picture as a base for a (at least qualitative) interpretation of the results. However, a mathematical approach was used to described the kineticks of the electrochemically-assisted deposition [2].

Different groups worked using this method and theliterature has soon becomes thick. To divide them rationally I have identified the following criterion: the first part regards all the papers that give us a better knowledge of the electrodeposition method and of the variables which govern it; then, the articles are listed according to the type of material deposited (silica, titania and others).

1.2 Basic Knowledge

In the last years, most of the papers were aimed to achieve two goals: the possibility to explore new applications and the creations of new materials, such as nanocomposites and different structures.

Nevertheless, there is a need to understand how the method works and which variables play an important role. In this section there is a collection of the main studies carried out over the years, which explains how to tune the thickness of the final films.

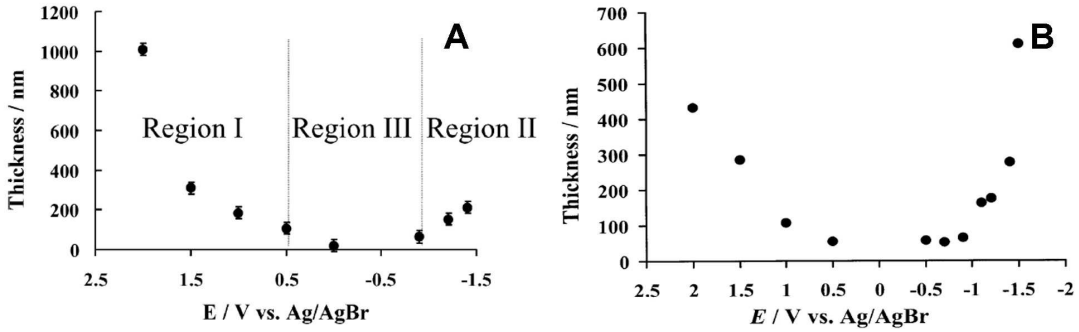

Figure 1.1: Thickness of the film in funcion of the applied potential for titania (A) and zirconia (B) precursors. (A) adapted from ref. [8]. (B) adapted from ref. [9]

1.2.1 Applied potential

The electrodeposition is based on the electrogeneration of a catalyst. Applying a negative potential the catalyst is the hydroxide ion, in fact the reduction of water and oxygen (reactions 1.3, 1.4, 1.5) occur in the range from -0.4 V and -0.7 V (vs Ag/AgCl) depending from the starting solution. Using a positive potential, the catalyst is represented by the proton.

Regarding silica precursors the strategy most used is the basic catalysis [1,3–7]. Applyig a more negative potential the thickness of the film increase reaching 18 μm for -1.6 V [5] and it seems that changing the potential of just 0.05 V (vs Ag/AgBr), the film is affected by this change [7].

The strategy to use a positive potential was devoleped for Titania and Zirconia precursors. In figure 1.1 reproduced from [8] and [9], one can see that the trend of both precursors is similar. In the range from 0.5 V to -0.5 V (see figure 1.1), the formation of the film is avoided, because no reduction or oxidation reactions occur on the lectrode surface. The thickness start to increase with the absolute value of the potential, *ceteris paribus*. Of course, it is impossible to give an absolute trend for the potential, without considering the other variables.

1.2.2 Deposition time

Keeping constant the potential, it is possible to tune the film thickness changing the duration of electrodeposition. It is easy to understand that the thickness increases with the deposition time. But also in this case, it results difficult to describe an absolute trend without taking into account the other variables.

Only for description purposes, one can split the influence of time into three different trends (figure 1.2 on page 5):

- linear. Liu *et al.* [7] found a progressive and linear trend for the deposition time, till 10 minutes (figure 1.2A. Separately, Wu *et al.* showed a quite linear trend for the deposition of hybrid silica films [6];

- exponential. Walcarius's papers [11, 12] shows that during the first three minutes of deposition, the time dependence of thickness seems to be exponential (figure 1.2B), with a lot of aggregates of particles stick on the surface electrode, generating a thick film around 5 μm, starting from tetraethoxysilane (TEOS) in mixture with (3-aminopropyl)triethoxysilane (APTES) or mercaptopropyltrimethoxysilane MPTMS [10].

- asymptotic. Aminopropylthiethoxysilane [4], titanium tetra-n-propoxide [8] and zirconium tetra-n-propoxide [9] show an asymptotic behavior to deposition time. After 30 minutes, the film stops to grow, due to a gradual blocking of the electroactive species on electrode surface (figure 1.2).

It is better to point out that the scales (3, 10, 90 minutes) and the starting solutions in the figure 1.2 are different. For this reason it is difficult to find an univocal trend for the deposition time.

1.2.3 Starting solution

Using electrochemical deposition, the starting solution changes its composition over the time. In fact, enhancing the sol-gel condensation, the amount of precursors decrease, while the formation of dimers, oligomers or particles increse. Keeping the solution to react for long time, also the pH increases in the entire bulk, not only near the electrode surface. For these reasons it is important to choose the correct initial composition of the solution.

In literature, the influence of starting solution was not studied in deep, only few papers allow us to understand the thickness dependence of the various reagents. Below, the main studies are summarized:

- increasing the initial precursor concentration the thickness of the film increases, *ceteris paribus*. A linear increase of the thickness was recorded for aminopropyltriethoxysilane up to 7.5% v/v in sol. Exceeded this percentage, the thickness reaches a cut off due to the insufficient concentration of hydroxide ions [4];

- the influence of water is not clear. Clearly, a certain amount of water is necessary for the formation of OH^-, as showed in reactions 1.3 and 1.4.

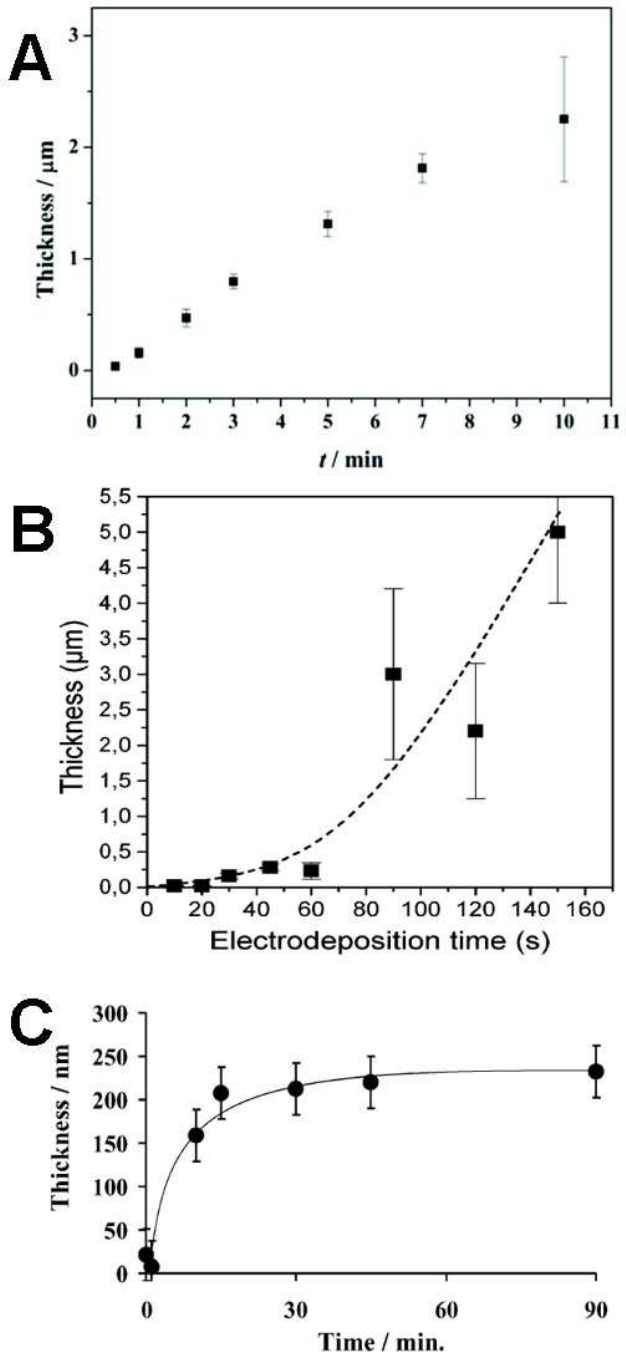

Figure 1.2: Deposition time dependence of the thickess. Three cases: (A) linear trend (adapted from ref. [7]) for sol-gel/carbon nanotubes composite films at -0.9 V vs Ag/AgBr; (B) exponential trend (adapted from ref. [10]) for amine-functionalized silica films deposited at -1.2 V; (C) asymptotic trend (adapted from ref. [8] for titania thin films on ITO deposited at -1.4 V vs Ag/AgBr wire

However, Shacham *et al.* [9] found a bell-like behaviour: adding 100 ppm of water, the thickness reaches its maximu, icreasing the concentration of water over 100 ppm, no effect was pointed out;

- another important result was obtained by Sibottier *et al.* [10]. The influence of aging time of the sol on the transition time from slow and fast condensation was recorded. They showed that increasing the time of hydrolysis, the condensation during deposition was enhanced due to the advancing state of the solution;

- the importance of electrolyte dissolved into the solution was studied by Collinson *et al.* [13] and Ding *et al.* [14]. The film formation takes place if the supporting electrolyte is chosen accurately: cathodic electrodepotion needs an electrolyte without acid properties, on the other side anodic elctrodeposition requires an electrolyte without basic properties. Also the concentration of electrolyte (KNO_3) plays an important role: higher concentration could lead to "overcatalysis". The reactions involved using nitrate as electrolyte will be listed in chapter four.

1.3 Silica-based Films

Many research groups focused their attention on the deposition of silica-based films. One of the reasons for this choice is the easiness to create tunable films, having controllable thicknesses and morphologies. Corrosion protection [15, 16], antireflection coatings [7] and sensors [17, 18] are three of the main applications.

As shown in references [13, 19, 20], the formation of thin inorganic silica films was used just to study the basic properties of the technique. Then, the major efforts were emplyed to find applications or new structures.

In this section the formation of hybrid films, mesoporous silica and nanocomposites will be described, trying to identify the most interesting works in the literature.

1.3.1 Hybrid organic-inorganic films

Silica-based hybrid organic-inorganic materials attracted the attention of many scientists due to their interesting application in electrochemical field [21], such as permselective coatings [22], ion exchange [23], molecular imprinting [24] and electrocatalysis [25].

Table 1.1: List of hybrid precursors used in combination with silica

Precursor	Abbreviation	ref.(s)
phenyl trimethoxysilane	PTMOS	[4, 26, 27]
bis-[triethoxysilyl] ethane	BTSE	[16, 28–30]
polypyrrole	ppy	[31]
dodecyltriethoxysilane	DTMS	[32–35]
dodecyltriethoxysilane	DTES	[6]
bis-[triethoxysilylpropyl]tetra-sulphide	BTESPT	[36]
methyltriethoxysilane	MTEOS	[37]
3-(aminopropyl)trimethoxysilane	APTMS	[17]
3-(aminopropyl)triethoxysilane	APTES	[4, 10, 38]
N-methylpyrrolidone	NMP	[7]
bis-[triethoxysilylpropyl]amine	BTSPA	[15]
methyltrimethoxysilane	MTMS	[28, 33]
propyltrimethoxysilane	PrTMOS	[4]
vinyltrimethoxysilane	VTMS	[33]
hemoglobin	Hb	[39]
glucose oxidase	GOD	[39]
polystyrene sulfonate	PSS	[40]
polyaniline	Pani	[41]
2-[2-(trimethoxysilyl)ethyl]-pyridine	—	[42]
octyltrimethoxysilane	O-TES	[43]
hexadecyltrimethoxysilane	HD-TES	[43]
3-azidopropyltrimethoxysilane	AzPTMS	[44–46]
3-mercaptopropyltrimethoxysilane	MPTMS	[10, 18, 37, 38, 45]

Hybrid materials have also been used in electro-assisted deposition and a series of precursors were deposited or co-deposited on different substrates (gold, ITO, stainless steel, aluminum alloys, carbon steel). In table 1.1, the principal precursors are listed.

1.3.2 Mesoporous silica

Ordered mesoporous silica-based materials were discovered for the first time in 1992 by Beck and co-workers [47, 48], obtained using sol-gel method and with the help of a surfactant-assisted synthesis. Since then, more and more articles have been published on this subject [49].

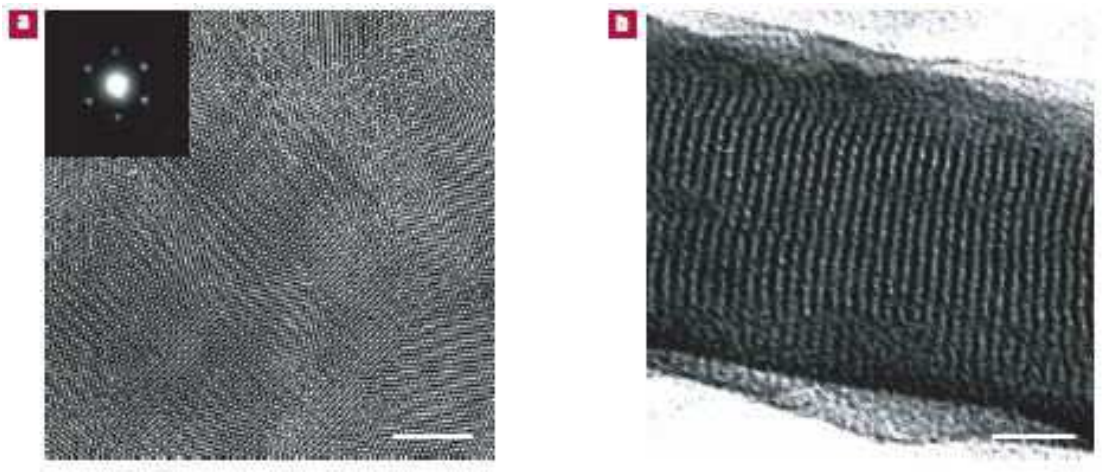

Figure 1.3: TEM images of ordered mesoporous and vertically-aligned silica films. Low magnification top-view (a), high magnification cross-sectional view (b). Scale bars: 50 nm (a) and 20 nm (b). Reproduced from ref. [11]

In 2007, Walcarius and co-workers published a paper in which they expose a new strategy to exploit electro-assisted deposition: the formation of ordered mesoporous and vertically-aligned silica films [11]. Using cetyl trimethylammonium bromide (CTAB) as a surfactant into the starting solution and applying a negative potential, a silica matrix template was created on the working electrode (figure 1.3).

The method was studied in deep changing the concentration of CTAB [50], understanding the importance of the counteranion [12], using different precursors [43] and creating nanocomposites [51]. In the last years, the research was based on functionalization of the mesochannels using redox molecules [44–46, 52].

The discovery has been so interesting that several groups have reproduced the technique separately [53–57].

1.3.3 Nanocomposites

An other advantage of electrodeposition is the possibility to co-deposit different materials and to control the final composition of the coating during deposition.

This fundamental aspect stimulated the study of numerous nanocomposites and consequently to brought the expansion of new applications, *e.g.* graded structure [5], electroanalysis [51], antireflection layers [7].

Among the most important examples, one could cite the possibility to modulate the dimension of copper NPs changing the applied potential [59]. The for-

Table 1.2: List of silica-based nanocomposites

Nanocomposite	Application(s)	ref.
CeO_2 - BTSPA	corrosion protection	[15]
zinc-doped - BTSE	corrosion protection	[29]
ppy - SiO_2	corrosion protection	[31]
DTMS - TiO_2	corrosion protection	[35]
clay - mesoporous silica	preconcentration electroanalysis	[51]
AuNPs - SiO_2	catalysis, optical filters	[3]
gold - SiO_2	catalysis, chemical sensing	[58]
copper - SiO_2	catalysis, sensing	[59]
SiO_2 - TiO_2	graded structure	[5]
carbon nanotubes - SiO_2	antireflection layers	[7]
PSS - SiO_2	ions exchange	[40]
pani - SiO_2	supercapacitors	[41]

mation of a coral-like gold structure was obtained with the help of co-deposition of silica matrix and consequently its removal [58].

In table 1.2 silica-based or silica-modified nanocomposites obtained over the years are listed.

1.4 Titania Films

The deposition of titania via electrochemical method results more difficult than silica deposition. Nevertheless, the general interest has led to deepening the concept of titania deposition. The major contributions found in literature are listed below:

- in 2004, Shacham *et al.* [8] demonstrated the possibility to deposit titania by electro-assisted deposition, using $Ti(O^nPr)_4$ precursor. Dye-doped titania was successfully performed by adding four dyes: Basic Blue 41, methylene blue, tris(2,2'-byridine)iron(II) and tris(2,2'-bipyridine)ruthenium(II);
- titanium oxide was deposit on pattern circuit and gold meshes [60]. Shacham *et al.* underline two of the strengths of the method: selective deposition on conductive surfaces and the feasibility to cover complex surfaces;
- graded structure of binary SiO_2-TiO_2 films was obtained by co-deposition of tetramethoxysilane (TMOS) and titanium tetraisopropoxide (TTIP). Both

depositions occur in the range from -1.2 V to -1.5 V, generating a thick layer of ca. 2.5 μm after 5 minutes of deposition. Increasing the Ti:Si ratio in the precursor, the thickness increases. Moreover, the different deposition time of TiO_2 and SiO_2 ensures the creation of a graded structure [5];

- titanium oxide was also used for corrosion protection of AA2024-T3 aluminum alloy [35]. In this case, DTMS and nano-scale TiO_2 particles were intercalated each other using dip-coating or cathodic deposition.

1.5 Conclusions

Summarizing, different aspects of electro-assisted deposition were studied over the years. However, basic knowledge needs to be depth, in order to explore new variables which can influence the process.

A significant number of studies was focused on applications, such as catalysis, corrosion protection, sensing and functional coatings.

Different research groups used electro-assisted technique for the deposition of hybrid organic-inorganic materials, mesoporous and nanocomposites silica-based. Moreover, titanium oxide can be deposited in combination with silica or alone, with greater effort.

It is simple to understand that the method can allow us to create complex structures and to modulate the thickness of sol-gel films in a precise way.

Bibliography

[1] Shacham, R.; Avnir, D.; Mandler, D. Electrodeposition of methylated sol-gel films on conducting surfaces. Adv. Mater. 1999, 11, 384-388

[2] Liu, L.; Walcarius, A. Kinetics of the electrochemically-assisted deposition of sol-gel films. Phys. Chem. Chem. Phys. 2017, 19, 14972-14983

[3] Toledano, R.; Mandler, D. Electrochemical codeposition of thin gold nanoparticles/sol-gel nanocomposite films. Chem. Mater. 2010, 22, 3943-3951

[4] Okner, R.; Favaro, G.; Radko, A.; Domb, A.J.; Mandler, D. Electrochemical codepositionn of sol-gel films on stainless steel: controllig the chemical and physical coating properties of biomedical implants. Phys. Chem. Chem. Phys. 2010, 12, 15265-73

[5] Liu, L.; Mandler, D. Electro-assist deposition of binary sol-gel films with graded structure. Electrochimica Acta 2013, 102, 212-218

[6] Wu, L.-K.; Zhang, X.-F.; Hu, J.-M. Corrosion protection of mild steel by one-step electrodeposition of superhydrophobic silica film. Corrosion Science 2014, 85, 482-487

[7] Liu, L.; Yellinek, S.; Tal, N.; Toledano, R.; Donval, A.; Yadlovker, D.; Mandler, D. Electrocemical co-deposition of sol-gel/carbon nanotubes composite thin films for antireflection and non-linear optics. J. Mater. Chem. 2015, 3, 1099-1105

[8] Shacham, R.; Avnir, D.; Mandler, D. Eletrodeposition of dye-doped titania thin films. J. Sol-Gel Sci. Technol. 2004, 31, 329-334

[9] Shacham, R.; Mandler, D.; Avnir, D. Electrochemically induced sol-gel deposition of zirconia thin films. Chem. Eur. J. 2004, 10, 1936-43

[10] Sibottier, E.; Sayen, S.; Gaboriaud, F.; Walcarius, A. Factor affecting the preparation and properties of electrodeposited silica thin films functionalized with amine or thiol groups. Langmuir 2006, 22, 8366-8373

[11] Walcarius, A.; Sibottier, E.; Etienne, M.; Ghanbaja, J. Electrochemically assisted self-assembly of mesoporous silica thin films. Nat. Mater. 2007, 6, 602-608

[12] Guillemin, Y.; Ghambaja, J.; Aubert, E.; Etienne, M.; Walcarius, A. Electro-assisted self-assembly of cetylmethylammonium-templated silica films in aqueous media: critical effect of counteranions on the morphology and mesostructure type. Chem. Mater. 2014, 26, 1848-1858

[13] Collinson, M.M.; Higgins, D.A.; Kommidi, R.; Campbell-Rance, D. Electrodeposited silicate films: importance of supporting electrolyte. Anal. Chem. 2008, 80, 651-656

[14] Ding, S.; Liu, L.; Hu, J.; Zhang, J.; Cao, C. Nitrate ions as cathodic alkalization promoters for electro-assisted deposition of sol-gel thin films. Scr. Mater. 2008, 59, 297-300

[15] Chen, C.; Dong, S., Hou, R.; Hu, J.; Jiang, P.; Ye, C.; Du, R.; Lin, C. Insight into the anti-corrosion performance of electrodeposited silane/nano-CeO_2 film on carbon steel. Surface & Coatings Technology 2017, 326, 183-191

[16] Gandhi, J. S.; Ooij, W.J. Improved corrosion protection f aluminum alloys by electrodeposited silanes. Journal of Materials Engineering and Performance 2004, 13, 475-480

[17] Zhang, Z.; Nie, L.; Yao, S. Electrodeposited sol-gel-imprinted sensing film for cytidine recognition on Au-electrode surface. Talanta 2006, 49, 435-442

[18] Tchinda, A.J.; Ngameni, E.; Walcarius, A. Thiol-functionalized porous clay heterostructures (PCHs) deposited as thin films on carbon electrode: towards mercury(II) sensing. Sensor and Actuators B 2007, 121, 113-123

[19] Deepa, P.N.; Kanungo, M.; Claycomb, G.; Sherwood, P.M.A., Collinson, M.M. Electrochemically dposited sol-gel-derived silicate films as a viable alternatve in thin-film design. Anal. Chem. 2003, 75, 5399-5405

[20] Liu, L.; Toledano, R.; Danieli, T.; Zhang, J.-Q.; Hu, J.-M.; Mandler, D. Electrochemically patterning sol-gel structures on conducting and insulating surfaces. Chem. Comm. 2011, 47, 6909-6911

[21] Walcarius, A. Electrochemical applications of silica-based organic-inorganic hybrid materials. Chem. Mater. 2001, 13, 3351-3372

[22] Wei, H.; Collinson, M.M. Functional-group effects on the ion-exchange properties of organically modified silicates. Anal. Chim. Acta 1999, 397, 113-121

[23] Petit-Dominguez, M.D.; Shen, H.; Heineman, W.R.; Seliskar, C.J. Electrochemical behavior of graphite electrodes modified by spin-coating with so-gel-entrapped ionomers. Anal. Chem. 1997, 69, 703-710

[24] Makote, R.; Collinson, M.M. Template recognition in inorganic-organic hybrid films prepared by the sol-gel process. Chem. Mater. 1998, 10, 2440-2445

[25] Kubota, L.T.; Gushikem, Y.; Perez, J.; Tanaka, A.A. Electrochemical properties of iron phthalocyanine immobilized on titanium (IV) oxide coated on silica gel surface. Langmuir 1995, 11, 1009-1013

[26] Sheffer, M.; Groysman, A.; Mandler, D. Electrodeposition of sol-gel films on Al for corrosion protection. Corrosion Science 2003, 45, 2893-2904

[27] Sheffer, M.; Groysman, A.; Starosvetsky, D.; Savchenko, N.; Mandler, D. Anion embedded sol-gel films on Al for corrosion protection. Corrosion Science 2004, 46, 2975-2985

[28] Jiang, L.-L.; Wu, L.-K.; Hu, M.-J.; Zhang, J.-Q.; Cao, C.-N. Electrodeposition of protective organosilane films from a thin layer of precursor solution. Corrosion Science 2012, 60, 309-313

[29] Wu, L.-K.; Hu, M.-J.; Zhang, J.-Q. Electrodeposition of zinc-doped silane films for corrosion protection of mild steels. Corrosion Science 2012, 59, 348-351

[30] Effect of electrodeposition potential on the corrosion properties of bis-1,2-[triethocysilyl] ethane films on aluminum alloy. Corrosion Science 2006, 51, 3944-3949

[31] Raveh, M.; Liu, L.; Mandler, D. Electrochemical co-deposition of conductive polymer-silica hybrid thin films. Phys. Chem. Chem. Phys. 2013, 15, 10876-10884

[32] Liu, L.; Hu, J.-M.; Zhang, J.-Q.; Cao, C.-N. Improving the formation and protective properties of silane films by combined use of electrodeposition and nanoparticles incorporation. Electrochimica Acta 2006, 52, 538-545

[33] Hu, J.-M.; Liu, L.; Zhang, J.-Q.; Cao, C.-N. Electrodeposition of silane films on aluminum alloys for corrosion protection. Progress in Organic Coatings 2007, 58, 265-271

[34] Zhang, X.; Chen, R.; Liu, Y.; Hu, J. Electrochemically generated sol-gel films as the inhibitor containers of superhydrophobic surface for active corrosion protection of metals. J. Mater. Chem. A 2016, 4, 649-656

[35] Li, M.; Yang, Y.-Q.; Liu, L.; Hu, J.-M.; Zhang, J.-Q. Electro-assisted preparation of dodecyltrimethoxysilane/TiO_2 composite films for corrosion protection of AA2024-T3 (aluminum alloy). Electrochimica Acta 2010, 55, 3008-3014

[36] Wu, L.-K.; Liu, L.; Li, J.; Hu, J.-M.; Zhang, J.-Q.; Cao, C.-N. Electrodeposition of cerium (III)-modified bis-[triethoxysilylpropyl]tetra-sulphide films on AA2024-T3 (aluminum alloy) for corrosion protection. Surface & Coatings Technology 2010, 204, 3920-3926

[37] Sayen, S.; Walcarius, A. Electro-assisted generation of functionalized silica films on gold. Electrochemistry Communications 2003, 5, 341-348

[38] Walcarius, A.; Sibottier, E. Electrochemically-induced deposition of amine-functionalized silica films on gold electrodes and application to Cu(II) detection in (hydro)alcoholic medium. Electroanalysis 2005, 17, 1716-1726

[39] Nadzhafova, O.; Etienne, M.; Walcarius, A. Direct electrochemistry of hemoglobin and glucose oxidase in electrodeposited sol-gel silica thin films on glassy carbon. Electrochemistry Communications 2007, 9, 1189-1195

[40] Gamero-Quijano, A.; Huerta, F.; Torres, D.; Montilla, F. Electrochemical behaviour of PPS-functionalized silica films prepared by electroassisted deposition of sol-gel precursors. Electrocatalysis 2015, 6, 33-41

[41] Torres, D.; Montilla, F.; Huerta, F.; Morallon, E. All electrochemical synthesis of polyaniline/silica sol-gel materials. Electrochimica Acta 2011, 56, 3620-3625

[42] Carrington, N.A.; Yong, L.; Xue, Z.-L. Electrochemical deposition of sol-gel films for enhanced chromium(VI) determiination in aqueous solutions. Analytica Chimica Acta 2006, 572, 17-24

[43] Despas, C.; Vodolazkaya, N.A.; Ghanbaja, J.; Walcarius, A. Preparation of ordered and oriented mesoporous silica thin films bearig octyl or hexadecyl groups by electrochemically assisted self-assembly and evaluation of their transport properties. J. Solid State 2015, 19, 2075-2085

[44] Vilà, N.; Walcarius, A. Electrochemical response of vertically-aligned, ferrocene-functionalized mesoporous silica films: effect of the supporting electrolyte. Electrochim. Acta 2015, 179, 304-314

[45] Vilà, N.; Ghanbaja, J.; Walcarius, A. Clickable bifunctional and vertically aligned mesoporous silica films. Adv. Mater. Interfaces 2016, 3, 1500440

[46] Vilà, N.; Ghanbaja, J.; Aubert, E.; Walcarius, A. Electrochemically assisted generation of highly ordered azide-functionalized mesoporous silica for oriented hybrid films. Angew. Chem. Int. Ed. 2014, 53, 2945-2950

[47] Kresge, C.T.; Leonowicz, M.E.; Roth, W.J.; Vartuli J.C.; Beck J.S. Ordered mesoporous molecular sieves synthesized by a liquid-crystal template mechanism. Nature 1992, 359, 710-712

[48] Beck J.S.; Vartuli J.C.; Roth, W.J.; Leonowicz, M.E.; Kresge, C.T.; Schmitt, K.D.; Chu, C.T-W.; Olson, D.H.; Sheppard, E.W.; McCullen, S.B.; Higgins, J.B.; Schlenkert, J.L. A new family of mesoporous molecular sieves prepared with liquid crystal templates. J. Am. Chem. Soc. 1992, 114, 10834-10843

[49] Mousty, C.; Walcarius, A. Electrochemically assisted deposition by local pH tuning: a versatile tool to generate ordered mesoporous silica thin films and layered double hydroxide materials. J. Solid State Electrochem. 2015, 19, 1905-1931

[50] Goux, A.; Etienne, M.; Aubert, E. Lecomte, C.; Ghanbaja, J.; Walcarius, A. Oriented Mesoporous Silica Films Obtained by Electro-Assisted Self-Assembly (EASA), Chem. Mater. 2009, 21, 731-741

[51] Maghear, A.; Etienne, M.; Tertis, M.; Sandulescu, R.; Walcarius, A. Clay-mesoporous silica composite films generated by electro-assisted self-assembly. Electrochimica Acta 2013, 112, 333-341

[52] Herzog, G.; Sibottier, E.; Etienne, M.; Walcarius, A. Electrochemically assisted self-assembly of ordered and functionalized mesoporous silica films: impact of the electrode geometry and size on film formation and properties. Faraday Discuss. 2013, 164, 259-273

[53] Xu, F.F.; Cui, F.M.; Ruan, M.L.; Zhang, L.L.; Shi, J.L. Structural ccharacteristics of oriented mesostructured silica thin films. Langmuir 2010, 26, 7535-7539

[54] Kang, H.S.; Lee, H.C.; Kwak, J.H. Electrodeposition of polypyrrole nanowires within vertically oriented mesoporous silica template. Korean Electrochem. Soc. 2011, 14, 22-26

[55] Del Valle, M.A.; Gacitùa, M.; Dìaz, F.R.; Armijo, R.; Del Rìo, R. Electrosynthesis and characterization of polythiophene nano-wires/platinum nanoparticles composite electrodes. Study of formic acid electro-catalytic oxidation. Electrochem. Acta 2012, 71, 277-282

[56] Rafiee, M.; Karimi, B.; Farrokhzadeh, S.; Vali, H. Hydroquinone functionalized oriented MCM-41 mesochannels at the electrode surface. Electrochim. Acta 2013, 94, 198-205

[57] Rafiee, M.; Karimi, B.; Arshi, S.; Vali, H.; Ethylenediamine-modified oriented MCM-41 at the electrode surface, cobalt adsorption ability and electrochemical performance. Dalton Trans. 2014, 43, 4901-4908

[58] Farghaly, A.A.; Collinson, M.M. Electroassisted codeposition of sol-gel derived silica nanocomposite directs thefabrication ofcoral-like nanostructured porousgold. Langmuir 2014, 30, 5276-5286

[59] Toledano, R.; Shacham, R.; Avnir, D.; Mandler, D. Electrochemical codeposition of sol-gel/metal thin nanocomposite films. Chem. Mater. 2008, 20, 4276-4283

[60] Shacham, R.; Avnir, D.; Mandler, D. Pattern recognition in oxides thin-film electrodeoposition: printed circuits. C. R. Chemie 2010, 13, 237-241

Chapter 2

Methods and Characterizations

In this chapter, the main methods and characterizations used during the PhD project are explained. The theory of design of experiments (DOE), cyclic voltammetry and ellipsometry will be briefly described in order to give a greater understanding of the subject. The details of the principal instruments used will be given in the section 2.4 on page 24. Anyway, each chapter presents the experimental section, because different apparatus and reagents were used depending on the study performed.

2.1 Design of Experiments (DOE)

One can imagine an experiment as a black box, in which it is necessary to put different *inputs* in order to receive one or more *outputs*. At this point, there are two problems:

- how to decide the best input;
- how to correlate the input with the output.

Design of experiments is a method that allow us to manage the experiments.

First of all, one has to decide the target (outputs), identifying the responce variables and choosing the most appropriate measurement systems. Consequently, the factors to be investigated and their measurements are determined together with the maximum and minum levels for each factor. Second, once the experiment skeleton has been obtained, it is necessary to establish any replicas and blocks (to isolate the sources of variation) and to identify both the variables that are not within the DOE and the so-called "out of control variables".

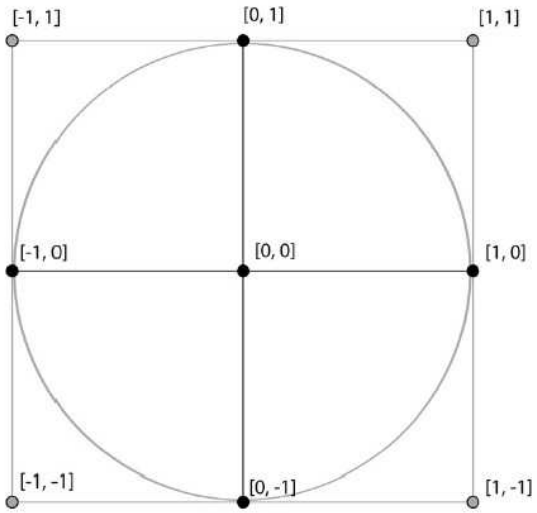

Figure 2.1: One-factor-at-a-time (circle). DOE (all the points)

It is advisable to keep in mind that factor ranges must be wide enough to generate the desired changes in responses and, in addition, it is useful to randomize experiments to avoid systemic or random errors [1].

Apart from the *trial and error* strategy, that is a non-mathematical approach to the problem, *one-factor-at-a-time* strategy is widely used in the engineering field, which is to choose an initial value for each factor, then to vary the levels of each factor in its own range, keeping the other constant factors at their base or central level. The disadvantage of this strategy is to leave unexplored a whole region of space (figure 2.1) that in the case of 2 factors still represents a modest percentage but grows rapidly as the size increases [2].

However, using factor plans allows systematic analysis of the system response. In fact, in a factorial experiment all (full factorial plan) or part (fractional factor plan) of combinations derived from possible factors levels are tested. One can quite understand how the design of experiment is a way of choosing examples in the design space to get the maximum number of information using the minimum of resources.

An important feature of a full factorial plan is the extremely efficient use of experimental data. In general, when all factors are investigated with the same number of levels, we talk about a family of L-factor factor plans and k factors, where Lk is also the number of tests required for a full system characterization. A factorial plan is said to be full (full factorial) when using all the possible combinations of factor levels. If L = 2, for k = 2 or k = 3 the factorial plane can be

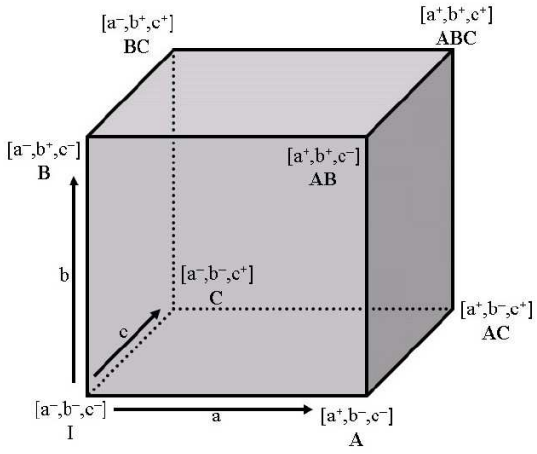

Figure 2.2: Full factorial plan with 3 factors and 2 levels (2^3 combinations)

represented geometrically in an euclidean space, respectively as a square or cube (figure 2.2); For k > 3, like a hypercube in a k-dimensional space.

Increasing the number of factors and levels, the total combinations increase exponentially, and therefore the number of tests required to run the experiment may not be sustainable. For this reason it is useful to use fractional factor plans as shown in figure 2.3 on the next page, *i.e.* a variation of the basic factorial plan in which only a subset of tests of the corresponding full factorial set is performed.

Considering the case where two factors interact each other, the benefits of using factorial experimentation are further understood. Two factors interact when the effect of a factor changes with the levels of the second factor: such interaction is defined as the first order (for example AB); This definition can also be extended to higher order interactions. In this way, interactions of the second or third order can be defined (*e.g.* ABC, ABCD).

DOE method was used in chapter 3, in fact the high number of experiments needed a rigorous method in order to perform as many experiments as possible.

2.2 Ellipsometry

The ellipsometer uses polarized light to characterize thin films and bulk materials. A wave is said to be polarized when the vibration of the electric vector associated with radiation has some preference about the direction, however always in a orthogonal plane to the wave vector k. There are three types of polarized light:

- linear: the oscillation direction of vector E is constant over time;

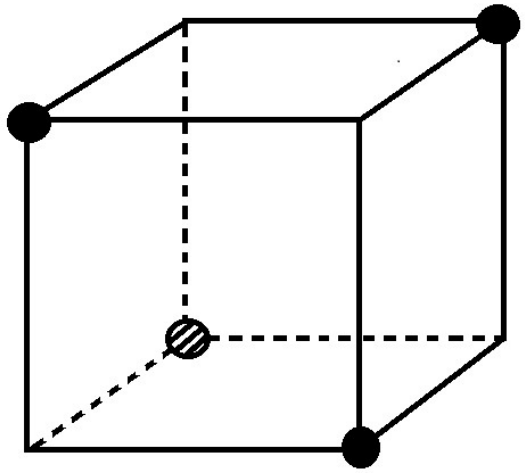

Figure 2.3: Fractional factorial plan 2^{3-1}

- circulate: the end of the vector E at a given point describes a circumference over time;
- elliptical: when the extremity of vector E at a given point describes an ellipse over time.

The polarization change is measured after the light reflects from the surface of the substrate. These measurements allow to derive the thickness and the optical constants (n, k) of the thin film. In fact, the elliptical measurement is expressed by two parameters for each wavelength-angle combination: Psi (Ψ) and Delta (Δ). These values can be linked to the complex reflection coefficient of Fresnel [3], given by the ratio between R_p and R_s (reflectance coefficients of the polarized light: type p- and type s-, respectively):

$$\rho = \frac{R_p}{R_s} = \tan(\Psi)e^{i\Delta} \tag{2.1}$$

When the light moves from a medium with a given refractive index n_1 in a second medium with refractive index n_2, both refraction and reflection occur. In figure 2.4 on the facing page, the incident light beam PO hits the point O at the interface between the two means with refraction index n_1 and n_2. Part of the beam is reflected as an OQ radius and part is refracted as an OS radius. The incidence angles relative to the normal interface are Θ_i, Θ_r and Θ_t respectively. The relationship between these angles is given by the law of reflection 2.2 and the law of Snell 2.3 [4, 5]:

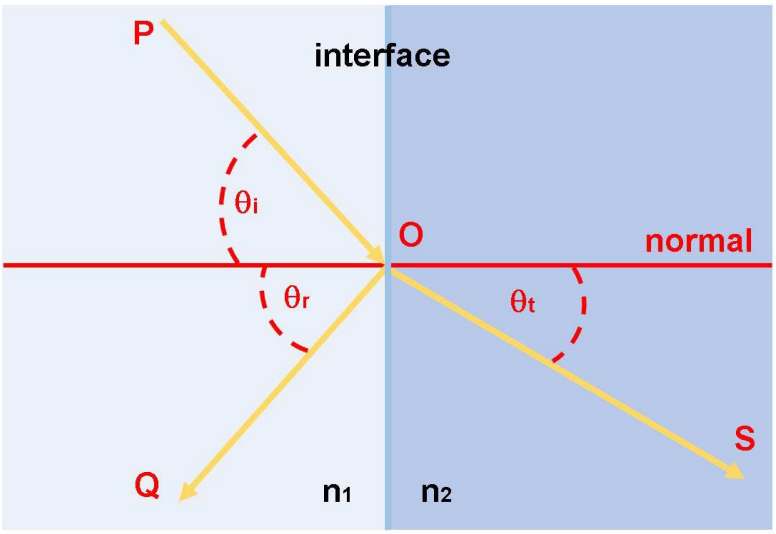

Figure 2.4: Reflection (OQ) and refraction (OS) of the light due to the different refractive index (n_1, n_2)

$$\Theta_i = \Theta_r \tag{2.2}$$

$$\frac{sin(\Theta_i)}{sin(\Theta_r)} = \frac{n_1}{n_2} \tag{2.3}$$

The fraction of the intensity of the incident radiation reflected by the interface is given by the reflection R, while the fraction refracted is given by the transmittance T (assuming non-magnetic behaviour).

The most common ellipsoid measurements regard the thickness (thanks to the phase information Δ which provides sensitivity up to sub-nanometric levels) and the refractive index. However, ellipsometry can also give information about the surface of the sample, such as roughness. It is important to underline that a film inhomogeneity along the thickness can cause a dependence of the refractive index. The presence of pores could induce anomalies in the behavior of optical properties; the existence of zones with different refractive indices would cause a different optical response of the material in comparison with that expected for the same pure material.

Typically, these values are determined analytically, that is, by means of a mathematical model that interpolates the instrumentś response. For example, the refractive index, $n(\lambda)$, for transparent materials can be described with the Cauchy dispersion model [6, 7], given by 2.4:

$$n(\lambda) = A_n + \frac{B_n}{\lambda^2} + \frac{C_n}{\lambda^4} \tag{2.4}$$

Where A_n, B_n and C_n are Causchy's parameters and λ is the wavelength in micron.

The application of ellipsometric characterization was widely used in this project. The thicknesses of the films were measured using ellipsometer in chapters 3 and 5 (section 5.1). Moreover, the optical properties of the films were measured in section 5.3.

2.3 Cyclic Voltammetry (CV)

During a cyclic voltammetry, the working electrode is immersed in the electrolytic solution under static conditions. A variable potential is applied at a constant speed, said scan rate (ν). The answer measured is the current in function of the potential. At a potential value, said inversion potential, the direction of the scan rate is inverted, in order to return to the starting potential value. In this way a triangular wave is produced, it is also possible to perform several consecutive cycles (figure 2.5A).

This current is due to two contributions:

- Capacitive contribution due to the formation of the double electrical layer that becomes more important as scan rate increases;
- Faradic contribution due to electronic transfer reactions on the surface electrode.

In cyclic voltammetry the faradic current is manifested in the form of oxidation and reduction peaks. The peak form is due to the staticity of the solution and the consequent decrease of the amount of reagent species able to reach the electrode surface by diffusion. The current begins to grow when the reagents begin the electronic transfer process. As the potential increases the reaction becomes faster, the gradient concentration on the electrode surface increases, such as the current. Before the gradient value reaches the maximum point, the diffusion layer starts to expand and the current decreases (figure 2.5B).

Once the potential is inverted, a current in the opposite direction begins to pass into the working electrode. As a result, the direction is anodic, the current is positive and the reactions are oxidative. Therefore, the cyclovoltammogram is characterized by two curves of current, whose shape depends on the type of process.

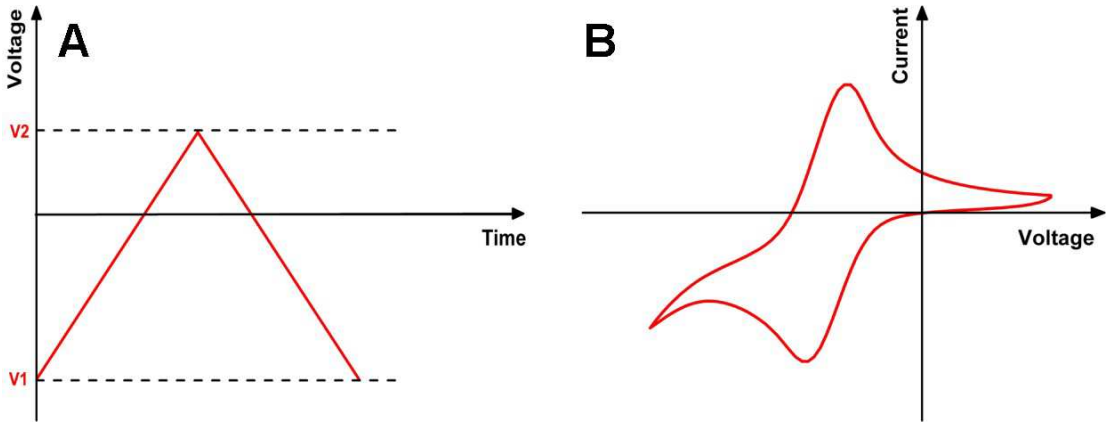

Figure 2.5: Trend of potential in a cyclic voltammetry measure (A). Example of a Cyclic voltammetry (B)

If the tested reaction is reversible then in the return scan there is a peak relative to the inverse oxidation reaction. Even the return scan signal has a maximum at a characteristic value of potential. The separation between cathodic and anodic peaks depends on the system's reversibility, the number of electrons exchanged in the process redox and temperature.

In a reversible process the peak potential value is independent of the scan rate, while the peak current value depends on the square root of ν, concentration and diffusion coefficient of the species involved in the redox process (equations 2.5 and 2.6 at 25°C) [8]. All of these parameters can be used to identify the nature of a reversible process.

$$I_p = 0.4463nFAC\left(\frac{nFC\nu D}{RT}\right)^{1/2} \tag{2.5}$$

$$I_p = 268600nAC(nD\nu)^{1/2} \tag{2.6}$$

For an irreversible process, there is no peak in the return scanning. Peak current depends on square root of the scan rate, but also on the transfer electronic coefficient (α). Moreover, the peak potential depends on the scan rate and moves cathodically. Due to the transfer electronic coefficient, the peak results enlarged and less intence than the reversible process. [9].

Cyclic voltammetries were performed in order to identify the potential at which occurs the reduction reaction of water (sections 3.3.2, 4.3). From an electrochemical point of view, an important application of this technique can be find in the

section 5.2 on page 68, in which the monitoring of redox reactions plays a fundamental role to explain the behaviour of the multilayer structure.

2.4 Thin Films Characterization. Other Techniques

During the doctorate project, we used different techniques in order to characterize thin film formation. Structural characterizations were obtained using X-ray diffraction and grazing incidence X-ray. Morphological characterizations were carried out using SEM, TEM and AFM.

In this section you will find a brief description of the instrument used.

X-ray diffraction (XRD) In order to evaluate the degree of transformation of amorphous titania in anatase-rutile, the thin-film XRD measurements were performed at 1.5° incidence using a Philips PW1710 diffractometer equipped with grazing-incidence X-ray optics, using CuKα Ni-filtered radiation at 40 kV and 40 mA. The samples were treated at 500°C before the characterization. Being stainless steel, a lot amount of hematite was establish on the surface, compromising the measurement. To avoid this technological problem, a thicker layer was deposited between the substrate and the titania layer. Moreover, in order to increase the signal a double layer of titania was deposited, the measurement were performed from 24 to 40 2θ and 15 seconds for each point taken.

Grazing incidence X-ray diffraction (GIXD) The structure of mesoporous films was also analyzed by grazingincidence X-ray diffraction (GIXD) using a Nonius Kappa CCD diffractometer equipped with an ApexII CCD detector (copper cathode lKα = 0.154184 nm). This would allow demonstrating the regular vertical orientation of mesopores, in fact the presence of the (10), (11), (20), and (21) signals indicates that the sample is made of hexagonal domains of regularly packed channels (figure 5.8 on page 80) [10, 11]. It has been shown that GIXD is a good technique for characterizing thin mesoporous films.

Field emission scanning electron microscope (FE-SEM) FE-SEM Zeiss Sigma HD, operated at 2 kV was used to analyze thin films multilayer silica-titania based. Images were obtained using carbon conductive tape. It is important to stress the fact that it is not simple to analyze a non-conductive thin films. An instrument more efficient than SEM was necessary. Electrons are liberated from

a field emission source and accelerated in a high electrical field gradient. Cross sectional views were obtained cutting the samples with a diamond tip. This method is used only for ITO samples, because stainless steel substrate is too ductile to be properly prepared.

Transmission electron microscope (TEM) Thanks to transmission electron microscopy (TEM), morphological analysis of the mesoporous ordered films has been achieved using a CM20 microscope at an acceleration voltage of 200 kV. Previously it has been noticed that with GIXD it is possible to characterize them structurally, but it is also important to show how the formation grows up. In figure 5.6 on page 77 you will observe the resolution of this microscope.

Using a FIB (Focused Ion Beam), a slice of the thin film was withdrawn, preserving the orientation of the mesoporous silica without destrying it. Different slices were placed on the TEM grid.

Atomic force microscope (AFM) AFM measurement were performed using Thermomicroscope Explorer Ecu+ apparatus (Veeco Instruments SAS). ITO samples were prepared scraching the film in order to obtain thickness data and morphological analysis of the surface. It was not possible to analyze stainless steel samples because the substrates were not completely flat.

Bibliography

[1] Vegliò, F. La Programmazione della Sperimentazione nello Sviluppo dei Processi Chimici. Ratio Mathematica 1995, 9, 37-53

[2] Toro, L.; Vegliò, F. Determinazione del Piano Sperimentale di una Sperimentazione Fattoriale a 2 e 3 Livelli con Confusione e Frazionata. Ratio Mathematica 1992, 195-210

[3] Morton, D.E.; Johs, B.; Hale, J. Optical monitoring of thin-films usin spectroscopic ellipsometry. Society of Vacuum Coaters 2002, 505, 856-7188

[4] Smith, D.R.; Pendry, J.B.; Wiltshire, M.C.K. Metamaterials and negative refractive index. Science 2004, 305, 788-792

[5] Yu, N.; Genevet, P.; Kats, M.A.; Aieta, F.; Tetienne, J.-P.; Capasso, F.; Gaburro, Z. Light propagation with phase discontinuities: generalized laws of reflection and refraction. Science 2011, 334, 333-337

[6] Li, J.; Wu, S.-T. Extended Cauchy equations for the refractive indices of liquid crystals. J. Appl. Phys. 2004, 95, 896-901

[7] Synowicki, R.A. Spectroscopic ellipsometry characterization of indium tin oxide film microstruture and optical constants. Thin Solid FIlms 1998, 313-314,394-397

[8] Laoire, C.O.; Mukerjee, S.; Abraham, K.M.; Plichta, E.J.; Hendrickson, M.A. Elucidating the mechanism of oxygen reduction for Lithium-air battery applications. J. Phys. Chem. 2009, 113, 20127-34

[9] Nicholson, R. Theory and application of cyclic voltammetry for measurement of electrode reaction kinetics. Anal. Chem. 1968, 37/11, 1351-1355

[10] Giordano, G.; Vilà, N.; Aubert, E.; Ghambaja, J.; Walcarius, A. Towards multi-layered, vertically-aligned and functionalized mesoporous silica films by

sequential electrochemically assisted self-assembly. Electrochimica Acta 2017, 237, 227-236

[11] Goux, A.; Etienne, M.; Aubert, E. Lecomte, C.; Ghanbaja, J.; Walcarius, A. Oriented Mesoporous Silica Films Obtained by Electro-Assisted Self-Assembly (EASA), Chem. Mater. 2009, 21, 731

Chapter 3

Preliminary Experiments

3.1 Introduction

In the chapter one, the cited literature reports on the influence of the most important parameters (potential, time, concentration of precursors, stirring, electrolyte) on the properties of the deposited layers (thickness, morphology, resistance to corrosion), and some of the studies are very well detailed with important key information. However, they are often made using different experimental methods and systems that cannot be easily compared. Therefore a clear picture of the fundamental aspects and of the real role played by the many parameters involved is still lacking, and many questions need for an answer, which is preliminary for the full development and application of this coating method.

This chapter is a first attempt to get a broader understanding of the key parameters and of their influence on the obtained coatings.

The fundamentals of the electrochemical deposition method involve many different theoretical aspects, and the practical results of the application of the method are the sum of many contributions. Therefore it is not easy to perform experiments taking everything into account or deciding what is most important. Furthermore the final coating is made of two layers, different in thickness and presumably different in density and degree of condensation. This makes the analysis of the results more complicated. Some authors rinsed [1] or blow-dried (with nitrogen [2]) the samples after deposition, assuming that the layer deposited by dipping could be removed leaving the electrodeposited layer mostly unaffected. Here, it was decided to take into account the thickness of the dipping layer by depositing it using the same solutions, but without any voltage applied.

In the next paragraphs, which are intended to be a preliminary approach to a systematic study, the effect of potential and time on the thickness was studied

using simple TEOS-based acidic solutions to coat planar stainless steel samples. Different starting solutions were tested, varying the amount of precursor, water and hydrochloric acid. The role of working temperature, oxygen concentration and the presence of KNO_3 until saturation were also tested.

The results were published in *Journal of Sol-Gel Science and Technology* [3].

3.2 Experimental

Reagents and apparatus Tetraethyl ortosilicate (98%) and Ethanol ($\geq$ 99.8%) were purchased from Sigma-Aldrich and used as received. Hydrochloric acid (1 M) was purchased from Labochimica srl.

Ethanol, distilled water, hydrochloric acid and tetraethyl ortosilicate (TEOS) were mixed, respecting the following parameters: C = SiO_2 g/L (from 50 to 150), R = H_2O/TEOS molar ratio (from 2 to 10) and H = HCl/TEOS molar ratio (from 0.05 to 0.02). The solutions were stirred for 1 h at room temperature ($\sim$21°C), in order to promote the hydrolysis.

A standard three electrode cell was used. The reference elecrode was a saturated calomel electrode (SCE) and the counter electrode was a platinum wire. The working electrode were obtained from a stainless steel sheet (AISI 304), protected on one side by a protective removable film. The surface was mirror-like polished and the roughness was the same for all samples. The surface of the plate was 20 mm $\times$ 10 mm $\times$ 1 mm. During cyclic voltammetry, an exposed area of $\sim$7 mm^2 was obtained masking the samples with Teflon tape. Teflon was used also in order to cover the edges of the working electrode during electrodeposition, left an exposed circular area of about 40 mm^2. An external thermostat was used, which was connected to the water jacket of the cell. No stirring was applied during the deposition. After application of the potential, the samples were withdrawn by a dip coater with a withdrarwal constant rate of ca. 100 μm/s.

During the extraction from the cell, a thin film is deposited by dip coating on the electrochemically deposited layer. The thin layer can be minimized using a low withdrawal rate, but can not be avoided. The samples were dried at room temperature for at least 24 h before any characterization.

Characterization The electrodeposition was obtained by using a potentiostat/galvanostat (EG&G PARC, Model 273A). The surface morphology of the films were investigated in low vacuum by scanning electron microscopy (SEM Philips XL30). The thickness was measured by a variable-angle spectroscopic ellipsometer (J. A. Wollam Co., Inc.) at icident angles of 70°, 75° and 80°, within a

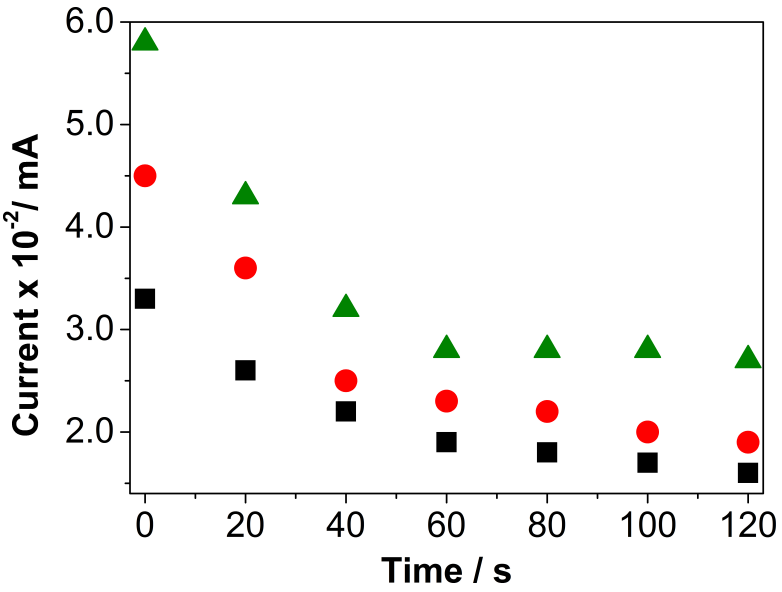

Figure 3.1: Chronoamperometric data. Deposition time: 2 min. Applied potentials: -0.7 V (*square*), -0.9 V (*circle*), -1.1 V (*triangle*)

wavelength range of 300-1700 nm. For each kind of solution, a cyclic voltammetry (CV) was performed with different switching potential and chronoamperometric (CA) data were acquired during the deposition runs.

3.3 Key Variables

3.3.1 Potential and time

With the help of cyclic voltammetry and using a blank solution with ethanol instead of TEOS, it was found that the reduction of water begins at -0.7 V vs. SCE. Therefore three different potentials were applied for 2 min (-0.7, -0.9 and -1.1 V vs. SCE) keeping constant the temperature and the solution ($C = 50$, $R = 6$ and $H = 0.01$).

As shown in figure 3.1, a chronoamperometry was acquired for each sample during the deposition. As expected, the initial current increases with the absolute value of the applied potential.

The thickness was measured by ellipsometry, although it was not trivial due to inhomogeneity of thickness. The mean value of the thickness and the optical constants were obtained by applying the Cauchy model.

Table 3.1: Thickness of silica films measured by ellipsometry in the central area of the samples

Sample	Potential (V vs SCE)	Time (min)	Thickness (nm)	Eet (nm)
$p1$	-0.7	2	125 ± 2	71 ± 3
$p2$	-0.9	2	121 ± 4	67 ± 4
$p3$	-1.1	2	197 ± 4	143 ± 5
$t1$	-0.9	30	181 ± 18	127 ± 18
$t2$	-0.9	120	338 ± 5	284 ± 6

Table 3.1 on the next page reports the thickness of the electrodeposited layers. As already observed, the final coating is made of a first layer deposited electrochemically, and a second one due to the withdrawal process after the electrodeposition. To take into account this last contribution to the total thickness, a silica film was deposited by simple dipping at open circuit potential. A thickness of 53.9 ± 1.0 nm was measured, which, subtracted to the total thickness, gives the estimated thickness (Eet) of the electrodeposited layer.

As reported in the literature, the thickness increases with the absolute value of the applied potential [4]. It increases also with time, but different trends are reported. Data published by Shacham et al. on TiO_2 [5] and ZrO_2 [6] coatings indicate that a constant thickness regime is reached after 10-15 min, but in a paper recently published by Farghaly et al. [7] the thickness of silica based nanocomposite films increases almost linearly with time up to the maximum tested period of 30 min. Here we show, even if with only three points, a linear increase up to 120 min.

3.3.2 Influence of starting solution

The thickness of the deposited layers was studied as a function of the concentration of precursor, water and hydrochloric acid. The potential and deposition time were fixed at -0.9 V vs. SCE and 5 min, respectively.

In order to avoid trivial errors, Design of Experiments (DOE) was used to plan the experiments. Three factors were considered (C, R, H) with two levels each: low and high concentration (Table 3.2). Therefore the full factorial design requires eight experiments, which are denoted with minuscule letters following the Yates's notation [8]. Experiments denoted with a single letter are aimed to test the influence of a single parameter, while experiments denoted with two or three letters are aimed to test the interaction between two or among three parameters.

Table 3.2: Factors and levels in DOE

Factor	Low	High
C	100	150
H	2	10
R	0.005	0.02

Table 3.3: Tested solutions

Solution	Ethanol (mL)	H_2O (mL)	HCl (1 M) (mL)	TEOS (mL)
(1)	28.7	2.6	0.4	18.3
c	18.1	3.8	0.6	27.5
r	16.9	14.4	0.4	18.3
cr	0.4	21.5	0.6	27.5
h	28.7	1.36	1.64	18.3
ch	18.1	1.94	2.46	27.5
rh	16.9	13.16	1.64	18.3
crh	0.4	19.64	2.46	27.5

The corresponding solution formulations are reported in 3.3 on the facing page.

Before the deposition, a CV was obtained for each solution. Assuming that, for the determination of hydrogen reduction potential, TEOS behaves as ethanol, solutions c, r and h, where TEOS was replaced with the appropriate amount of ethanol were used. The results are shown in figure 3.2 on the next page. By increasing the concentration of bi-distilled water and of HCl, the current increases, but the potential at which hydrogen evolution occurs remains constant.

During the deposition, the potentiostat provides the current as a function of time (chronoamperometry, CA). The current depends on the nature of the solution, but also on the thickness of the silica layer that is forming, on the size, amount and morphology of the pores. To the best of our knowledge, these aspects weren't studied thoroughly, although they are important both from the points of view of the understanding of the process and of the practical application. At the beginning current always decreases, according to the trend of figure 3.3 on page 35, but after this we observed two different behaviors:

- combinations that had a factor H with a low level (0.005) followed the same trend as shown in figure 3.3A, with a continuous decrease of the current with time;

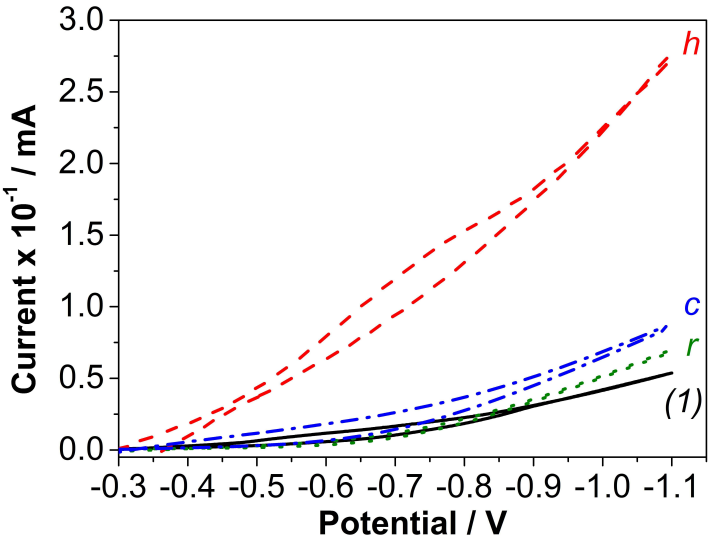

Figure 3.2: Cyclic voltammetry. Scan rate 200 mV/s. Switching potential: -1.1 V vs SCE

- combinations that had a factor H with a high level (0.02) show a trend similar to the one shown in figure 3.3B, with an increase of the current after about 20 s until to reach a constant value.

According to Shacham at al. [6] by plotting i^{-1} as a function of $t^{1/2}$ a linear dependence can be observed, at least in the first period of the deposition (figure 3.3, insets). This behavior can be explained assuming diffusion-controlled conditions following the Cottrell equation 3.1 for semi-infinite diffusion [9, 10]

$$i(t) = \frac{nFAC_0D^{1/2}}{(\pi t)^{1/2}} \tag{3.1}$$

valid only for short time period, while the deviation from linearity for long periods is due to the finite nature of the film.

The trend shown in figure 3.3 has been observed in the electrochemical deposition of metals and has been discussed in terms of three contributions: adsorption, 2D nucleation and growth and 3D nucleation with diffusion-controlled growth [11]. The mechanism of film deposition in the case described here is, of course, different and the observed trend cannot be explained in the same way, even if some analogy might be found. A specific study was done to relate the shape of the current-time curves with the morphology of the deposited layers. This study will be described in chapter 3.

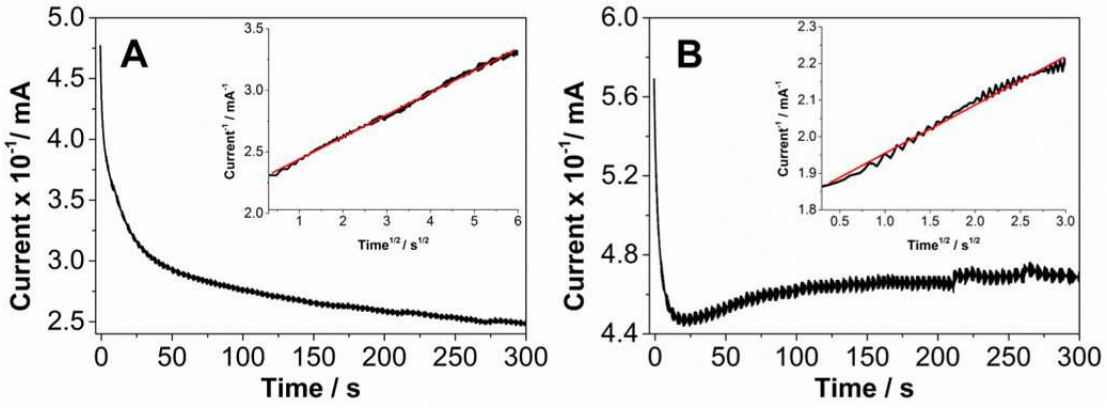

Figure 3.3: Chronoamperometric data. Deposition time: 5 min. Applied potential: -0.9 V vs. SCE. Sample *cr* (A) and sample *rh* (B)

Table 3.4: Composition and ellipsometric thickness data of samples used to evaluate the influence of the solution composition

Samples	Thickness (nm)	Dipping (nm)	Eet (nm)
(1)	300 ± 14	149 ± 2	151 ± 14
c	580 ± 16	233 ± 4	347 ± 16
h	449 ± 9	140 ± 3	309 ± 9
ch	586 ± 26	204 ± 2	382 ± 26

After deposition the samples were withdrawn from the solution and dried as already described in the experimental section. After few seconds the samples *r*, *cr*, *rh* and *crh* cracked on the whole surface (figure 3.4B), while the samples with a low water content ($R = 2$, corresponding to the treatments (1), *c*, *h*, *ch*) were free of cracks, at least in a wide central area (figure 3.4A). It was, of course, impossible to get ellipsometric data in the first four samples, due to scattering. The thickness of the other samples is reported in table 3.4. Also in this case layers at null voltage were produced to get the dipping thickness and estimate the electrochemical thickness.

It is interesting to compare the dipping thickness and the estimated electrodeposited thickness. The dipping thickness clearly increases, as known, with precursor concentration, but seems to slightly decrease with acid concentration, which might be related to the structure of the hydrolyzed species and to the related viscosity of the sol. Considering the estimated electrochemical thickness, quite reasonably it increases with precursor concentration, according to Okner

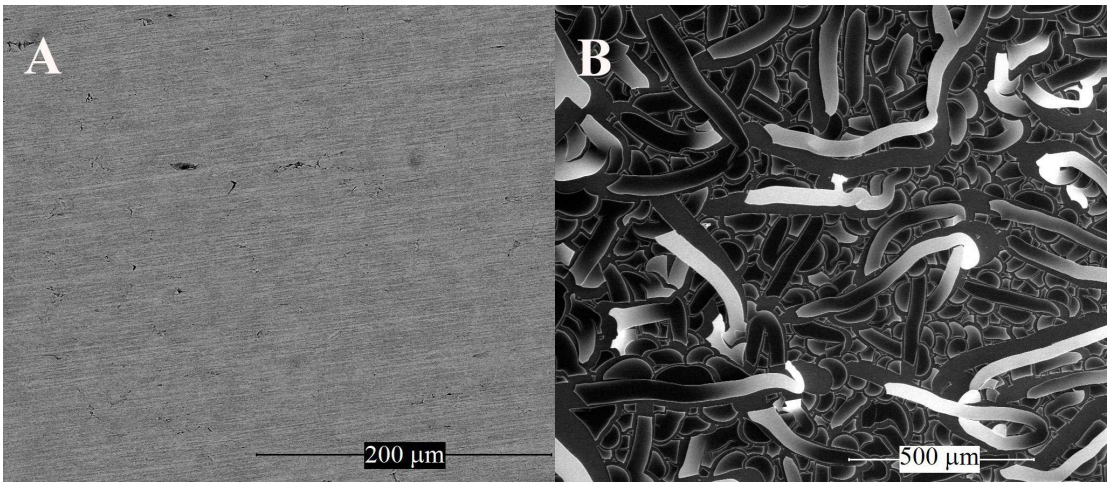

Figure 3.4: ESEM micrographs. Sample (1) deposited at -0.9 V vs SCE for 5 min (A). Sample *cr* deposited at -0.9 V vs SCE for 5 min (B).

at al. [12]. It also increases with the factor H, i.e. with the acidity of the solution. One might argue that starting from a lower initial pH should minimize the local increase of pH due to protons consumption at the sample surface, thus decreasing the layer grow and consequently the thickness at a given deposition time. However, a lower pH the hydrolysis rate of the precursor increases. More hydrolyzed species should be therefore available in the solution, prompt to condense at the sample surface. The higher thickness when both C and H are high seems to confirm this tentative explanation.

3.3.3 Temperature, oxygen and electrolyte

The temperature is an important variable, because it affects the kinetics of diffusion and promotes Ostwald ripening, changing the morphology of the film [13].

The concentration of oxygen in solution might also be important. The electrolyte is usually considered as not directly participating in the electron-transfer reaction. However, as pointed out by Collinson et al. [14], the electrolyte's chemical properties can enable direct reactions at the electrode surface or reactions with species electrogenerated at an electrode surface. Potassium nitrate was indeed used by Ding et al. [15] to promote OH^- production by the reaction 3.2

$$NO_3^- + H_2O + 2e^- \rightarrow NO_2^- + 2OH^- \tag{3.2}$$

Therefore these three further parameters were tested. The starting solution

Table 3.5: Thickness, measured by ellipsometry, of layers deposited at $T = 41°C$

Samples	Thickness (nm)	Eet (nm)
T	173 ± 3	120 ± 3
oT	241 ± 2	187 ± 3
eT	222 ± 2	168 ± 2

used for these experiments had $C = 50$, $R = 6$ and $H = 0.01$. A potential of -0.9 V vs. SCE was applied for 5 min. Three experiments were run: at 41°C in the absence of oxygen and KNO_3 in solution (T), at 41°C in the presence of oxygen in solution (oT), at 41° C in the presence of KNO_3 in solution (eT). The oxygen saturation was ensured by bubling O_2 into the solution in the cell for 20 min and blowing O_2 above the solution during the whole deposition, whereas the absence of oxygen was guaranteed by bubbling argon into the solution for 20 min before the deposition. For the experiment eT the solution was saturated with KNO_3.

All the samples were qualitatively better (more homogeneous, crack-free) than those obtained at room temperature, suggesting that process temperature may be an important factor for obtaining good quality layers. However, a more systematic study is need to support this feeling.

The thickness of the coatings deposited in the three experiments are reported in table 3.5. The dipping thickness for this solution (the same used for testing the influence of potential and time) is 53.9 ± 1.0 nm. It can be seen, by comparing these results with those reported in table 3.1, that all three parameters affect the thickness by increasing it.

In figure 3.5, chronoamperometry suggests a correlation between thickness and current, and that oxygen seems to have a greater effect than the electrolyte. The CA curves for the samples eT and T present an uncommon behavior which is still unexplained, but that is reproducible.

3.3.4 Importance of shape

Another aspect that has to be taken into account when measuring the thickness of the electrodeposited layer is related to the shape of the sample. It is known from the electroplating practice that the deposited layers are thicker at sharp corners and edges, and thinner in recessed areas due to the inhomogeneous distribution of the electric field. In the case of electrochemical sol-gel deposition for the same reason the reduction reactions should not occur homogeneously on the surface, generating a strong pH gradient and, as a consequence, a variation of the thickness

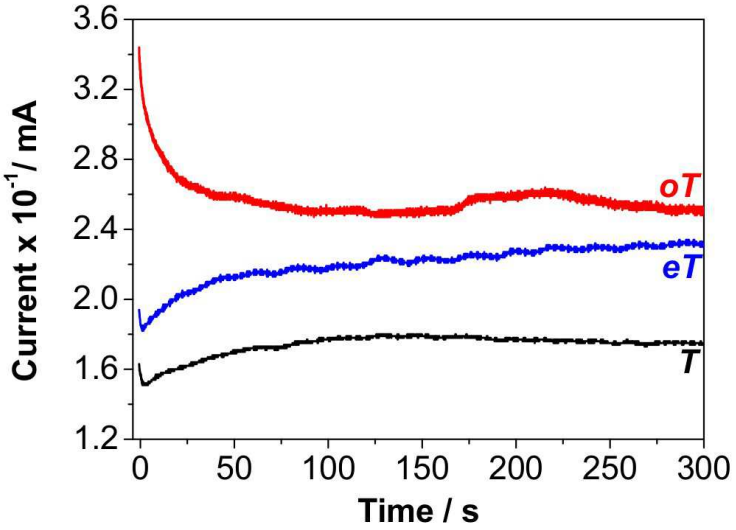

Figure 3.5: Chronoamperometry of samples T, eT, oT. Applied potential: -0.9 V vs SCE. Deposition time: 300 s

from the edge to the center of the sample.

To estimate this effect a stainless steel sample was coated using a solution characterized by $C = 50$, $R = 6$ and $H = 0.01$, at -0.7 V for 5 min at 27°C. Figure 3.6 on the facing page shows the Environmental Scanning Electron Microscope (ESEM) image of the layer at the edge where the thickness is about 5 μm. The thickness was also measured at the center of the sample and in between the edge and the center by ellipsometry, obtaining values of 90 and 120 nm, respectively.

To minimize the edge effect all the samples used for this study were masked at the edges with a teflon tape, leaving an exposed area of about 40 mm^2.
The use of teflon tape reduced the edge effect, even if it was not completely eliminated. The morphology of the central area of a coated sample can be seen in the ESEM image taken using backscattered electrons in figure 3.7 on page 40.

Figure 3.8 shows the thickness of a stainless steel plate (30 mm × 30 mm × 1 mm) after the electrodeposition process, without the masked edge. As we can observe the deposition is not homogeneous. A thicker broken film is formed on the cusp-shaped edge, moving three millimeters from the edge, a thickness of 588 nm was measured. As the distance from the cusp increases, the thickness decreases, taking into account that the thickness of the dipping layer is around 132 nm.

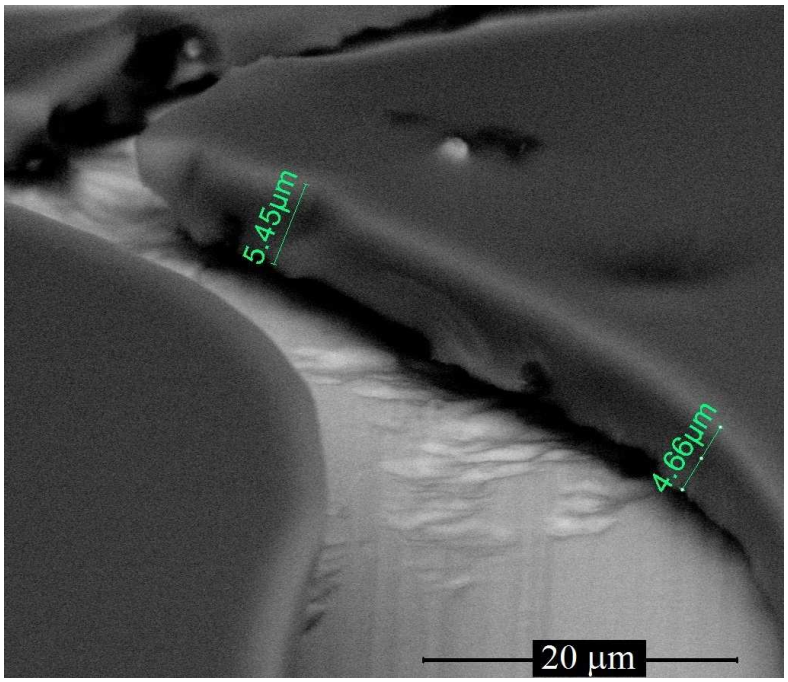

Figure 3.6: ESEM image of SiO_2 film deposited at -0.7 V vs SCE for 5 min at 27°C. Detail of the edge

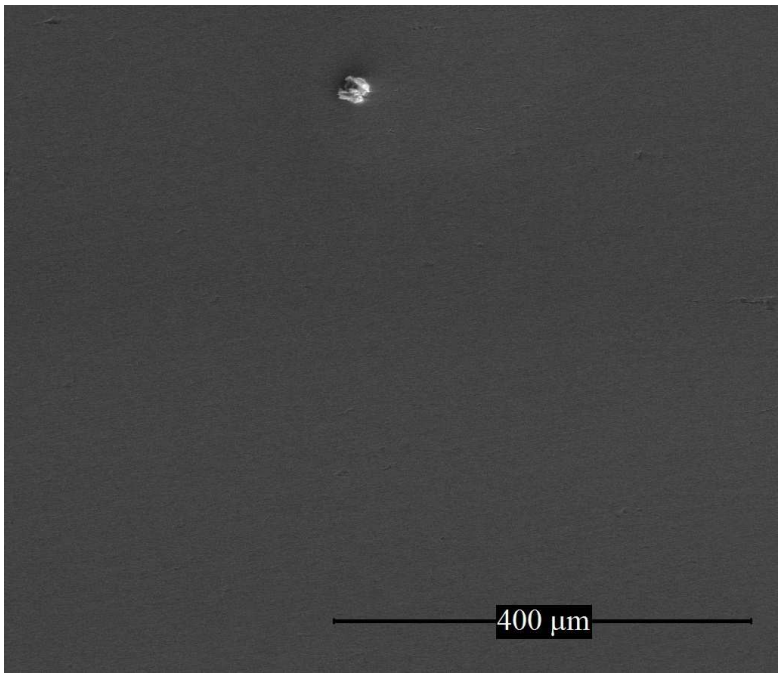

Figure 3.7: ESEM micrographs of SiO_2 film deposited at -0.7 V vs SCE for 2 min at 27°C

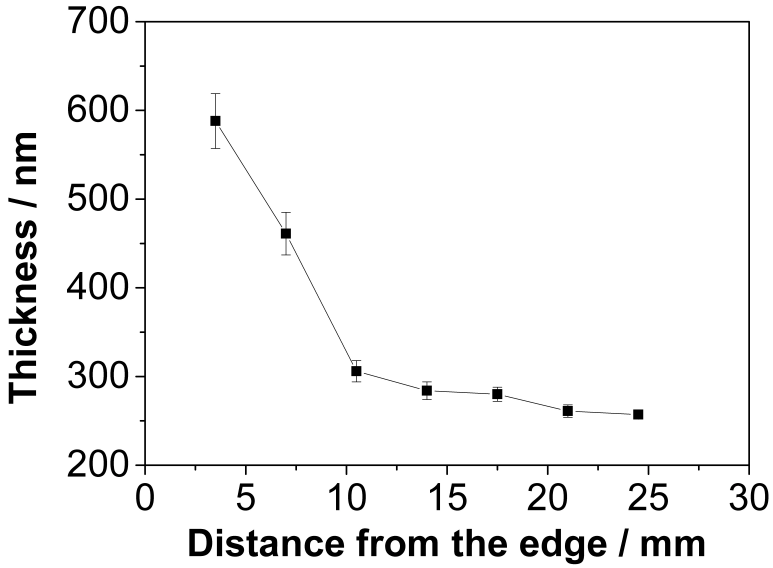

Figure 3.8: Corresponding thickness of an electrodeposited inhomogeneous plate of stainless steel

3.4 Pulsed Potential

With increasing time, the initially acidic sol becomes more and more basic at increasing distances from the surface of the working electrode (due to the diffusion of hydroxyl ions), and hydrolysis and condensation are promoted not only at the surface, but also in the sol producing complex species which add to the surface layer in a non-homogeneous way [16]. Although an exact picture of the process is not available yet, it seems clear that it would be necessary to limit the reactions at the substrate surface by avoiding the enlargement of the "basic zone". Samples obtained by keeping the potential for 15 min showed the complete delamination of the obtained thick layer.

In this paragraph we present a new approach adopted to avoid this unwanted effect. In the pulsed potential method, the time for sol homogenization is given by stopping the production of OH^- with the substrate remaining inside the sol.

The results were published in *The Journal of Physical Chemistry C* [17].

3.4.1 Experimental

Tetraethyl orthosilicate (≥99.0%), Methyl Triethoxysilane (>90%) (MTES) and Ethanol (≥99.8%) were purchased from Sigma Aldrich and used as received. Potassium nitrate (KNO_3) was purchased from Carlo Erba.

The coating solution was prepared by mixing ethanol (31.5 mL), 10 mL of bi-distilled water, 0.5 mL of hydrochloric acid (0.1 M), 6.4 mL of TEOS and 1.63 mL of MTES (70:30 molar ratio) as precursor of silica. The solution was pre-hydrolyzed overnight at room temperature under stirring. Before the deposition, KNO_3 (0.03 M) was mixed using magnetic stirring, until complete dissolution.

The electrodeposition was obtained by using a potentiostat/galvanostat within a three-electrode cylinder cell (diameter: ∼4 cm). The reference electrode was a saturated calomel electrode (SCE) and the counter electrode was a glassy carbon plate (16 mm × 20 mm). The working electrodes were obtained from a stainless steel sheet (AISI 304), protected on one side by a protective removable film. The surface was mirror-like polished and the roughness was the same for all samples. The dimensions of the plates were 30 mm × 30 mm × 1 mm. Teflon was used to mask the edges of the samples during the depositions leaving an exposed circular area of about 200 mm^2. No stirring was applied. After deposition the samples were withdrawn at a low constant speed to minimize the thickness of the layer deposited by dip-coating.The samples were dried at room temperature for at least 24 h before the characterization.

Intermitted duty-cycles were used (figure 3.9 on the following page) between

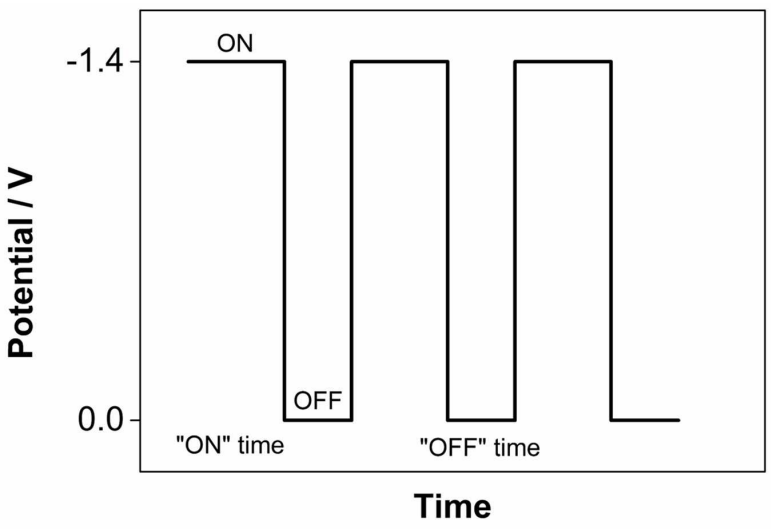

Figure 3.9: Schematic representation of the intermitted duty-cycles used for the pulsed potential experiments

a maximum potential of -1.4 V ("ON") and a minimum of 0 V ("OFF") vs the reference electrode, with a ON time of 4, 5 and 6 s, and a "OFF" time ranging between 2.5 and 7 s with changes of 0.5 s. In all the experiments the total "ON" time was 300 s, i.e. each cycle was repeated from 50 (6 s $\times$ 50 = 300 s) to 75 (4 s $\times$ 75 = 300 s) times.

The thickness was measured by a variable-angle spectroscopic ellipsometer (J. A. Wollam Co., Inc.) at incident angles of 70° and 80°, within a wavelength range of 300-1200 nm. The thickness was fitted using a Cauchy model.

3.4.2 Result and discussion

In this experiment all the three main parameters which allow to modulate the film thickness, *i.e.* the concentration of the precursor in the sol, the applied potential and the total deposition time, were kept constant. However, the deposition time was divided in different numbers of intervals by cycling the potential as described in 3.4.1, changing the "ON" (potential at -1.4 V) and the "OFF" (open circuit, OCP) times.

This procedure favors the neutralization of the hydroxide ions produced at the substrate surface at the beginning of the deposition by the protons in solution (the pH of the sol is equal to 3), when the accumulation of OH^- is still small. Recalling that the diffusion layer is proportional to $(\pi Dt)^{1/2}$, where D is the

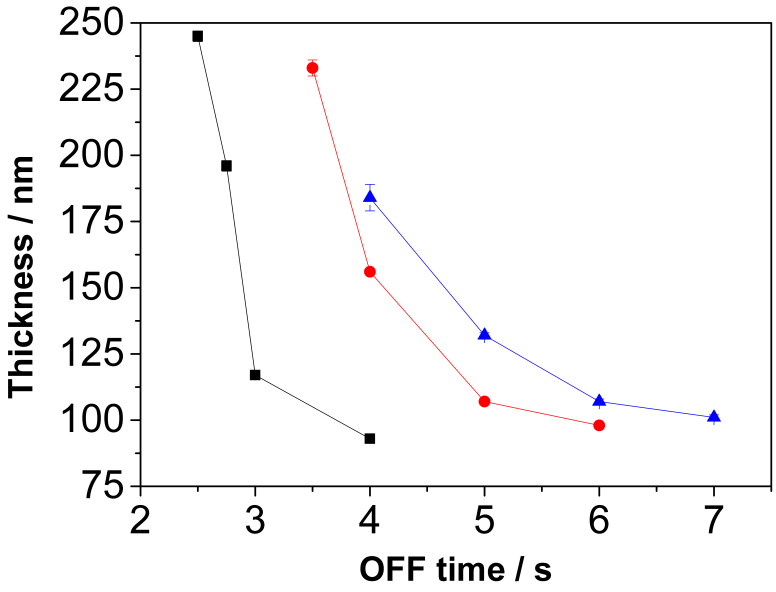

Figure 3.10: Thickness of the film in function of the "OFF" time in the three different cases: number of intervals equal to 75 (black square, 4 s), 60 (red circle, 5 s), 50 (blue triangle, 6 s). Applied potential: -1.4 V. Total deposition time: 300 s

diffusion coefficient (estimated to be $4000\mu m^2/s$) and t the deposition time, after only 5 seconds hydroxide ions are capable of reaching distances of 250 μm [16].

It was observed that setting the potential at -1.4 V, for a deposition time of 300 s (without any interruption) the film exhibited cracks over the entire surface. No cracks were observed, instead, if the total time of 300 s was divided in much shorter intervals. In figure 3.10 three cases are presented. In the first case, the deposition time was divided into 75 intervals of 4 s ("ON" time) each (black square), in the second case the number of intervals was equal to 60, each length being 5 s (red circle), in the last case the time has been divided into 50 intervals of 6 s each (blue triangle). Four different "OFF" times were selected, in such a way to describe a general trend, which is similar in all the three cases.

It may be observed that:

- using an equal number of intervals, the thickness increases with decreasing the "OFF" time;
- using an equal "OFF" time, the thickness increases with decreasing the number of intervals.

These results are consistent with the diffusion of OH^- ions away from the

surface and their neutralization in the acidic sol. At longer "OFF" times the neutralization of the local basic environment is more effective, and the deposition is always starting from an initial pH condition. At shorter "OFF" times the hydroxyl concentration increases at the surface because of accumulation at each "ON" step, increasing the rate of layer growth.
The same happens with increasing the "ON" time (or reduction of the number of intervals).

The quality of the coating was quite good using this approach.

3.5 Conclusions

Silica thin films were deposited by the electro-assisted deposition, based on the electrochemically generation of hydroxide ions, with the aim to test different parameters involved in the process. Submicron thicknesses were measured with ellipsometry by using Cauchy's model. The influence of potential and time were studied. According to the literature the thickness grows with the increase of both, though any asymptote with deposition time was not identified.

Solutions with different C, R and H ratios were tested, and the thickness was found to increase with both C and H. The effect of R on the thickness could not be checked, as films cracked at R = 10.

Temperature seems an important factor in the electrodeposition process, from the point of view of thickness, thickness uniformity and integrity.

The presence of oxygen and KNO_3 in solution influences the amount of hydroxide ions at the interface, thus increasing the thickness.

In the second part of experiments a pulsed potential is applied to the sample always immersed in the sol.

The thickness is increased in several steps, by cycling the potential between a maximum value of -1.4 V ("ON") and a minimum value of 0 V ("OFF"). It was demonstrated that the thickness may be increased by decreasing the "OFF" time, at constant number of intervals, or by decreasing the number of intervals at constant "OFF" time.

Apart from the specific results obtained in this study, which must be considered as preliminary, it seems important to stress the fact that a systematic approach was adopted, trying to analyze the different factors that make experimentation difficult, looking for possible solutions, and putting the basis for a more complete and analytic investigation.

Bibliography

[1] Deepa, P.; Kanungo, M.; Claycomb, G.; Sherwood, P.M.A.; Collinon, M.M. Electrochemically deposited sol-gel derived silicate films as a viable alternative in thin-film deisgn. Anal. Chem. 2003, 75, 5399-5405

[2] Liu, L.; Hu, J.-M.; Zhang, J.-Q.; Chao, C.-N. Improving the formation and protective properties of silane films by the combined use of electrodeposition and nanoparticles incorporation. Electrochim. Acta 2006, 52, 538-45

[3] Giordano, G.; Durante, C.; Gennaro, A.; Guglielmi, M. Electrochemical Deposition of Silica Sol-Gel Films on Stainless Steel. Preliminary Analysis of Key Variables. J. Sol-Gel Sci. Technol. 2015, 76, 233-240

[4] Shacham, R.; Avnir, D.; Mandler, D. Electrodeposition of methylated sol-gel films on conducting surfaces. Adv. Mater. 1999, 11, 384-388

[5] Shacham, R.; Avnir, D.; Mandler, D. Eletrodeposition of dye-doped titania thin films. J. Sol-Gel Sci. Technol. 2004, 31, 329-334

[6] Shacham, R.; Mandler, D.; Avnir, D. Electrochemically induced sol-gel deposition of zirconia thin films. Chem. Eur. J. 2004, 10, 1936-43

[7] Farghaly, A.A.; Collinson, M.M. Electroassisted codeposition of sol-gel derived silica nanocomposite directs thefabrication ofcoral-like nanostructured porousgold. Langmuir 2014, 30, 5276-86

[8] Vegliò, F. La programmazione della sperimentazione nello sviluppo dei processi chimici. Ratio Math. 9, 37-53

[9] Leventis, N. Electrochemically assisted sol-gel process for the syntesis of polysiloxane films incorporating phenothiazine dyesanalogous to methylene blue. Structure and ion-transport properties of the films via spectroscopic and electrochemical characterization. Chem. Mater. 1997, 9, 2621-31

[10] Lyons, M.E.G. Electroactive polymer electrochemistry. Part 1: fundamentals. Springer US, Boston, 1994, 487

[11] Mendoza-Huizar, L.H.; Robles, J.; Palomar-Pardavé, M. Nucleation and growth of cobalt onto different substrates. Part II. The upd-opd transition onto a gold electrode. J. Electroanal. Chem. 2003, 535, 39-45

[12] Okner, R.; Favaro, G.; Radko, A.; Domb, A.J.; Mandler, D. Electrochemical codepositionn of sol-gel films on stainless steel: controllig the chemical and physical coating properties of biomedical implants. Phys. Chem. Chem. Phys. 2010, 12, 15265-73

[13] Brinker, C.J.; Schere, G.W. Sol-Gel science: the physical and chemistry of sol-gel processing. Academic Press Inc, London, 1990

[14] Collinson, M.M.; Higgins, D.A.; Kommidi, R.; Campbell-Rance, D. Electrodeposited silicate films: importance of supporting electrolyte. Anal. Chem. 2008, 80, 651-656

[15] Ding, S.; Liu, L.; Hu, J.; Zhang, J.; Cao, C. Nitrate ions as cathodic alkalization promoters for electro-assisted deposition of sol-gel thin films. Scr. Mater. 2008, 59, 297-300

[16] Walcarius, A.; Sibottier, E.; Etienne, M.; Ghanbaja, J. Electrochemically assisted self-assembly of mesoporous silica thin films. Nat. Mater. 2007, 6, 602-608

[17] Giordano, G.; Durante, C.; Gennaro, A.; Guglielmi, M. Multilayer deposition of silica sol-gel films by electrochemical assisted techniques. J. Phys. Chem. C 2016, 120, 28820-24

Chapter 4

Silica 3D Growth

4.1 Introduction

This chapter analyzes the deposition of silica by means of chronoamperometric data. The starting solution consists of a mixture of water, ethanol, hydrochloric acid, potassium nitrate and tetraethyl orthosilicate.

As explained in the first capter, when a sufficient negative potential is applied, hydroxide ions are generated only in the proximity of the electrode surface along with H_2, thanks to the reduction reactions of protons and water according to the reactions

$$H_3O^+ + 2e^- \rightarrow H_2 + OH^- \tag{4.1}$$

$$2H_2O + 2e^- \rightarrow H_2 + 2OH^- \tag{4.2}$$

Alternatively, in the presence of nitrate the reduction of NO_3^- to ammonia involves the concomitant formation of OH^-.

$$NO_3^- + 6H_2O + 8e^- \rightarrow NH_3 + 9OH^- \tag{4.3}$$

In both cases the consequence is the raising of the local pH, while the bulk solution remains acidic. The sol-gel formation is based upon a condensation reaction, which can evolve according two different ways:

$$\equiv Si - OR + HO - Si \equiv \quad \rightarrow \quad \equiv Si - O - Si \equiv + ROH \tag{4.4}$$

$$\equiv Si - OH + HO - Si \equiv \quad \rightarrow \quad \equiv Si - O - Si \equiv + H_2O \tag{4.5}$$

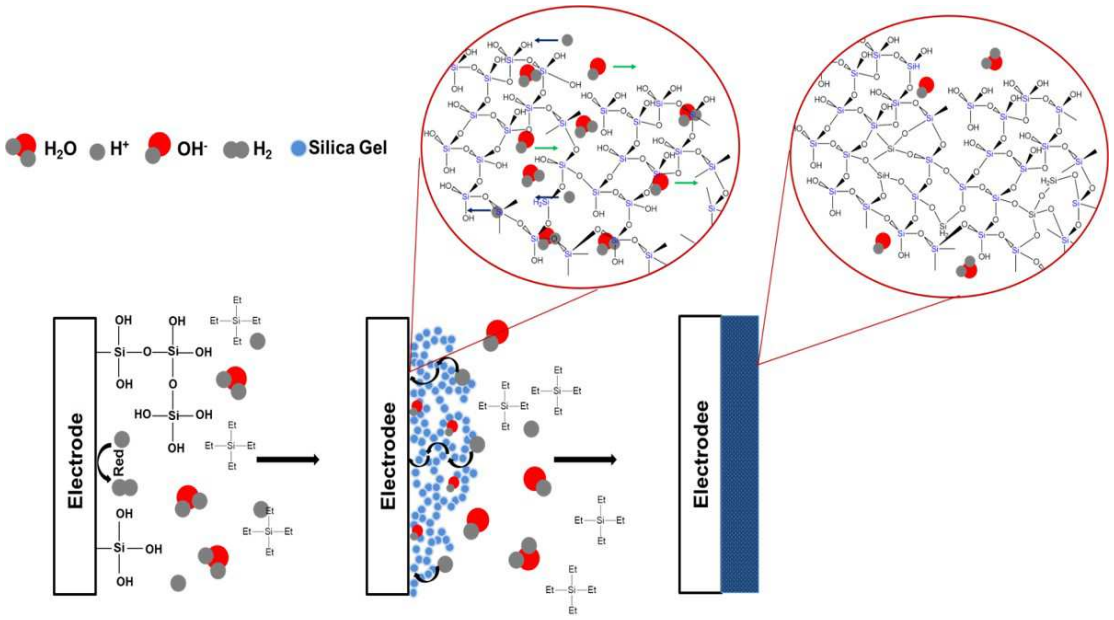

Figure 4.1: Pictorial view of electroactivated silica deposition mechanism

Where, in the present case, R is an ethyl orthosilicate, reactions 4.4 and 4.5 are catalyzed in both acidic and basic environments, forming 3D network on the substrate. However, different pH lead to different structures; in particular, denser structures are created in a basic environment. At this point, it is easy to understand that the raising of the pH near the electrode leads to the formation of a dense thin films. A schematic representation of the process is shown in figure 4.1

Despite the resulting films may be very homogeneous and uniform, in the previous chapter we pointed out some critical aspects, stressing the fact that there is a need for more basic knowledge to better understand the potentiality of the deposition method, such as understanding the current-time behavior [1].

Aim of this chapter is to highlight the strong relationship between standard galvanic deposition of metals and electrochemically assisted deposition of sol-gel. In order to analyze the current transients, the applied potential and the concentration of precursor were changed, keeping starting solution and potential constant, respectively. Furthermore, the thickness in function of time was evaluated by using an ellipsometer. It was found that the silica film grows linearly with time, reaching a thickness of 15 μm after 15 minutes. The results were published in *Journal of Electroanalytical Chemistry* [2].

4.2 Experimental

Reagents and apparatus Tetraethyl orthosilicate (≥99.0%), HCl (≥37%) and ethanol (≥99.8%) were purchased from Sigma Aldrich and used as received. Potassium Nitrate (>98%) was purchased from Carlo Erba.

The starting solutions for electrodeposition were prepared by mixing, in the following order, ethanol, distilled water, hydrochloric acid and TEOS as precursor for silica. The solutions were pre-hydrolyzed for 1 h at room temperature under stirring. Before the deposition, suitable amount of KNO_3 was added to the solution for obtaining a concentration of 0.03 M KNO_3 and was mixed using magnetic stirring, until complete dissolution.

The electrochemical deposition was accomplished by using a potentiostat galvanostat Bio-Logic SP-300 in a three-electrode electrochemical cylinder cell (diameter: ∼4 cm). Saturated calomel electrode (SCE) and glassy carbon plate (1.6 cm × 2.0 cm) were employed as reference and counter electrode, respectively. The working electrodes were obtained from a stainless steel sheet (AISI 304), protected on one side by a protective removable Teflon tape. The surface was mirror-like polished and the roughness was the same for all samples. The dimensions of the plates were 30 mm × 30 mm × 1 mm.

Electrochemical analyses were carried out on an exposed area of approximately 7 mm^2, which was obtained by applying a mask of adhesive Teflon. Teflon was used also for masking the edges of the samples during the depositions, where a circular area of about 200 mm^2 was let exposed. Deposition was accomplished in thermostated and unperturbed solution.

Characterization After silica deposition, the samples were withdrawn by a dip coater with a withdrawal constant rate of ca. 100 μm/s, then they were dried at room temperature for at least 24h before each characterization.

The surface morphology and the composition of the films were investigated in low vacuum by Scanning Electron Microscopy (SEM, Philips XL30), while the thickness was measured by a variable-angle spectroscopic ellipsometer (J. A. Wollam Co., Inc.) at incident angles of 70°, 75° and 80°, within a wavelength range of 300-1200 nm. The thickness was fitted using a Cauchy model. Cyclic voltammetry (CV) and chronoamperometry (CA) were recorded in the same three electrode configuration employed for electro-assisted deposition.

Table 4.1: Starting solution composition. Samples and solution labels refer to the SiO_2 concentration expressed in g/L

	Water (mL)	HCl (0.1 M) (mL)	Ethanol (mL)	TEOS (mL)	KNO_3 (g)
$C30$	10	0.5	34.00	5.5	0.152
$C50$	10	0.5	30.35	9.15	0.152
$C70$	10	0.5	26.69	12.81	0.152
$C110$	10	0.5	19.37	20.13	0.152

4.3 Results and Discussion

In classical sol-gel deposition, hydrolysis or condensation of silicon alkoxides occur under acidic or alkaline conditions, respectively. Since all species are hydrolyzed at an early stage of the reaction, they can condense to form small oligomeric species (clusters) with reactive Si-OH groups. Under these conditions, reactions at terminal silicon atoms are favored. This results in polymer-like gels; that is, small clusters undergo condensation reactions with each other to give a polymer-like network with small pores. The electrodeposition of sol-gel is based on the local electrochemical generation of OH^- or H_3O^+ to trigger the rate of sol-gel reactions; this involves that other parameters must be taken into account, including cell geometry, working potential, ion conductivity, etc.

In particular, the choice of starting solution is a critical point for the electrodeposition method, since it is known that reagents play different roles during deposition. In the case of basic catalysis, the hydrolysis is performed in a fairly acidic electrolyte and the polycondensation is promoted at the electrolyte-electrode surface by the local increase of OH^- concentration as the result of H_3O^+ and/or H_2O reduction according to equations 4.1 and 4.2. However, H_3O^+ and H_2O not only participate in the reduction reaction at the working electrode surface, but they are key variable in the sol-gel process; in fact water accelerates polycondensation of silica gel and H_3O^+ permits a faster hydrolysis of alkoxide groups.

Therefore, H_3O^+ concentration must be kept as low as possible, and as a consequence an electrolyte is necessary in order to attenuate the ohmic drop in solution. In particular, when KNO_3 is employed, the supporting electrolyte cannot be considered completely innocent since it favors the generation of hydroxide groups at the working electrode surface (equation 4.3) [3], and it reduces the gelification time [4]. In the present investigation the amount of water, hydrochloric acid and supporting electrolyte were kept fixed for all the experiments, whereas TEOS amount was varied. Experimental conditions are summarized in table 4.1.

Before electrodeposition cyclic voltammetry was collected using a blank solution, without TEOS precursor, obtained by mixing 10 mL H_2O + 0.5 mL HCl (0.1 M) + 39.5 mL of EtOH, (figure 4.2A).The corresponding CV clearly resembles a resistant behavior (figure 4.2A, curve a) as a result of a too high ohmic drop for the low ion conductivity (pH = 3). To prevent ohmic drop, a fixed amount of electrolyte was considered; in particular $LiClO_4$ and KNO_3 were tested and in both case a clear shift of H_2 evolution was observed, for KNO_3 even more evident (figure 4.2A, curve c). A reduction peak is also present at -1.04 and -1.09 V vs SCE in both electrolytes, whose nature is not clearly appointable.

Typically electrochemical assisted deposition experiments were carried out at a fixed applied potential in a H_2O/EtOH/HCl/KNO_3/TEOS mixture. The average thickness of deposited silica layer from $C30$ solution (table 4.1 on the facing page) was measured, after a potentiostatic treatment at E_{app} = -1.2 V vs. SCE for 900 s, by using the scanning electrochemical microscopy (figure 4.2B). The film was 15 μm thick and showed cracks on the whole surface. The formation of cracks is due to the evaporation of the solvent, which leads to strong tensions (figure 4.2B). In order to monitor the film growth, thickness was analyzed in a deep only in the initial stages of the process since, according to Walcarius et al. [5], silica layer breaks down when exceeding a thickness of 400 nm. Therefore, several experiments were arranged and stopped at 7, 15, 30, 60 s.

It must be stressed that, while the electrode is extracted from the batch, a layer is deposited by dip coating on the electrodeposited layer. This can be reduced by using a very low withdrawal rate, but cannot be avoided. Therefore, in order to remove the layer obtained by the unavoidable dipping contribution, the samples were rinsed in pure ethanol after deposition for few seconds. Figure 4.2C shows that the silica thickness grows linearly with time. It is important to underline that the sample deposited in 7 seconds did not present a completely covered surface, hence the thickness measured is referred to the coated area. Moreover it is important to underline that no crystalline phases were observed, but only amorphous silica was deposited.

In figure 4.3A and B the effect of the applied potential and of TEOS concentration were investigated by chronoamperometry. Figure 4.3A reports the current transients recorded with a TEOS concentration of 30 g/L at different applied potentials. It is evident that for E_{app} > -1.05 V vs. SCE, the current decays almost exponentially to a constant value, similarly to what expected from a diffusion controlled process following the Cottrell equation for semi-infinite diffusion. However, for more negative potentials, current shows a more complex behavior, since at first current decreases till reaching a minimum point after about 4 s, and it subsequently increases with different slopes in the time range 4 $\div$ 10 s and 10 s

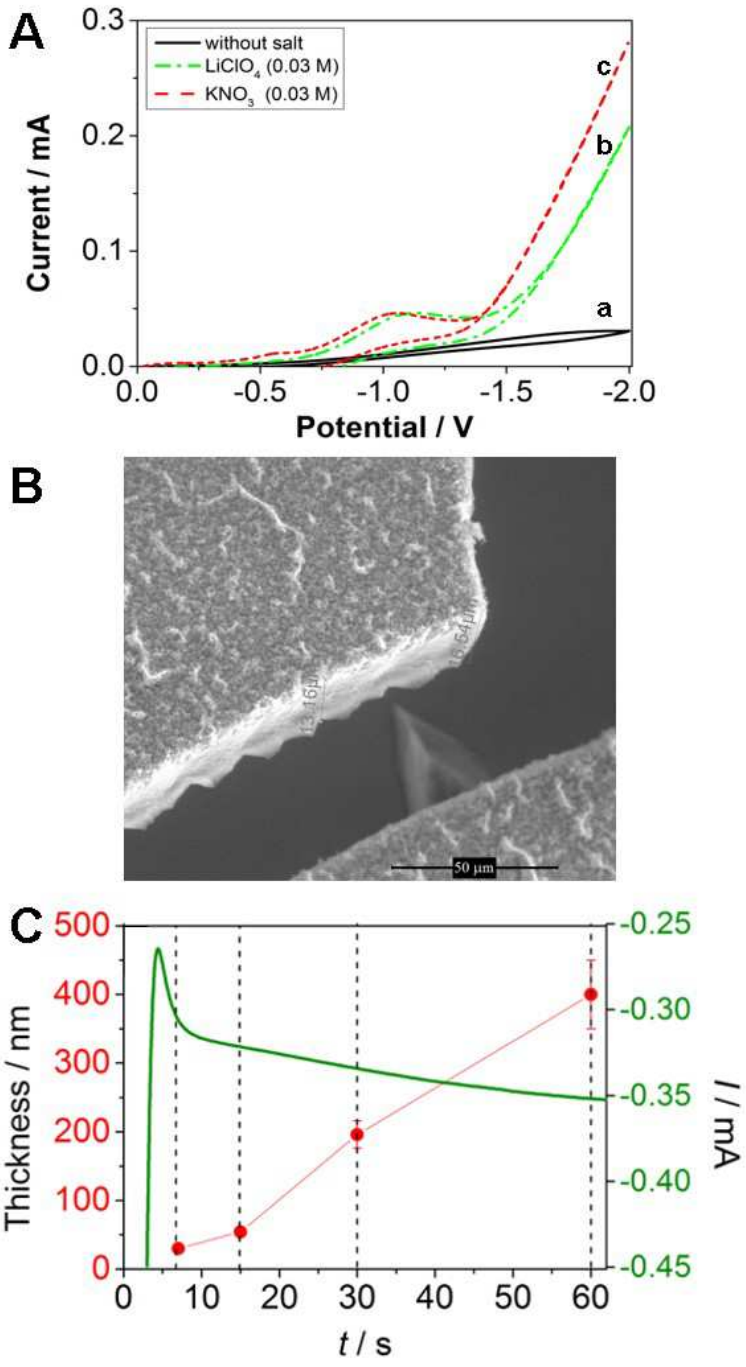

Figure 4.2: Cyclic Voltammetry at stainless steel electrode, in a H_2O/EtOH/HCl mixture with "a" KNO_3 0.03 M; "b" $LiClO_4$ 0.03 M and "c" without supporting electrolyte. $\nu = 50$ mV/s (A). SEM image of silica film obtained after a deposition of 900 s at E_{app} = -1.2 V vs. SCE in solution $C30$: crack detail (B). Thickness of electrodeposited layer as function of time and the corresponding current transient recorded at E_{app} = -1.2 V vs. SCE, in solution $C30$ (C).

to ∞, until a constant value is reached (figure 4.3A). Similar current transients were found in figure 3.3. In those experiments, protons concentration was ranged between 0.03 M and 0.05 M and no electrolyte was added; the current peak was more broad and placed at longer times (about after 20 seconds).

Current transients recorded at E_{app} = -1.2 V vs SCE but with an increased TEOS concentration result even more complicate (figure 4.3B) and resemble the typical two-dimensional cylindrical growth and progressive nucleation current transient. Taking the $C70$ sample as reference, the current transient can be divided into three time intervals (figure 4.4A). At the beginning, the current decays as in the case of double layer charging current. In the second interval the current increases, whereas in the third interval there are an initial increase in the current, a maximum, and a decrease in the current. In particular, $C50$, $C70$ and $C110$ transients clearly show a maximum at about 10 s after which the current decreases again (figure 4.3B). It is worth noting that depending on TEOS concentration, current shows damped oscillations till a constant value after 100 s, 150 s and 300 s for $C50$, $C70$ and $C110$, respectively (figure 4.3C).

In the case of electrodeposition of conducting materials, current transients depend on the nucleation and on the growth of either independent or overlapping nuclei. Figure 4.4C shows the dimensionless current transient for 3D nucleation with diffusion-controlled growth for progressive nucleation [6], which is derived by the theory according to the formula:

$$\frac{I}{I_m} = \frac{A}{\left(\frac{t}{t_m}\right)^{0.5}}\left[1 - \exp\left(-B\left(\frac{t}{t_m}\right)^2\right)\right] \tag{4.6}$$

Where A and B are constants, whereas I_m is the maximum deposition current, which occurs at time, t_m. The two major features affecting the current transient shape is the deposition current (I_{dep}) due to nucleation and growth of metal nuclei and the overlap current (I_{over}), which accounts for the two opposing effects: independent nuclei growth and nuclei overlap, that results in a point of relative maximum.

A similar equation can be derived for instantaneous nucleation model [6]

$$\frac{I}{I_m} = \frac{C}{\left(\frac{t}{t_m}\right)^{0.5}}\left[1 - \exp\left(-D\left(\frac{t}{t_m}\right)\right)\right] \tag{4.7}$$

It is worth noting that besides the parameters A, B, C and D, the two models differ for the exponentials in the second term that switchs from 1 to 2 passing from instantaneous to progressive nucleation. It is evident the parallelism between the dimensionless current transients for electrochemical deposition (figure

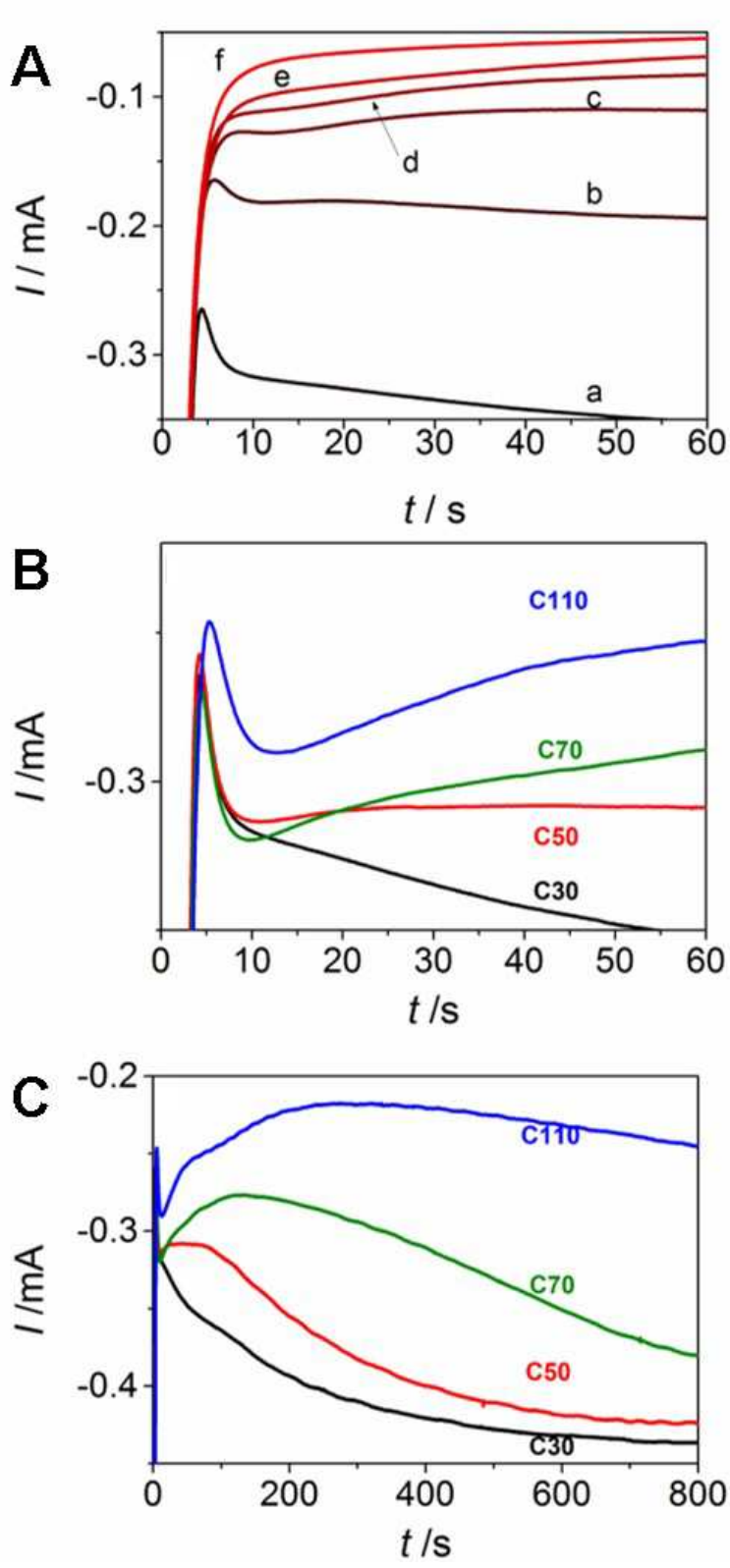

Figure 4.3: Current transients at different applied potential. (a) -1.2 V, (b) -1.1 V, (c) -1.05 V, (d) -1.03 V, (e) -1.01 V, (f) -1.0 V. Starting solution: *C*30 (A). Current transients at different TEOS concentration: (1) 30 g/L, (2) 50 g/L, (3) 70 g/L, (4) 110 g/L. Applied potential: -1.2 V (B). Current transient curves in an extended time window (C).

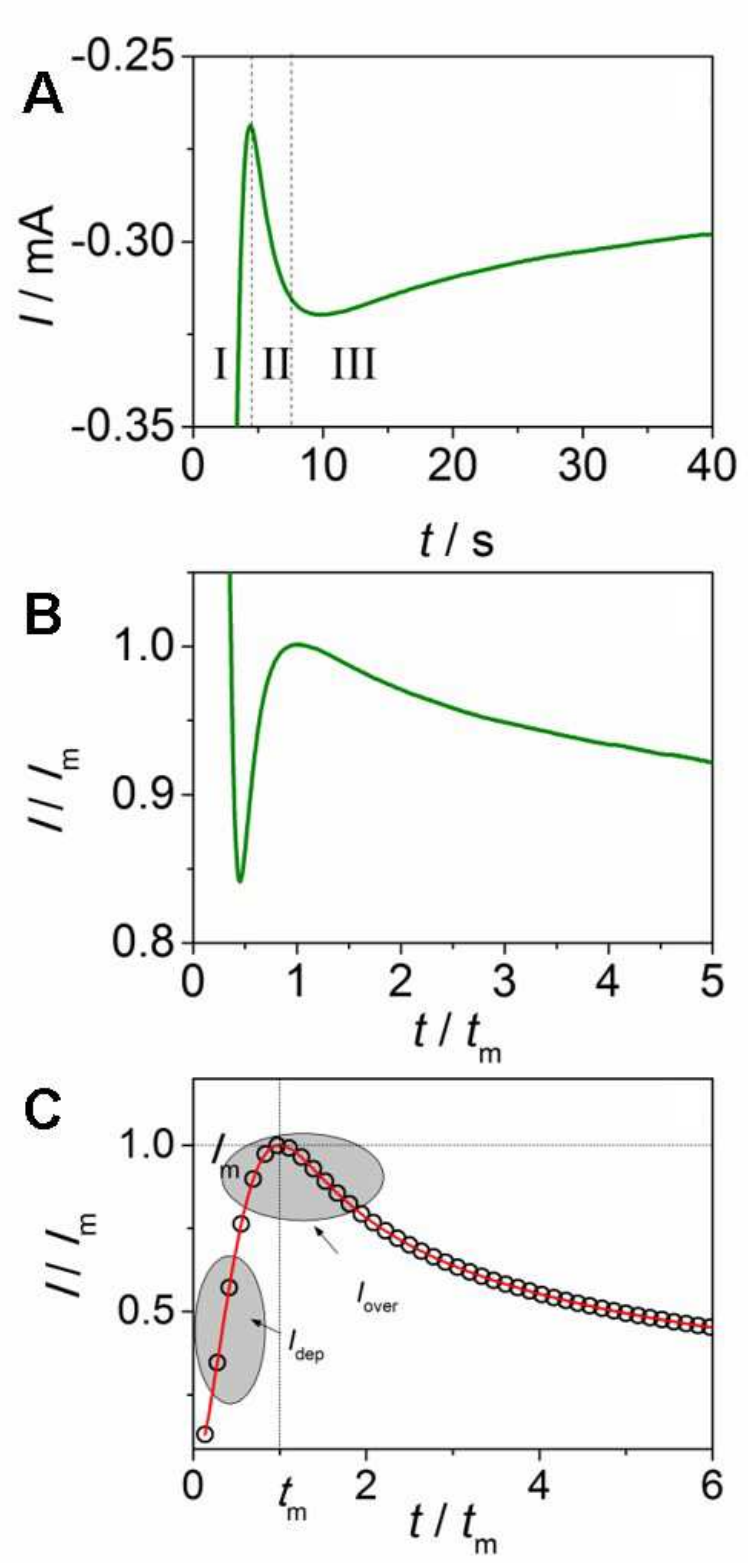

Figure 4.4: Close view of current transient for electro-assisted deposition of $C70$ (A). Dimensionless current transient for electro-assisted deposition of $C70$ (B). Dimensionless current transient for 3D nucleation with diffusion-controlled growth for progressive nucleation (C).

4.4B) and the transient calculated from metal deposition theory (figure 4.4C). It is worth noting that whether 2D and 3D growths of conductive materials like polypyrrole [7], polyaniline [8, 9], silicon [10], silver [11–13] are a well-known processes, this is the first time that the 3D-like-growth of silica-gel was observed using chronoamperometry.

However, the two deposition processes differ for two substantial properties: (i) deposited silica is not an electronic conductor but an ionic conductor. In fact, the ionic conductivity of silica surfaces depends on the concentration of Si-OH groups and on the adsorbed water or other polar molecules [14]. Therefore, the charge carriers are protons, and the electrochemical process must occurs exclusively at the accessible electrode surface. (ii) The only redox reaction of interest at the electrode surface is the H_3O^+ reduction, since TEOS is not redox active. Therefore, there is not electron transfer between silica precursors and the stainless steel electrode. However, TEOS condensation is a consecutive reaction of H_3O^+ reduction, which affords the activating specie OH^- electrogenerated at electrode surface. Therefore, nucleation and growth of silica nuclei depends directly to H_3O^+ reduction and therefore to the observed current transient.

Bearing this in mind, we have rationalized the three different zone in the current transient in figure 4.4A according to the following sequence.

- In the first stage H_3O^+ is reduced according to the reaction 4.1; the current decreases due to depletion of H_3O^+ in the diffusion layer, at the same time the electrogenerated OH^- trigger TEOS condensation and the result is the nucleation of silica-gel nuclei over the electrode surface. The local basic environmental favors the reaction at central silicon atoms of oligomer units, that affords a network of big particle and large pores (colloidal gels) (figure 4.1);

- In the second stage, current rises due to an increased availability of protons nearby the electrode surface i.e. inside the hydrated silica-gel layer. In fact, the number of protons increases at the increasing of the silica nuclei formation, since the surface of silica-gel is covered by Si-OH groups, which act as proton donors. In this way protons can migrate through the porous silica gel structure and by hopping along neighboring $Si\text{-}O^-$ sites to the electrode surface, where they react. It must to be stressed that at this stage the electrode surface is not completely covered by silica gel, but where it is present, it is only few nm thick, as reported previously in the paper. In the same way, the electrogenerated OH^- are driven out the diffused silica gel trough pores by the electric field, catalyzing the condensation of fresh TEOS in the proximity of silica-gel/electrolyte interphase. The depletion of

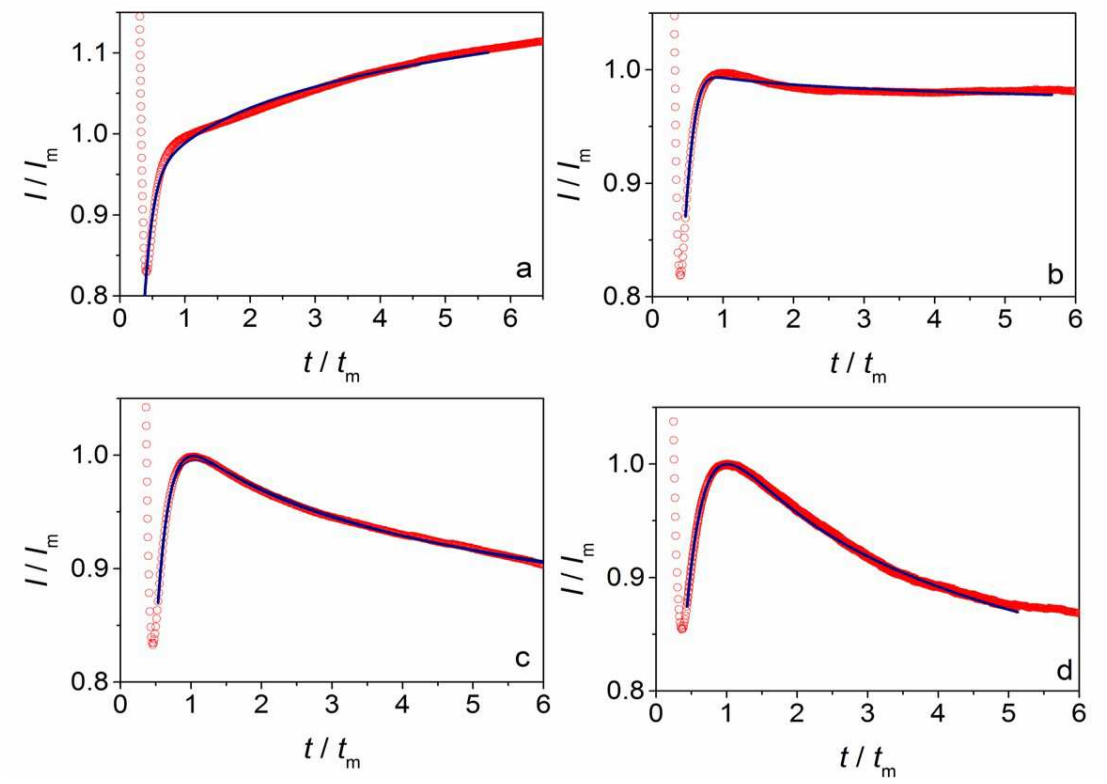

Figure 4.5: Dimensionless current transient plots comparing the experimental data to the fitting with a pseudo 3-D nucleation formula reported in equation 4.7. Red circles: experimental data; black lines simulated current transients.

protons inside the silica gel layer is compensated by the transport of proton from the bulk solution (figure 4.1). The migration of protons and hydroxide anions assure the ionic conductivity inside the silica-gel layer, an aspect that was well documentated by Anderson and Parks [14] and other [15–18];

- In the third stage current transient reach a maximum point and then decreases due to the opposite effect of the increasing number of Si-OH group nearby the electrode surface and the slow migration of protons from bulk solution and inside a thicker silica-gel layer. In fact, the conductivity of the silica-gel decreases when the volume fraction of the isolating phase (Si-O-Si) increases [16].

Table 4.2: Fitting parameters for current transient in figure 4.5 according to equation 4.8

	A	B	C	$p \times 10^{-2}$	q	R^2
$C30$	0.989 ± 0.001	1.0 ± 0.1	8.5 ± 0.4	6.17 ± 0.05	1.52 ± 0.04	0.993
$C50$	2.1 ± 0.1	0.4 ± 0.2	8.3 ± 0.3	0.91 ± 0.02	1.4 ± 0.2	0.959
$C70$	2.2 ± 0.3	0.45 ± 0.06	5.2 ± 0.1	6.10 ± 0.02	1.14 ± 0.05	0.998
$C110$	1.07 ± 0.07	0.96 ± 0.06	3.63 ± 0.06	10.26 ± 0.03	1.02 ± 0.03	0.998

4.3.1 Data fitting

The dimensionless expressions of the current transients for electroactivated silica deposition at E_{app} = -1.2 V vs. SCE and at different TEOS concentration are reported in figure 4.5.

The dimensionless current transients were tentatively compared with theoretical expression for progressive nucleation given in equation 4.6, however, even though the dimensionless current transients were similar in shape at least for $C70$ and $C110$ to the theoretical transients, they differ in magnitude. The heavy mismatch between theoretical and experimental points confirms that electrochemical deposition can not be fully analyzed in the framework of classical nucleation and growth theory [6]. In fact, according to the model proposed in the previous paragraph, proton migration inside the silica hydrated layer must be taken in account. Figure 4.5 on the previous page reports also the dimensionless current transients fitted with an empirical expression (equation 4.8) similar in the form to the theoretical one (equation 4.6).

$$\frac{I}{I_m} = \frac{A}{\left(\frac{t}{t_m}\right)^p}\left[B - \exp\left(-C\left(\frac{t}{t_m}\right)^q\right)\right] \tag{4.8}$$

A good matching between experimental points and the fitting function was found without constraining the coefficients A, B, C and the exponentials p and q. Fitting results are resumed in table 4.2 for sake of comparison. The total volume of the solution has been kept constant and equal to 50 mL. A comparison between the theoretical model for progressive nucleation (equation 4.6) and the empirical equation employed for fitting the experimental data highlights that the two model differ substantially, especially for the exponential terms, since p and q varies in the range $0.06 \div 0.1$ and $1.5 \div 1$ with respect to 0.5 and 2 of the theoretical model. The two terms of the equation prevail at different deposition time; in particular the first term prevail for $t > t_m$, whereas the second term, which account for the type of nucleation, prevails for $t < t_m$. Therefore since q was found to range

between $1 < q < 1.5$, this could be an evidence for a mechanism switching from a progressive nucleation ($q = 2$) to an instantaneous nucleation ($q = 1$) at the increasing of TEOS concentration.

4.4 Conclusions

Using chronoamperometry a novel aspect of electrochemical sol-gel deposition was studied. A pseudo 3D-like growth of silica was investigated on stainless steel in a standard three-electrode cell. Changing the potential and the starting solution, current-time behavior was marked out and unexpectedly we found that, at least qualitatively, there is a fairly agreement with the nucleation and growth theory for electrodeposition, in fact, three different zone were observed. Bearing in mind that the only redox reaction at the electrode surface is the H_3O^+ reduction, we rationalized the current transient according to the availability of H_3O^+ close to the electrode surface and the migration of H_3O^+ through the porous silica gel structure along neighboring Si-O^- sites to the electrode surface. The current transients we also fitted with an empirical formula, which has highlighted the mismatching with respect the preogressive nucleation and growth theory.

Bibliography

[1] Giordano, G.; Durante, C.; Gennaro, A.; Guglielmi, M. Electrochemical Deposition of Silica Sol-Gel Films on Stainless Steel. Preliminary Analysis of Key Variables. J. Sol-Gel Sci. Technol. 2015, 76, 233-240

[2] Giordano, G.; Durante, C.; Gennaro, A.; Guglielmi, M. Electrochemical 3D-growth of amorphous silica gel. J. Electroanal. Chem. 2017, 784, 153-158

[3] Collinson, M.M.; Higgins, D.A.; Kommidi, R.; Campbell-Rance, D. Electrodeposited silicate films: importance of supporting electrolyte. Anal. Chem. 2008, 80, 651-656

[4] Brinker, C.J.; Schere, G.W. Hydrolysis and condensation II, sol-gel Sci. Phys. Chem. Sol-Gel Process, Elsevier 1990, 96-233

[5] Walcarius, A.; Sibottier, E.; Etienne, M.; Ghanbaja, J. Electrochemically assisted self-assembly of mesoporous silica thin films. Nat. Mater. 2007, 6, 602-608

[6] Scharifker, B.R.; Monstany, J. Three-dimensional nucleation with diffusion controlled growth, J. Electroanal. Chem. 1984, 177, 13-23

[7] Asavapiriyanont, S.; Chandler, G.K.; Gunawardena, G.A.; Pletcher, D. The electrodeposition of polypyrrole films from aqueous solutions, J. Electroanal. Chem. 1984, 117, 229-244

[8] Córdova, R.; Del Valle, M.A.; Arratia, A.; Gómez, H.; Scherebler, R. Effect of anions on the nucleation and growth mechanissm of polyaniline, J. Electroanal. Chem. 1994, 377, 75-83

[9] Komsiyska, L.; Tsakova, V.; Staikov, G. Electrochemical formation and properties of thin polyaniline films on Au(111) and p-Si(111), Appl. Phys. 2007, 87, 405-409

[10] Bieber, A.L.; Massot, L.; Gibilaro, M.; Cassayre, L.; Taxil, P.; Chamelot, P. Silicon electrodeposition in molten fluorides, Electrochimica Acta 2012, 65, 282-289

[11] Milchev, A.; Scharifker, B.; Hills, G. A potentiostatic study of the electrochemical nucleation of silver on vitreous carbon, J. Electroanal. Chem. 1982, 132, 277-289

[12] Hills, G.J.; Schiffrin, D.J.; Thompson, J. Electrochemical nucleation from molten salts I. Diffusion controlled electrodeposition of silver from alkali molten nitrates, Electrochimica Acta 1974, 19, 657-670

[13] Toschev, S.; Milchev, A.; Vassileva, E. Electronmicroscope investigation of the initial stages of silver electrodeposition, Electrochimica Acta 1976, 21, 1055-1059

[14] Anderson, J.H.; Parks, G.A. The electrical conductivity of silica gel in the presence of adsorbed water, J. of Phys. Chem. 1968, 72, 3662-3668

[15] Tatsumisago, M.; Honjo, H.; Sakai, Y.; Minami, T. Proton-conducting silica-gel films doped with a variety of electrolytes, Solid State Ionics 1994, 74, 105-108

[16] Wasiucionek, M.; Breiter, M.W. Ionic conductivity of silica gels and dynamic properties of their pore liquids studied by impedance spectroscopy and polarized-light spectrofluorimetry, Solid State Ionics 2000, 136-137, 453-456

[17] Schober, T. Proton conductivity in silica gels, Ionics 2006, 12, 131-134

[18] Livage, J. Sol-gel Ionics, Solid State Ionics 1992, 50, 307-313

Chapter 5

Multilayer deposition

5.1 Multilayer of Amorphous Silica

5.1.1 Introduction

Although the method is, in principle, simple and a deep knowledge has been obtained on both the science behind the process and the technological aspects related to the different coating strategies, there are still limitations to the extensive use of sol-gel. A particularly important point is the difficulty to obtain thick layers and, somehow related to it, the difficulty to coat objects with complex or hidden surfaces.

The thickness is limited by the shrinkage of the gel and the resulting mechanical stresses arising when the deposited gel film dries under the constrain of the substrate. Above a certain critical thickness, that depends on the chemical composition, but mainly on the structure of the gel and on its initial density, the layer starts to crack and with increasing of its thickness it may even detach completely from the substrate. This is a well-known phenomenon, described at the beginning of the nineties by Brinker [1] and Scherer [2] shown that the maximum thickness obtainable by a single step dip-coating deposition does not exceed 1 μm. Our experience is that it is very difficult to obtain silica layers exceeding 0.5 μm if a simple TEOS solution is used. Different strategies have been studied in the past: increasing the compliance of the gel and its initial density by using organically modified tetraethoxysilane-methyltriethoxysilane (TEOS-MTES) sols [3], adding denser silica nanoparticles (colloids) to a TEOS-MTES sol [4], incorporation of a polymer as stress-relaxing agent [5–7], multilayer deposition, with each deposition step followed by a thermal treatment able to relax the stresses [8]. The last strategy is, of course, time consuming, even if in specific cases automatic

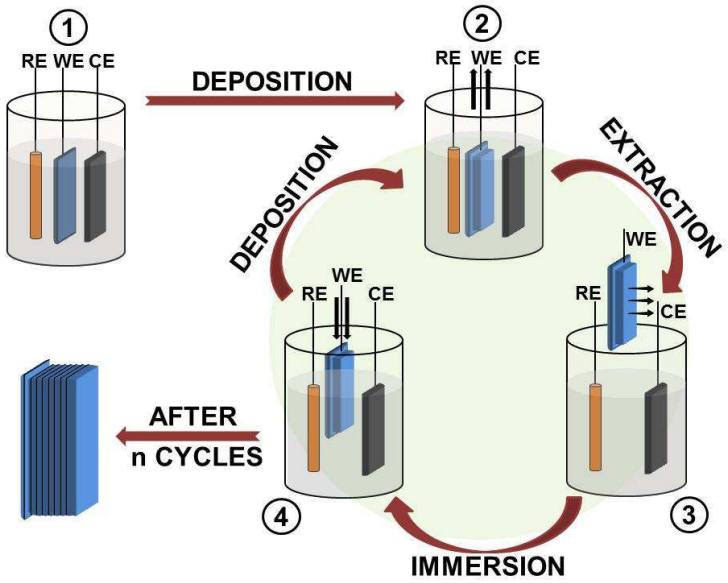

Figure 5.1: Schematisation of multilayer deposition process

deposition-rapid thermal annealing systems may be used.

During the experimental work, described in chapter 3 [9], it was observed that, increasing the deposition time to increase the thickness, the homogeneity of the layer progressively got worse and above a critical thickness of few tenths of micrometer the layer was destroyed. This was, in some way, not expected as it was believed that an increased density of the layer was the premise for a thicker critical thickness, unlike what happens during the dip coating process, in which an heat treatment is necessary in order to densify the film.

Starting from this observation it was decided to deepen the comprehension on the experimental findings. In this chapter we report the results of our study: the deposition of multiple layers by repeated extraction and re-immersion of the sample from the batch after electrochemical assisted deposition, as shown in figure 5.1.

The results were published in *The Journal of Physical Chemistry C* [10].

5.1.2 Experimental

Tetraethyl orthosilicate (≥99.0%), Methyl Triethoxysilane (>90%) (MTES) and Ethanol (≥99.8%) were purchased from Sigma Aldrich and used as received. Potassium nitrate (KNO_3) was purchased from Carlo Erba.

The coating solution was prepared by mixing ethanol (31.5 mL), 10 mL of

bi-distilled water, 0.5 mL of hydrochloric acid (0.1 M), 6.4 mL of TEOS and 1.63 mL of MTES (70:30 molar ratio) as precursor of silica. The solution was pre-hydrolyzed overnight at room temperature under stirring. Before the deposition, KNO_3 (0.03 M) was mixed using magnetic stirring, until complete dissolution.

The electrodeposition was obtained by using a potentiostat/galvanostat within a three-electrode cylinder cell (diameter: ∼4 cm). The reference electrode was a saturated calomel electrode (SCE) and the counter electrode was a glassy carbon plate (16 mm × 20 mm). The working electrodes were obtained from a stainless steel sheet (AISI 304), protected on one side by a protective removable film. The surface was mirror-like polished and the roughness was the same for all samples. The dimensions of the plates were 30 mm × 30 mm × 1 mm. Teflon was used to mask the edges of the samples during the depositions leaving an exposed circular area of about 200 mm^2. No stirring was applied. After deposition the samples were withdrawn at a low constant speed to minimize the thickness of the layer deposited by dip-coating.The samples were dried at room temperature for at least 24 h before the characterization.

For multilayer deposition, the samples were extracted and reinserted in the cell after 5 minutes, with the idea to allow the solution to return to the initial pH conditions (neutralization of OH^- by means of protons). In order to measure the thickness for each layer, different samples were produced for one deposition, two depositions, etc. (each data corresponds to a different sample), assuming that the deposited layers were not affected by further immersion in the solution.

The thickness was measured by a variable-angle spectroscopic ellipsometer (J. A. Wollam Co., Inc.) at incident angles of 70° and 80°, within a wavelength range of 300-1200 nm. The thickness was fitted using a Cauchy model.

5.1.3 Results and discussion

The premise to this work was the difficulty to increase the thickness of the deposited layer by simply increasing the deposition time. The homogeneity of the layer was getting worse when time was increased and the layer started to crack above a critical thickness. This is usual when coatings are deposited by traditional methods (dipping, spinning, etc.), as sol-gel layers obtained from acidic solutions are subjected to a large structural contraction upon drying, which in a constrained system (substrate-film) determines a tensile stress, increasing with the layer thickness. With the electrochemical deposition the local basic environment is expected to get denser and stiffer gel, thus increasing the critical thickness at which the film starts to crack. In fact, for a dip coating process it is necessary to densify and condensate the film, with the help of an heat treatment between a

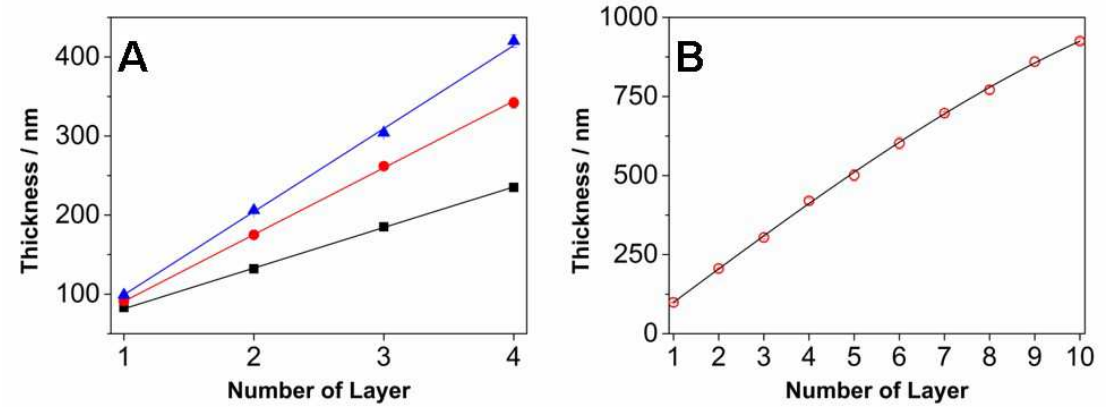

Figure 5.2: Thickness of the first four layers deposited at -1.2 V for 100 s (black square), -1.2 V for 150 s (red circle), -1.3 V for 150 seconds (blue triangle) (A). Thickness of the first ten layers deposited at -1.3 V 150 s (B)

layer and the other.

The electrodeposition of a sol-gel layer may be controlled by two main variables: potential and time. The multiple deposition experiments were made by changing both these parameters. Taking as a reference condition a potential of -1.2 V vs. SCE and a deposition time of 150 seconds, the potential was lowered to -1.3 V vs. SCE keeping the time constant, and the time was decreased to 100 s keeping the potential constant.

In figure 5.2A it may be observed that in the reference conditions the thickness of each layer is about 85 nm. Increasing the potential, the thickness increases to about 100 nm for each layer, while decreasing the deposition time the thickness decreases to about 50 nm. Both the variations were expected. The increase with potential is due to the higher amount of OH^- produced at the surface of the working electrode. The decreasing with decreasing deposition time is obvious.

Four layers were deposited in the three experimental conditions, while up to ten layers were deposited at -1.3 V vs. SCE and 150 s (figure 5.2B) obtaining a total thickness close to 1 μm (about 925 nm).

In all the three cases the thickness increases linearly with the number of layers. When ten layers are deposited a slight deviation from linearity is observed from the seventh layer.

In all the experiments the final results were very uniform and homogeneous coatings, as shown in figure 5.3 on the facing page, which refers to a 10 layers sample, and is representative of the all set of samples.

These experimental data suggest that:

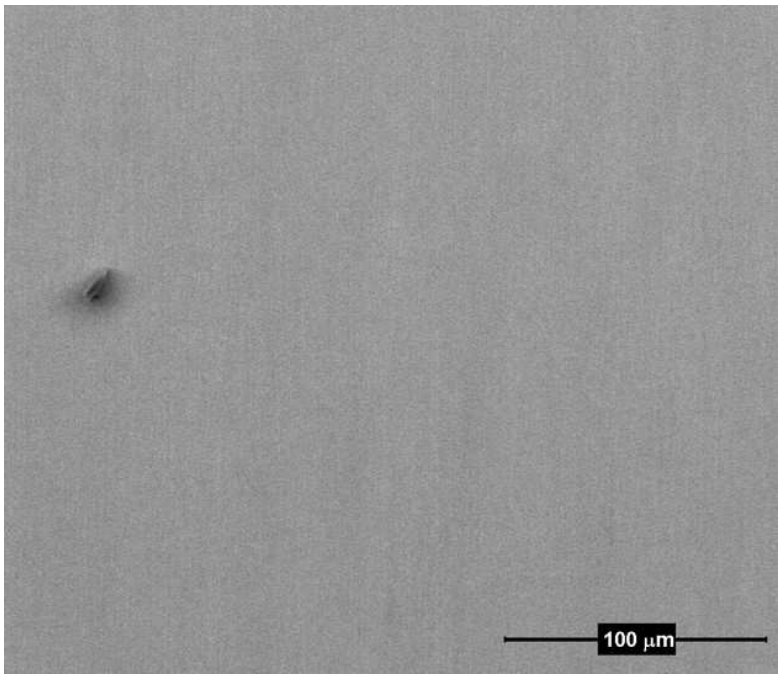

Figure 5.3: SEM image (BSE). Top view of the first ten layers deposited at -1.3 V 150 s

- the film building process is not affected by the previously deposited layers, at least up to a certain thickness;
- the film is stable against re-dissolution in the sol when it is re-immersed;
- very good quality films can be obtained.

All of the above observations are not trivial.

The surface where the deposition of a further layer occurs is moving away from the conducting metal substrate layer after layer, but the availability of hydroxyl ions at the new surface seems to be unchanged. The reason may be that the film has sufficient porosity to allow water and oxygen reduction to occur on the working electrode and, as a consequence, to not affect the production of OH^-.

The second point, concerning the stability of the deposited multilayer film, is related to what may be easily observed if a substrate is coated by a simple dip-coating procedure using an acidic sol and, after extraction, it is re-immersed in the same sol. The process may be repeated several times, but the thickness does not increase at all, or at least not by an additive process. This has been checked once again during the experiments with the solution used in this work.

The condensation reactions occurring in the layer after deposition are evidently not sufficient to get a stable, interconnected gel, and it re-dissolves in the sol when re-immersed. Only after thermal treatment (or a quite long drying time) a second layer may be deposited on the first one, thus doubling the thickness. What, instead, happens in the electro-assisted deposition is the formation of the film in a locally basic environment, that is known to increase the rate of condensation and, therefore, its physical-chemical stabilization is favored. As a matter of fact, the film can be re-immersed in the sol immediately after its extraction, with no dissolution of the gel layer.

5.2 Multilayer of Ordered Mesoporous Silica

This part of experiments was developed at Centre National de la Recherche Scientifique (CNRS) - Laboratoire de Chimie Physique et Microbiologie pour l'Environnement (LCPME) in Nancy, under the supervision of Alain Walcarius and in collaboration with Neus Vilà. The results were published in *Electrochimica Acta* [72].

5.2.1 Introduction

Nanostructuration of electrode surfaces has emerged as an ubiquitous mean to enhance the performance of many electrochemical systems, with applications in various fields such as catalysis and electrocatalysis [11–13], sensors and electroanalysis [13–15], energy conversion and storage [15–18], bioelectrochemistry [19, 20], or nanomotors [21]. Electrochemical techniques suit well in the elaboration of nanostructured surfaces [22, 23] and template electrodeposition is now becoming an accepted versatile method for getting nanomaterials coated electrodes [24–26]. They can be generated either by direct reduction of a metal precursor in the presence of a suitable hard or soft template (to get nanostructured metallic coatings [26–28]), or indirectly, by electrochemically-triggered pH changes likely to induce the formation of selected compounds (metal oxides [29], sol-gel or layered double hydroxide materials [30], mesoporous silica and organically-modified silica [30, 31]) on electrodes.

Ordered mesoporous silica-based materials are attractive in electrochemistry because they combine a rigid inorganic network ensuring fast mass transport processes with a very rich organosilane chemistry enabling the covalent attachment of numerous accessible organofunctional groups [15,31,32], which is notably interesting in the field of electrochemical sensors [32–34]. An important point governing the performance of mesoporous thin films on electrode is the control of porosity, morphology and pore orientation, to keep them accessible from surfaces [35–39]. An ideal configuration is provided by vertically-aligned mesopores [40, 41], but this is not easily achieved by conventional evaporation-induced methods used to generate such deposits [42]. Nowadays, two robust approaches are available to generate highly ordered silica films with mesochannels perpendicular to the underlying support:

- the Stöber solution growth process [43];
- the electrochemically assisted self-assembly method [44, 45];

among some others [40, 46, 47].

When used as electrode modifier, they offer promising avenues for applications as permselective coatings (size and charge selectivity) [48, 49], including antifouling surfaces [50, 51] or molecular sieving membranes [52, 53], electrochemical sensors based on preferential accumulation/detection of target species via complexation [54, 55] or lipophilic effects [56, 57], electrochemical bioassays [58, 59], electrocatalysis [60–62], or electrochemiluminescence sensors [49, 63].

The electro-assisted self-assembly (EASA) method combines the electrochemical interfacial surfactant templating (*i.e.*, assembly of amphiphilic molecules under potential control [64]) and electrochemically assisted sol-gel deposition of the silicate phase [65], in a self-assembly growth process [29, 44, 45, 66]. It involves the cathodic polarization of an electrode immersed in a hydrolyzed sol solution containing the silica precursor (e.g., tetraethoxysilane, TEOS) and a surfactant template (*i.e.*, cetyltrimethylammonium bromide, CTAB), in order to generate the hydroxide ions that are necessary to catalyze polycondensation of the precursor species and induce the formation of transient surfactant hemimicelles around which the silica film is growing in the form of hexagonally packed one dimensional channels of about 2 nm in diameter perpendicularly to the electrode surface. One can prepare such films, either potentiostatically or galvanostatically, on various electrode materials (carbon, gold, platinum, copper, indium-tin oxide, or silicon wafer) [44, 45, 67, 68]. They can be obtained in an organically-modified form, either by post-synthesis grafting [60] or via co-condensation routes [54, 60, 61, 69], but the more versatile approach combines EASA with click chemistry [70, 71]. To date, their thickness can be only varied *ca.* in the 25-150 nm range by tuning the precursor concentration or adjusting the electrosynthesis conditions (applied potential or current density, deposition time) [45]. Moreover, unwanted silica aggregates can form over the thin film, especially at long deposition times or highly cathodic potentials [44], as a result generated OH^- species in a diffusion layer of hundreds of micron thick, contributing to bulk silica precipitation in that region in addition to the expected mesoporous film growth.

In this section, we have thus evaluated how to get aggregate-free films with larger thicknesses, by developing a sequential EASA method. The basic idea is applying the deposition potential intermittently, to deposit one layer on the "ON" position while keeping the system relaxing when "OFF", and repeating the sequence to get multilayers. This is basically achievable for 'classical' sol-gel deposits described in the previous section [10], but not necessary for surfactanttemplated mesoporous silica films because the presence of the surfactant phase can act as an insulating barrier for sequential deposition. We have tested the "ON-OFF" approach with rinsing the electrode between each deposition cycle. The obtained coatings have been characterized by transmission electron microscopy and grazing-incidence X-ray diffraction, and their permeability properties were investigated by cyclic voltammetry. It will be also demonstrated that such films can be functionalized with redox moieties (ferrocene) being electrochemically accessible over the whole multilayer thickness.

5.2.2 Experimental

Reagents and apparatus Tetraethoxysilane (TEOS, Alfa Aesar, 98%,), cetyl trimethylammonium bromide (CTAB, Acros, 99%), $NaNO_3$ (Fluka, 99%), HCl (Riedel de Haën, 1 M solution), hexamminoruthenium chloride $[Ru(NH_3)_6]Cl_3$, Sigma-Aldrich, 98%), and Ethanol (Merck, 95-96%) were from commercial sources and used as received. 3-azidopropyltrimethoxysilane (AzPTES) has been prepared from 3-chloropropyl triethoxysilane (Sigma Aldrich, 95%,) and sodium azide (Acros, 99%), as described in [70].

Ethynylferrocene, (Sigma Aldrich, 97%), ascorbic acid (Merck, 99%), copper acetate (Prolabo, 97%) and dimethylformamide (DMF, Sigma-Aldrich, 99%) were used for the preparation of the ferrocene-functionalized silicabased films from the azide-functionalized films via azide-alkyne cycloaddition reaction.

The films have been prepared by modifying the electrochemically-assisted self-assembly method employed for the preparation of single layer silica thin films. Such process involves the application of a negative potential to an electrode surface (indium-tin oxide, ITO plates (surface resistivity 8-12 Ω), from Delta Technologies) dipped in a hydrolyzed sol solution containing 200 mM TEOS as silane precursor, and CTAB as template in a concentration close to the critical micelle concentration (corresponding to a C_{CTAB}/C_{silane} ratio = 0.32). The pH of the sol is adjusted to 3 by addition of HCl 0.1 M. The applied potential induces a gradient concentration of hydroxide ions which leads to increasing pH locally at the electrode/solution interface, which contributes to catalyze the poly-condensation of the silane precursors. At the same time, the applied cathodic potential induces a transient organization of surfactant hemi-micelles onto the electrode surface, which contributes to the self-assembly of surfactants and the hybrid inorganic network, and film growth orthogonally to the electrode surface in a vertically-aligned hexagonal mesostructure [44, 45].

In order to get multilayered silica thin films, the cathodic potential was applied up to four consecutive times (-1.3 V, optimized value [45]) for selected periods (in the range 5-15 s). Between each polarization period ("ON"), the electrode was disconnected ("OFF" period) and removed from the electrochemical cell to be rinsed in order to avoid disordered polymerization of the silica precursors. The electrodeposition time was fixed at 15 s for the formation of the first layer since it is the minimum time required to initiate the film growth.

For subsequent deposition cycles, the cathodic potential was applied for times of 5, 10 or 15 s, depending on the experiment. At the end of the process, the multilayered films obtained were thoroughly rinsed with water and kept at 130°C overnight.

An analogous experimental procedure was followed in the case of the preparation of multilayered azide-functionalized films, starting from sol solutions containing TEOS and 3-azidopropyltriethoxysilane (AzPTMS) as silica precursors (TEOS/AzPTMS molar ratios ranging from 90/10 to 60/40) in addition to CTAB. Further functionalization of the verticallyoriented multilayered azide-functionalized films was achieved with an azide-alkyne Huisgen cycloaddition reaction leading to the formation of a triazole core substituted at the 4 position. Once the multilayered azide-functionalized films were obtained and the CTAB template removed (by extraction in 0.1 M HCl ethanolic solution for 10 min), a second step based on a click chemistry approach allowed further functionalization and incorporation of ferrocene moieties in the films. Briefly, the azide-functionalized silica films deposited on ITO were dipped in the dark for 18-24 h in a solution of $BuOH/H_2O$ (20 mL) of ethynylferrocene (10.0 mg), $CuSO_4$ H_2O (2.0 mg) and ascorbic acid (10.5 mg) in order to enable derivatization of the azide-based films via 'click chemistry' into a ferrocene-functionalized material. After this period, the films were thoroughly rinsed with water firstly, ethanol and acetonitrile for 10 min in each solvent in order to remove the possible unreacted ethynylferrocene and traces of the catalyst that could be remaining on the ITO surface and subsequently dried.

A three electrode configuration was employed for the electrochemical measurements, including the electrogeneration, the evaluation of the permeability properties, and the characterization of the ferrocene-functionalized silica-based mesoporous films. The voltammetric curves were recorded using a platinum rod as counter electrode, an Ag/AgCl reference electrode (Metrohm) and ITO plates as working electrodes where the hybrid films were deposited. The electrochemically-assisted deposition was carried out using a home-made electrochemical cell with a configuration allowing placing the working electrode at the bottom. A stainless steel counter electrode and AgCl-coated silver wire pseudo-reference electrode completed the electrochemical setup.

Characterization All the electrochemical experiments were performed using a μAutoLab III potentiostat (Eco Chemie) monitored by the GPES software.

Morphological analysis of the mesostructured films has been achieved by transmission electron microscopy (TEM) using a CM20 microscope at an acceleration voltage of 200 kV. The film thickness was evaluated routinely by atomic force microscopy (AFM, apparatus Thermomicroscope Explorer Ecu+, Veeco Instruments SAS) on scratched samples. The film structure was analyzed by grazing-incidence X-ray diffraction (GIXD) using a Nonius Kappa CCD diffractometer equipped with an ApexII CCD detector (copper cathode ($\lambda_{K\alpha} = 1.54184$ $\mathring{A}$), as previously described [45]. Uncertainties on the measured lattice parameters were estimated

from multiple measurements and were found to be 0.2 $\AA$. Fourier transform infrared spectroscopy (FTIR) measurements were performed using a Nicolet 8700 apparatus equipped with a diffuse reflectance accessory. FTIR was used to evidence the presence of azide and/or 1,2,3-triazole functionalities in the synthesized films [70].

5.2.3 Results and discussion

As stated in the introduction, a straightforward way to increase the thickness of EASA-based mesoporous silica films implies longer deposition times. In doing so, however, silica aggregates are formed in addition to the ordered and oriented mesoporous film. This is evidenced by SEM (see figure 5.4A showing cross-sections of a uniform thin film obtained at short deposition time (part A_1) and a thicker film with numerous aggregates at longer times (part A_2), the underlying film exhibiting also significant cracks).

GIXD data (5.4B) also demonstrate the existence of the vertically-aligned hexagonal mesostructure (through characteristics spots in the equatorial plan [45], see part B_1), with additional out-of-plane rings for thicker films (see part B_2) originating from the presence of randomly distributed mesoporous silica particles with wormlike structure. Such unwanted aggregates arise from the fact that the catalyst (hydroxyl ion) is formed in a region at the electrode/solution interface much thicker by several orders of magnitude over the film thickness. As far as time evolves, the catalyst concentration profile at the interface (diffusion layer) extends according to $(\pi Dt)^{1/2}$ (with D is the diffusion coefficient for the catalyst and t the deposition time). The thickness of this layer containing the catalysts is much larger than that of the mesoporous silica film (see part C_1 in figure 5.4 on the next page), and silica aggregates are formed essentially in this diffusion layer, on the top of the uniform thin film, when extending the deposition period (*i.e.*, typically over 20 s) as schematically illustrated in figure 5.4 (part C_2).

If wishing to increase the thickness of such ordered and oriented mesoporous silica films, it is thus necessary to find a way circumventing the problem of the thick diffusion layer leading to bulk precipitation of silica aggregates at longer deposition times. What is proposed here is a sequential EASA process. In doing so, the deposition potential is only applied for short periods (typically ON times in the range 5-15 s) interrupted with open-circuit 'rest' times (figure 5.5A). Such ON-OFF scheme is then repeated successively to get the multilayer film. During OFF time, the electrode is removed from the sol and washed with a precursor-free water/ethanol solution. This is required to eliminate as much as possible the OH^- ions electrogenerated on the electrode surface, which would remain still

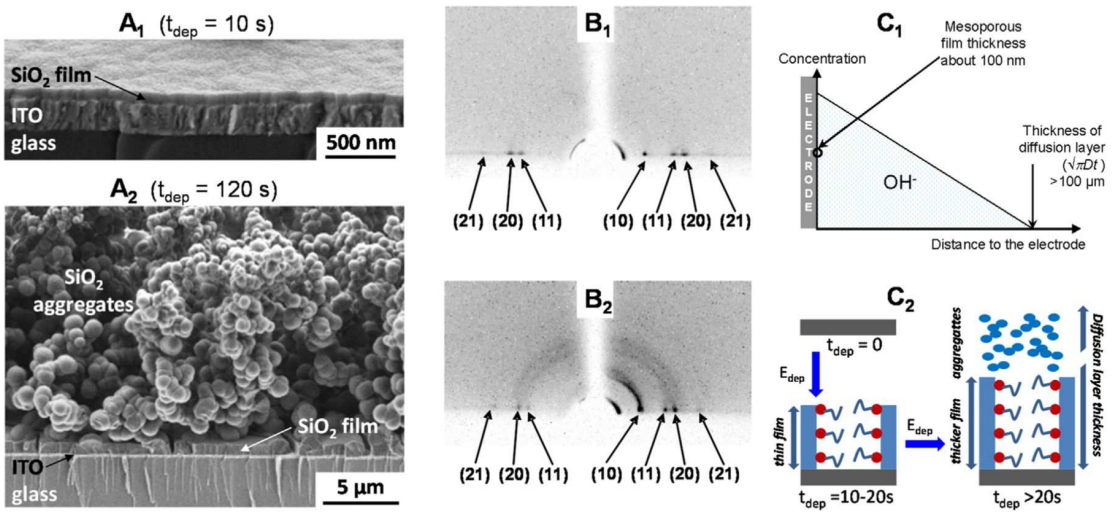

Figure 5.4: (A) Cross-section SEM views of thin (A_1) and thick (A_2) mesoporous silica films prepared by EASA at respectively short and long deposition times (t_{dep} = 10 or 120 s); (B) corresponding GIXD patterns for thin (B_1) and thick (B_2) films (indicating also the (10), (11), (20) and (21) signals characteristics of the hexagonal $p6m$ symmetry with $C6$ rotation axis perpendicular to the surface); (C) schematic representation of the catalyst concentration profile at the electrode/solution interface (C_1) and illustration of thin and thick deposits formed at short and long deposition times (C_2)

present at the interface for a significant time even at open-circuit, leading to continuation (yet slowly) of the precursors polycondensation (as previously pointed out from quartz microbalance measurements, see supporting information in [44]). The importance of removing/washing the electrode during OFF time is illustrated by AFM images recorded for two-layer films (figure 5.5B) prepared either with keeping the electrode in the sol solution between the two consecutive deposition periods (figure $5.5B_2$) or with removing/washing it (figure $5.5B_1$), showing clearly the formation of much more silica particles in the former case. On the basis of scratched films(figure $5.5B_3$), AFM imaging also provides a way to estimate the film thickness (figure $5.5B_4$). Finally, one has to stress that significant current values (of the same order of magnitude when reaching steady-state) are observed when applying the cathodic potential in the successive deposition steps (figure $5.5A_2$), thanks to the permeable wetted gel enabling the electrolysis to be performed and OH^- catalyst to diffuse through the silica gel walls (because it cannot pass the hydrophobic barrier made of surfactant molecules in the mesopore channels). If applying a drying and heat treatment (120°C, as typical for strengthening the silica network) after the first deposition step, the film becomes impermeable (as previously demonstrated using hydrophilic redox probes in solution [37,56,73]) and no further deposition can be made.

Morphological characterization

The microscopic morphology of multilayered mesoporous silica films was first analyzed by transmission electron microscopy (TEM). Cross-section TEM micrographs (as shown in figure 5.6A-C for 2-4 layers, all prepared with "ON" times adjusted at 15 s) demonstrate that thin and uniform multilayers can be indeed obtained and that the vertical orientation of mesopore channels is maintained is all layers. The thickness of the last layers (3^{rd} and especially 4^{th} ones) was lower than the two first ones, suggesting slower growth kinetics. A possible explanation is the progressively larger resistance to mass transport through thicker deposits, resulting in lower amounts of OH^- catalyst at the interface and consequently slower film growth. This is also supported by slightly longer times required to get steady-state current values in the successive electrolytic deposition steps (see bottom of figure 5.4A). An enlargement of the interlayer region (figure $5.6A_2$) reveals that it is extremely thin (nm range) and that mesopore channels seem to stay online from one layer to the adjacent one, suggesting possible keeping of transport properties. TEM top views (figure 5.7) confirm the hexagonal arrangement of mesopores up to the 4^{th} layer.

The pore diameter is around 2 nm and pore-to-pore distance equal to 4 nm,

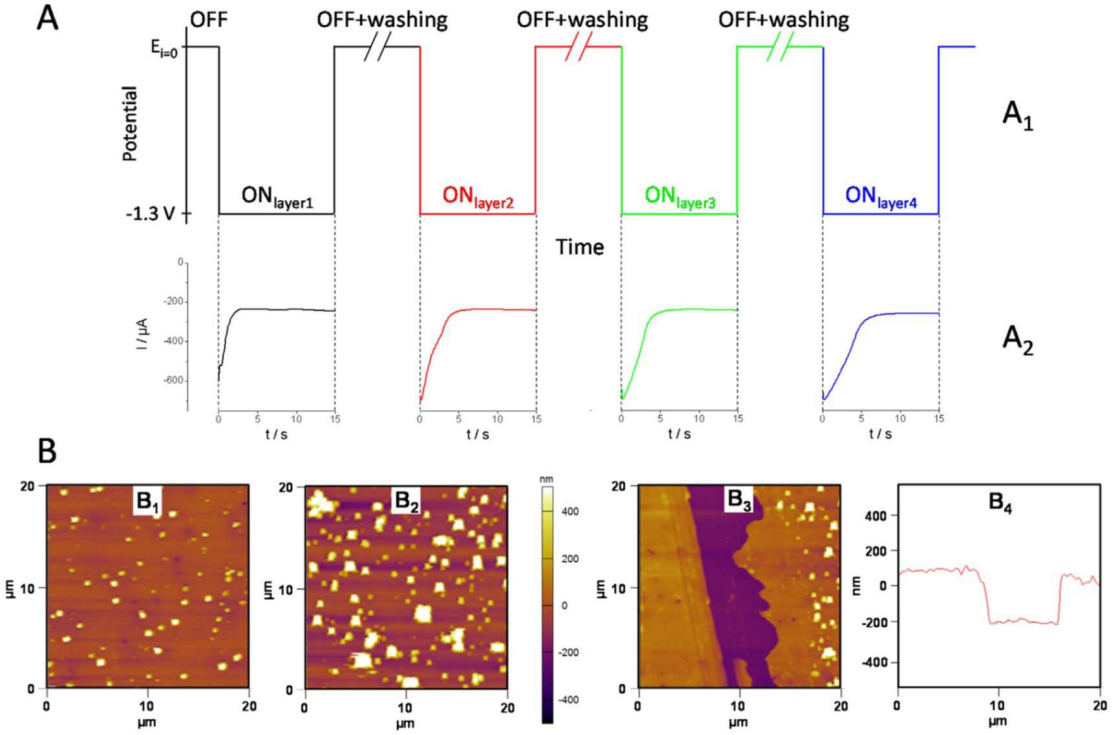

Figure 5.5: (A) Illustration of the sequential EASA method (A_1) and corresponding currents (A_2) recorded during periods of applied potential (ON) interrupted by open-circuit times during which the electrode was removed from the sol solution and washed (OFF + washing). (B) AFM imaging of a two-layer film obtained after washing the electrode (B_1) or not (B_2) between two successive deposition steps; image obtained for a scratched film (B_3) and corresponding line scan used to evaluate the film thickness (B_4)

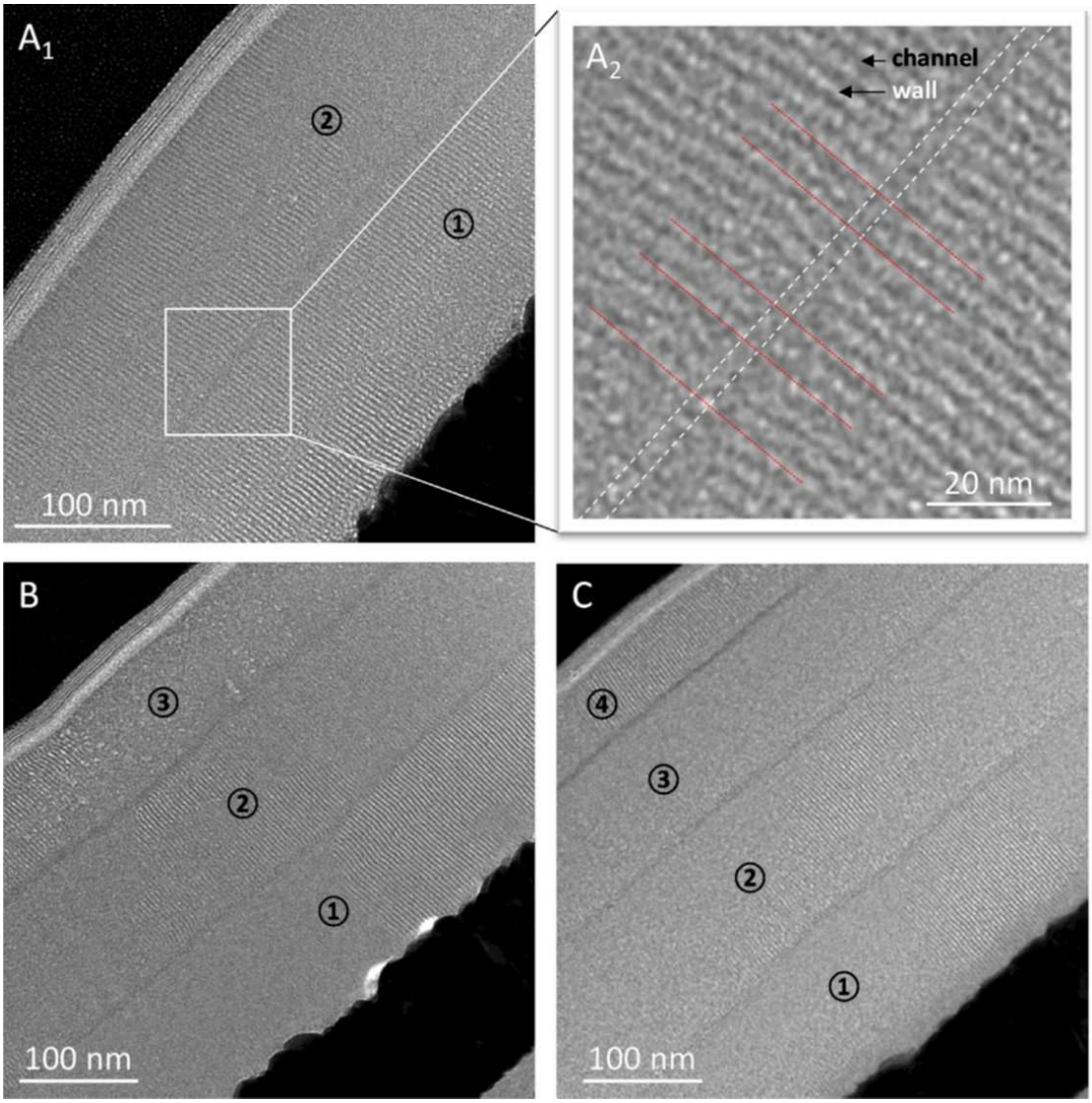

Figure 5.6: TEM micrographs of electrogenerated multilayer mesoporous thin films prepared by the sequential EASA method: cross-section views of two-layer (A), three-layer (B) and four-layer (C) films (A_2 is a magnified view at the intersection between two electrodeposited layers in which white dashed lines represent the interlayer domain and the red ones illustrate the pore orientation maintained in both sides of the interface). The thin layer visible on the top of each sample is an artefact linked to the way in which slices of the film have been cut

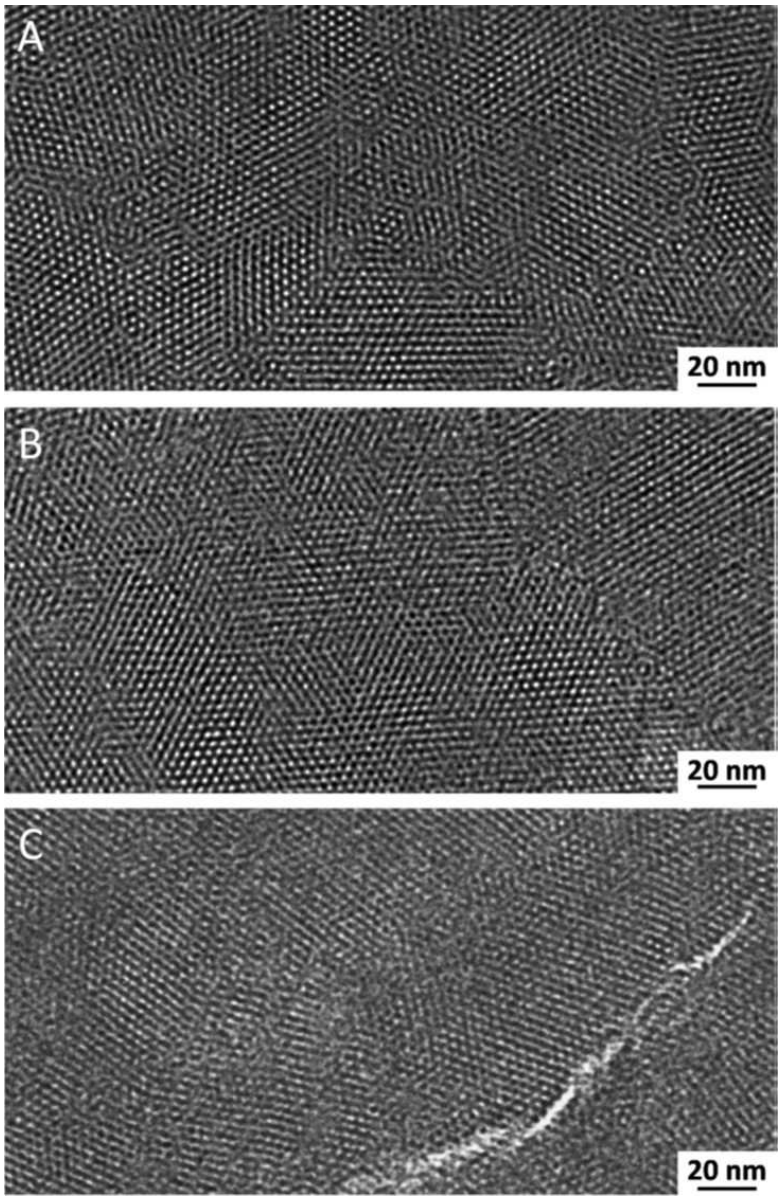

Figure 5.7: TEM micrographs of electrogenerated multilayer mesoporous thin films prepared by the sequential EASA method: top views of two-layer (A), three-layer (B) and four-layer (C) films

consistent with values reported for other CTAB-based mesoporous silica thin films [31,74]. For the thicker multilayered film (figure 5.7C), one can notice the presence of a small defect being possibly a crack (originating from mechanical stress due to shrinking in the course of heat treatment, as common for thick silica films [75]), but it can also be due to the fact that TEM imaging requires the removal of the film from its support and its transfer on a TEM grid (which can result in some physical damages to such thin membranes).

The high degree of mesostructural order and the vertically-aligned hexagonal structure are confirmed by GIXD measurements performed on the films on their substrate (figure 5.8 on the following page). As shown, well-defined spots in the equatorial plan, with typical (10), (11), (20) and (21) plans for an orthogonally oriented hexagonal structure [45], are obtained for all samples from 1 to 4 layers. The lattice parameter remains constant at *ca.* 4.04 ± 0.02 nm, regardless the film thickness, confirming the pore-to-pore distance value estimated above from TEM. Almost no additional out-of-plane rings can be evidenced, indicating no or very few silica particles/aggregates, except for the thickest 4-layers sample in which on can notice a small contribution of such silica particles with wormlike structure. This confirms the good quality of both the mesostructure and its vertical orientation over the whole multilayered films.

The first silica layer was always obtained by applying the cathodic potential for 15 s since it is the minimum time required in order to ensure the film growth. Nevertheless it is possible to tune the thickness of the multilayer film by adjusting the electrodeposition time. Typical results are shown for 2-4 layers electrodeposited at times ranging from 5 to 15 s (figure 5.9 on page 81). In all cases, lengthening the deposition period for layers 2-4 resulted in increasing the multilayer film thickness, the maximal value achievable while keeping the mesostructural order being 400 nm. Film growth in the presence of CTAB template is much faster than without (getting a 400 nm pure silica gel film required 4 deposition steps at -1.3 V for 150 s each [10]). The film thickness was proportional to the total electrolysis time: for instance, the 15-5-5-5 four-layers film has a similar thickness as the 15-15 two-layers one, because the overall deposition time was the same in both cases (*i.e.*, 30 s in this case).

In terms of thickness, reproducibility of multilayer deposition was good, with standard deviation values of *ca.* 5% (n = 3); see, for example the thickness of the first and second layers being constant independently on the film was made of 2, 3 or 4 layers (figure 5.6 on page 77). As before mentioned, the process has however a limit arising from the restricted diffusion of OH^- catalyst through thicker films (levelling off starting to be noticeable in figure 5.6 for 4^{th} layers). This restriction is also supported by the fact that the amount of charge necessary to form the

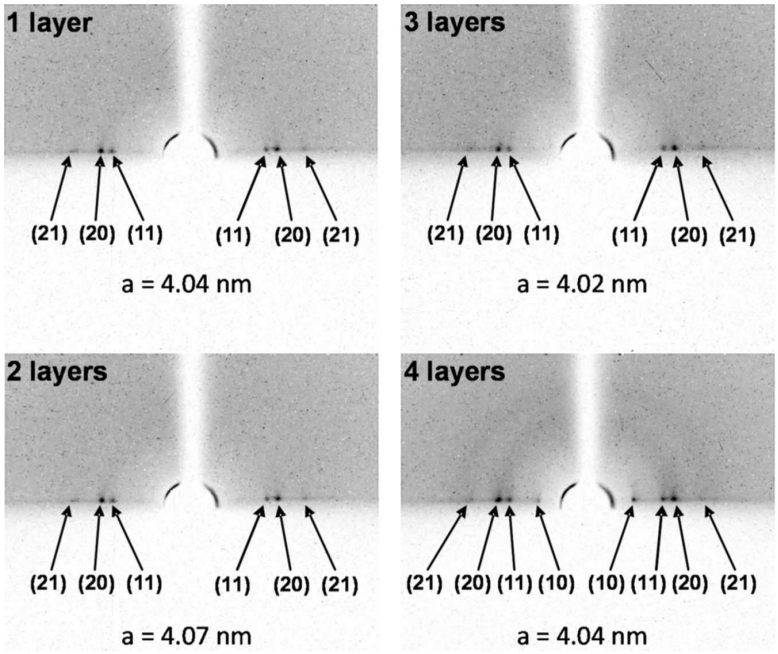

Figure 5.8: GIXD patterns for electrogenerated multilayer mesoporous thin films prepared by the sequential EASA method (1-4 layers), indicating also the (10), (11), (20) and (21) signals characteristics of the vertically-aligned hexagonal mesostructure and lattice parameters (a)

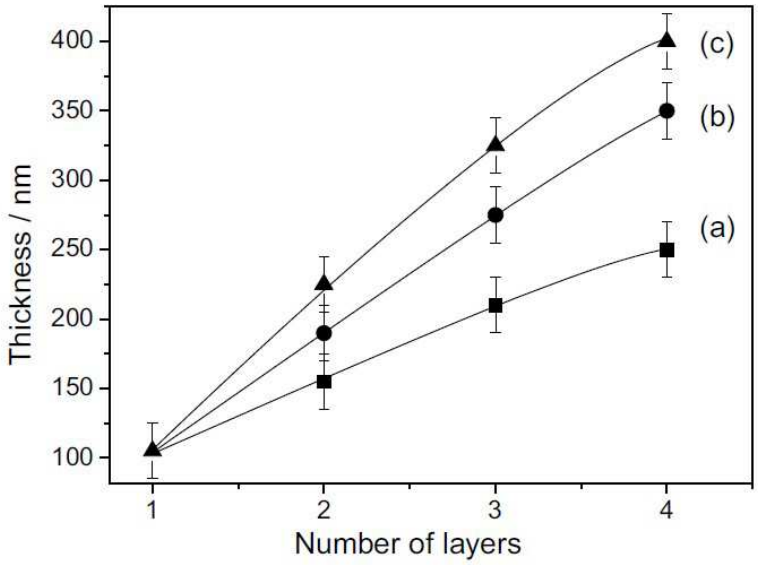

Figure 5.9: Thickness of the first layer deposited at -1.3 V for 15 s and the subsequent 2-4 layers deposited at the same potential for (a) 5 s, (b) 10 s and (c) 15 s

film (*i.e.* corresponding to the amount of generated OH^- catalyst) is increasing with the number of layers. For instance, for the 15-15-15-15 four layers film, the charges passed during the successive 15 s deposition times (figure 5.5A2) were 3.9, 4.4, 4.7 and 5.3 mC, respectively for layers 1 to 4, while in the same time, layer thicknesses decreased from *ca.* 100 nm (1^{st} layer) to 50 nm (4^{th} layer). It means that even if generating more OH^- catalyst species, their restricted diffusion through thicker films resulted in slower film growth of outermost layers.

Electrochemical characterization

Cyclic voltammetry (CV) measurements, performed respectively before (figure 5.10A) and after surfactant extraction (figure 5.10B), were carried out in order to evaluate the quality and permeability properties of the silica films using a redox probe (*i.e.*, $Ru(NH_3)_6^{3+}$ 1 mM) in solution. For as-prepared films, the absence of electrochemical response indicates that the silica film is uniformly deposited over the whole ITO surface and free of defects because the electroactive species are not able to diffuse through the surfactant templated film.

Figure 5.10A shows that it is indeed the case for the multilayer films, except for the thicker ones (especially the 4 layers one) for which a small signal starts to grow. This signal is much smaller than on bare ITO and wave-shaped, indicating

the presence of some individual small defects (probably cracks originating from shrinkage during heat treatment, as also observed for mesoporous silica thick films prepared by evaporation-induced self-assembly [75]), in agreement with TEM analysis (figure 5.7C). After template removal the multilayered silica films were all highly permeable, exhibiting CV responses of the same order of magnitude or even larger than that recorded on bare ITO (figure 5.10B). This indicates clearly that the interlayer regions between successive layers individually generated by EASA do no prevent mass transport issues through the multilayered films. This was already suggested above on the basis of TEM observations (figure 5.7 on page 78), but such morphological analysis was restricted to portions of the film. The communication/continuity between the mesochannels of consecutive layers is evidenced regardless the film thickness and number of layers. The larger current values observed for film-modified electrodes, as greater for thicker films, are explained by some accumulation of the positively-charged redox probe onto the negatively-charged silica surface [33, 76]. The peak-to-peak separation of 60 mV demonstrates fast electron transfer kinetics. A study at various potential scan rates (see results on figure 5.11 on page 84 for a 4 layers film) indicates diffusion-limited charge transfer processes (peak currents directly proportional to the square root of scan rate, see right insert in figure 5.11 on page 84), yet with leveling off at scan rates larger than 70 mV s^{-1}, as explained by some resistance to mass transport through the film (such deviation was not observed on bare electrode). All these results indicate good accessibility to the multilayered and oriented mesoporous silica films prepared by layer-by-layer EASA deposition.

A more quantitative analysis of the electrochemical parameters is however prevented by the difficulty to evaluate the probe concentration in the film (because of an unknown added contribution due to its accumulation onto the silica walls by electrostatic interactions). The only discussion one can provide here is related to the increase in the slope of $Ivs\nu^{1/2}$ plot with the number of layers (see right insert in figure 5.11 on page 84), meaning that (according to the Randles-Sevcik equation) the product $\sqrt{D_f} \times C_f$ (where D_f is the apparent diffusion coefficient of the probe in the film and C_f its concentration in the film) is larger than in solution ($\sqrt{D} \times C$ with D the diffusion coefficient of the probe in solution and C its concentration). As D_f is expected to be smaller than D (because of some resistance to mass transport in such confined environment [12]), this behavior confirms the accumulation of the positively-charged probe in the negatively-charged film (C_f larger than C) and this effect is more important for thicker films (larger binding capacity). A final observation is the asymmetric variation of peak potentials for film electrodes (figure 5.11). While no noticeable variation of the cathodic peak potential values with scan rate is observed (consistent with fast electron transfer

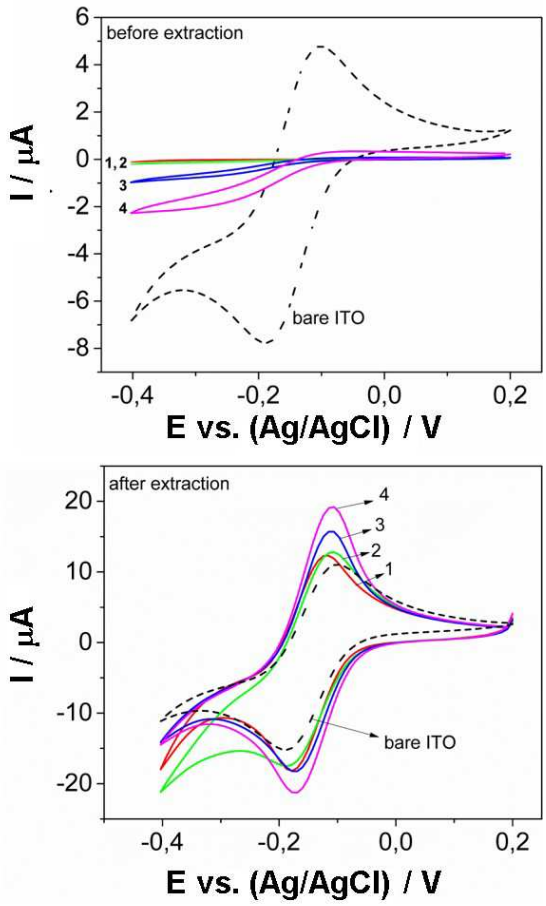

Figure 5.10: Cyclic voltammetry of 1 mM $Ru(NH_3)_6{}^{3+}$ performed on ITO electrodes respectively covered with a single layer (1, red line), two-layers (2, green line), three-layers (3, blue line) and four-layers (4, violet line) of mesoporous silica films, respectively before (A) and after surfactant extraction (B); the curves have been recorded at 20 mV s^{-1} (A) or 80 mV s^{-1} (B). The corresponding responses at bare ITO electrode are also shown (black dashed lines)

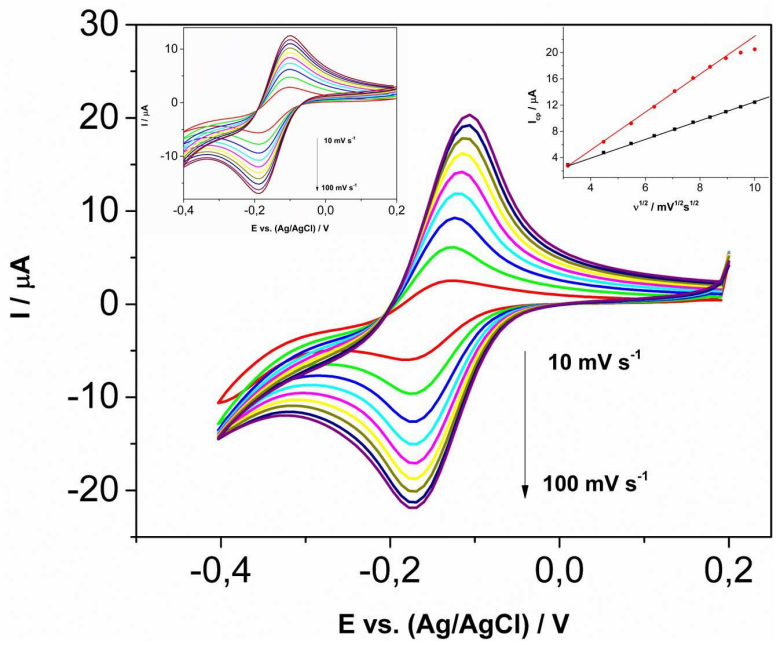

Figure 5.11: Cyclic voltammetry of 1 mM $Ru(NH_3)_6{}^{3+}$ performed on ITO electrode covered with a four-layers mesoporous silica film, at various potential scan rates ranging from 10 mV s^{-1} to 100 mV s^{-1}. The data observed at bare ITO are shown in the left insert and the corresponding variations of cathodic peak currents with square root of scan rate are given in the right insert

rates for the $Ru(NH_3)_6^{3+/2+}$ redox couple [77]), a positive shift is seen for the anodic peak potentials (E_{pa}) with rising scan rates (ν). This is explained by charge compensation requiring the ingress of an electrolyte anion from the solution into the film when oxidizing $Ru(NH_3)_6^{3+/2+}$ into $Ru(NH_3)_6^{3+}$, and such diffusion of anionic species through negatively-charged mesochannels is known to be a strong rate-determining process [48,78]. Using Laviroń formalism [79], one can estimate from the E_{pa} *versus* ν plot an apparent heterogeneous rate constant of 0.9 s^{-1} (α = 0.5) for such slow anodic reaction. On bare ITO, both cathodic and anodic processes are fast because there is no restriction to charge neutralization.

Functionalization of multilayered mesoporous silica films with redox moieties

To get further insight in the accessibility properties of the multilayer films, series of mesoporous silica samples (1 to 4 layers) functionalized with azido groups have been prepared (by cocondensation of TEOS and AzPTMS in 80:20, 70:30 and 60:40 molar ratios in the presence of CTAB, according to a known procedure [70]). They gave rise to well-ordered and oriented mesostructures as for the films prepared from only TEOS (data not shown). They were then derivatized with ferrocene groups by exploiting the Huisgen coupling reaction between the azido groups in the film and ethynylferrocene in solution, the effectiveness of such click chemistry being evidenced by FTIR (not shown), via the progressive vanishing of the asymmetric stretching band associated to the presence of $-N_3$ terminal groups at 2095 cm^{-1} and concomitant emergence of a broad and intense absorption band around 1595 cm^{-1} indicating the formation of 1,2,3-triazole rings [70, 71].

Typical voltammetric responses of these films are shown in figure 5.12. They first indicate that the click reaction occurred in the whole thickness of the multilayered deposits as the ferrocene signals increased continuously when passing from 1 to 4 layers (figure 5.12A,B). Consistent with the above permeability results (figure 5.10B), this means that the click reagent (ethynylferrocene) is likely to diffuse through the entire depth of the film, including passing through the interfacial region between two consecutive layers. Moreover, the amount of ferrocene incorporated is proportional to the film thickness, as the trend for films prepared in the 15/5/5/5 s deposition series (figure 5.12A) and the 15/15/15/15 ones (figure 5.12B) is parallel to the variations in film thickness as a function of the number of layers (see respectively curves (a) and (c) in figure 5.9 on page 81). The electrochemical response of these ferrocene-functionalized films is based on an electron hopping mechanism because this is the only way to exchange electrons between adjacent redox sites in such insulating material [80]. The observation of

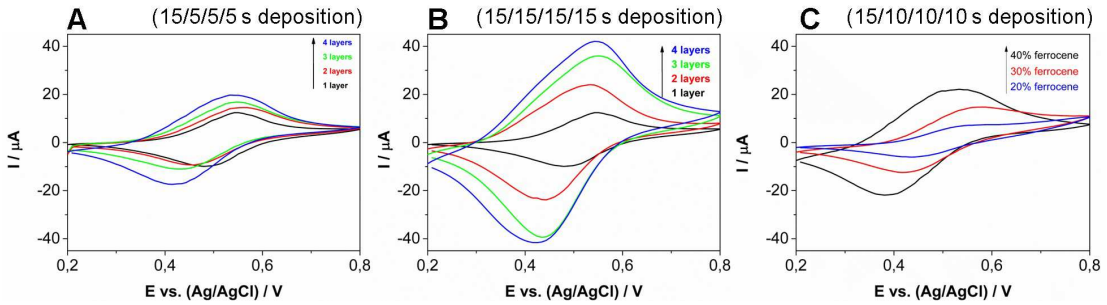

Figure 5.12: Cyclic voltammetry responses of ferrocene-functionalized multilayered mesoporous silica films: (A,B) 1 to 4 layers films prepared from 40:60 AzPTMS/TEOS ratio respectively at (A) 15/5/5/5 s and (B) 15/15/15/15 s deposition times; (C) 4 layers films prepared from 40:60, 30:70 and 20:80 AzPTMS/TEOS ratios at 15/10/10/10 s deposition time. The curves have been recorded in acetonitrile (+0.1 M $TBAClO_4$) at a scan rate of 20 mV s^{-1}

ferrocene electroactivity in the multilayered deposits is thus an indirect evidence that these groups have been successfully attached to the silica walls in the whole film thickness, even at the bottom of mesopore channels, since ferrocene groups must be close enough to the underlying electrode surface to initiate the electron transfer process. As for single-layer films [70], it is possible to tune the degree of functionalization by varying the AzPTMS/TEOS molar ratio in the synthesis medium, resulting in proportional voltammetric responses (as illustrated in figure 5.12C for four-layer films prepared at 15/10/10/10 s deposition times and 20 to 40% organosilane) with respect to the amount of ferrocene in the material.

5.3 Silica/Titania Multilayer for Optical Applications

5.3.1 Introduction

After experiencing the solidity of the multilayer technique, both with hybrid silica (TEOS/MTES) and functionalized mesoporous silica, the next step was to intercalate different oxides.

The formation of optical coating via sol-gel method is well known by decades [81–84]. Their applications as antireflective coatings for silicon solar cell get in continuous research [85,86]. Graded structures based on the different refractive index of amorphous titania [87] or using the codeposition of silica and titania [88] were

successfully obtained via electron beam evaporation and electro-assisted deposition, respectively. Recently, titania multilayer was used for corrosion protection of AISI 304 stainless steel [89] and the formation of TiO_2/AlOOH was promoted in order to enhance the interference color of the coating [90].

In this section, the possibility to intercalate silica-based films (low refractive index) and amorphous titania (high refractive index) via electro-assisted deposition is demonstrated. The hydrolysis and condensation reactions of titania precursors are just like silica [91]:

$$\equiv Ti - OR + H_2O \quad \rightarrow \quad \equiv Ti - OH + R - OH \tag{5.1}$$

$$\equiv Ti - OH + HO - Ti \equiv \quad \rightarrow \quad \equiv Ti - O - Ti \equiv +H_2O \tag{5.2}$$

$$\equiv Ti - OR + HO - Ti \equiv \quad \rightarrow \quad \equiv Ti - O - Ti \equiv +R - OH \tag{5.3}$$

As Liu and Mandler [88] showed, the kinetics is different. Two starting solutions were properly optimized in order to obtain similar thicknesses for titania and silica thin films. Optical properties of the multilayer were characterized using ellipsometer, such as the reflection in p-polarized light and the dispersion of the refractive index n on ITO and stainless steel substrates.

The results presented in this section are in submission on *Journal of Sol-Gel Science and Technology*.

5.3.2 Experimental

Reagents and apparatus Tetraethyl orthosilicate (TEOS, ≥99.0%), methyl triethoxysilane (>90%) (MTES) and ethanol (≥99.8%), titanium(IV) isopropoxide (TTIP, 97%), acetylacetone (AcAc, >98%) were purchased from Sigma Aldrich and used as received. Potassium nitrate (KNO_3) was purchased from Carlo Erba. Hydrochloric acid (0.1 M) was purchased from Labochimica srl.

Silica solution was prepared by mixing in order ethanol (30.5 ml), bidistilled water (10 ml, 0.03 M KNO_3), TEOS (6.4 ml) and MTES (1.6 ml). HCl (0.1 M) was added till reaching pH 3.0. The solution was stirred for 1h to ensure the hydrolysis.

Two solution were prepared for titania deposition. The first one was obtained by mixing TTIP (2.37 ml), AcAc (0.82 ml) and ethanol (20 ml) for 30 minutes, then 20 ml of bidistilled water (0.2 M KNO_3) were added drop by drop. The two solutions were stirred for 1h to ensure the hydrolysis.

Potentiostat/galvanostat Bio-Logic SP-300 was used for electrodeposition in a three-electrode electrochemical cylinder cell (diameter: $\sim$ 40 mm) configuration. Satured calomel electrode (SCE) and glassy carbon plate (16 mm $\times$ 20 mm) were employed as reference and counter electrode, respectively. The working electrodes were obtained from a stainless steel sheet (AISI 304), protected on one side by a protective removable Teflon tape. The surface was mirror-like polished and the roughness was the same for all samples. The dimensions of the plates were 30 mm $\times$ 30 mm $\times$ 1 mm; electrochemical depositions were carried out on an exposed area of $\sim$ 200 mm^2, which was obtained by applying an adhesive Teflon mask. For ITO substrate, the working electrodes were obtained from Corning alkaline earth boro-aluminumsilicate glass, 50 mm $\times$ 75 mm $\times$ 0.7 mm, Indium Tin Oxide coated one surface, R_s = 5-15 Ω, purchased from Delta Technologies.

Deposition of silica films occurred at -1.2 V for 100 s, then titania films were deposited at -1.1 V for 100 s, following the same procedure used in 5.1.2 on page 64.

Characterization After silica-titania deposition, the samples were withdrawn by a dip coater with a withdrawal constant rate of ca. 100 μm/s, then they were dried at room temperature for at least 24h before each characterization.

Cross-sectional view of multilayer films was investigated in high vacuum by Field Emission Scanning Elecron Microscope (FE-SEM), Zeiss sigma HD, operated at 2 kV.

Reflection measurements were obtained using ellipsometer (J. A. Wollam Co., Inc.) and the refractive index dispersion of silica and titania was calculated with the help of Cauchy model, within a wavelength range of 300-1000 nm.

X-ray diffraction (XRD) was obtained using Philips PW 1710, with Cu K_α Ni-filtered radiation.

5.3.3 Results and discussion

As explained in the first chapter, the deposition of titania via electrochemical deposition is not simple, because the modulation of the thickness and the control of the homogeneity are more difficult. Nevertheless, titanium oxide is very interesting from the point of view of applications. As shown in the section 1.4 on page 9, graded structure and protective coating were created by Liu and Mandler [88] and Li *et al.* [92], respectively.

The intercalation of silica and titania in a multilayer format meets several applications within linear optic.

Below, the possibility to create SiO_2-TiO_2 multilayer via electrodeposition technique on stainless steel (SS) and indium tin oxide (ITO) substrates is demonstrated: four intercalated layers were deposited using the same applied potential and deposition time (-1.2 V for 100 s for silica solution and -1.1 V for 100 s for titania solution).

Morphological and structural characterizations

In this work the starting solution of titanium oxide was optimized in order to obtain thin films having thicknesses comparable to those obtained with silica solution.

Four layers were deposited both on ITO and stainless steel. However, it was possible to verify the structure only on ITO samples: cross-sectional view of the central area of the multilayer was obtained using FE-SEM at 2 kV, as shown in figure 5.13.

The results show that the films are homogeneous, keeping constant the thickness over the whole deposited area. This aspect is important for any optical applications. However, if the total thickness reaches the value around 500-600 nm, a detachment of the multilayer from the substrate could occur during the evaporation of the solvent, as shown in figure 5.13D.

In order to obtain a coating by the multilayer depositon, an heat treatment at 60°C for 1h is needed only after the deposition of the second titania layer, in order to guarantee the adhesion of the second layer on the first one. The other layer (first, third and fourth) do not need any heat treatment. According to Liu and Mandler [88], the deposition of titanium oxide gets less adhesion to the substrate and for this reason it is necessary to improve the condensation of sol-gel by means of the evaporation of the solvent. Skipping this step, the third layer of silica replaces the second layer of titania, which is solubilized in the ethanol/water mixture. As one can observe, the thickness of the films is around 100 nm for both silicium and titanium oxides.

Treating thermally at 500°C for 5h the titania layer, the formation of anatase and rutile was verified, as shown in figure 5.14 on page 91. A broady peak of hematite was observed, due to the oxidation of the stainless steel substrate, which begins around 500°C. The peak of potassium chloride is originated from KNO_3 and from satured calomel electrode, used as reference electrode for the electro-assisted deposition.

The phase transformation of titanium oxide could be interesting: the refractive index increases passing from amorphous titania (2.2) to anatase (ca. 2.4) or rutile (ca. 2.6).

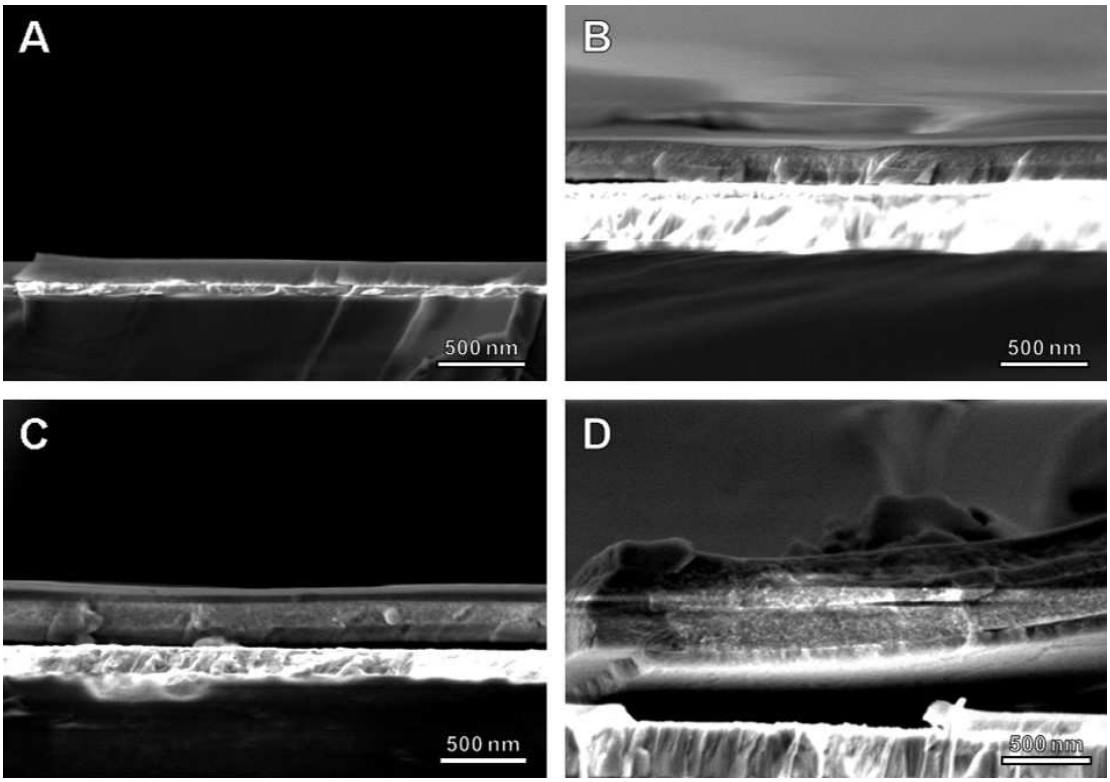

Figure 5.13: FE-SEM images of multilayer silica-titania based on ITO. Cross sectional view of one layer (A), two layers (B), three layers (C) and four layers (D). EHT: 2 kV. Magnification: 100000 X

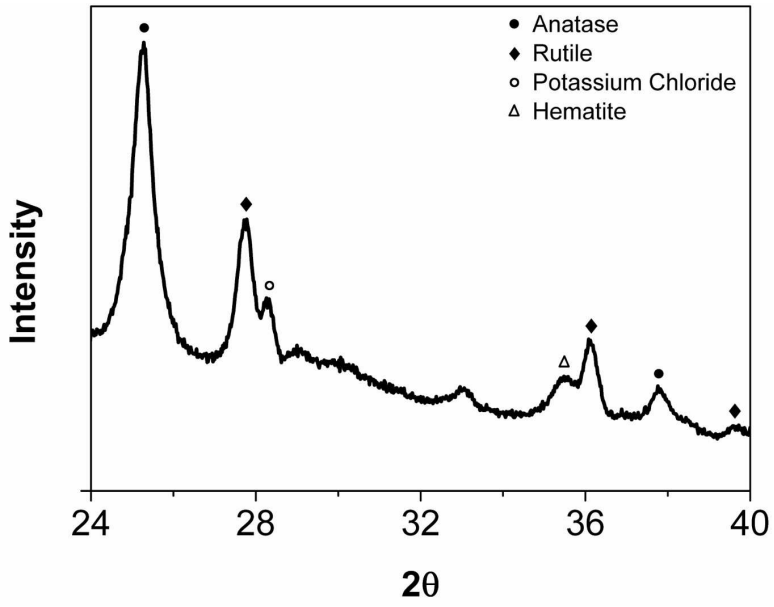

Figure 5.14: X-ray diffraction of SiO_2-TiO_2 multilayer treated at 500°C for 5 h

Optical characterizations

The reflection of p-polarized light at different angles (from 20° to 60°) was obtained on stainless steel and ITO substrates by ellipsometer. For the bare stainless steel substrate, the reflection at 600 nm is around 35%, on the other hand for ITO bare material it reaches a value of ca. 5%.

Depositing a single layer of titania, the reflection increases slightly in the range from 400 nm to 550 nm, on the contrary the reflection decreases when only one layer of SiO_2 is deposited (see figures 5.15C and 5.16C).

The reflection starts to increase when SiO_2 and TiO_2 are coupled together creating a double layer, thanks to the different values of refractive index (Bragg effect). Depositing four layers the refraction bands can be observed (centered around 450 nm for ITO and 550 nm for SS, see figures 5.15F and 5.16F).

As described in tables 5.1 and 5.2, the reflection increases up to 15% using only 4 layers. The refractive bands can be modulated by changing the thicknesses of the two layers, but this is not the purpose of this work.

In order to have a comparison with the theory, a reflection fitting was performed using the following procedure:

- modeling the real substrates;
- fitting the single layers of silica and titania on the bare substrate;

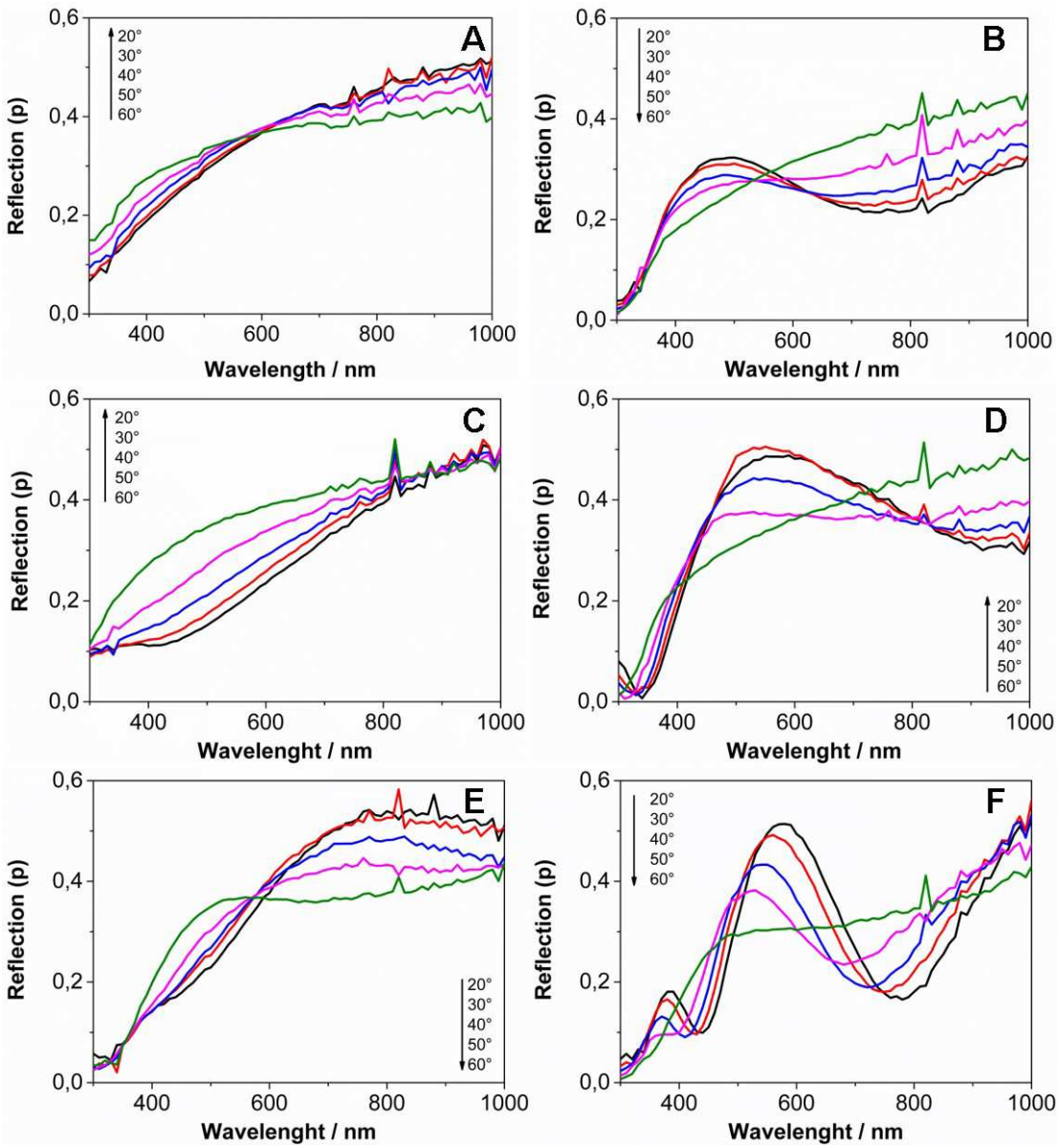

Figure 5.15: Reflection p-polarized on stainless steel substrate. Bare stainless steel (A), TiO_2 one layer (B), SiO_2 one layer (C), two layers SiO_2-TiO_2 (D), three layers SiO_2-TiO_2-SiO_2 (E), four layers SiO_2-TiO_2-SiO_2-TiO_2 (F). Reflection at 20° (black line), 30° (red line), 40° (blue line), 50° (magenta line), 60° (green line)

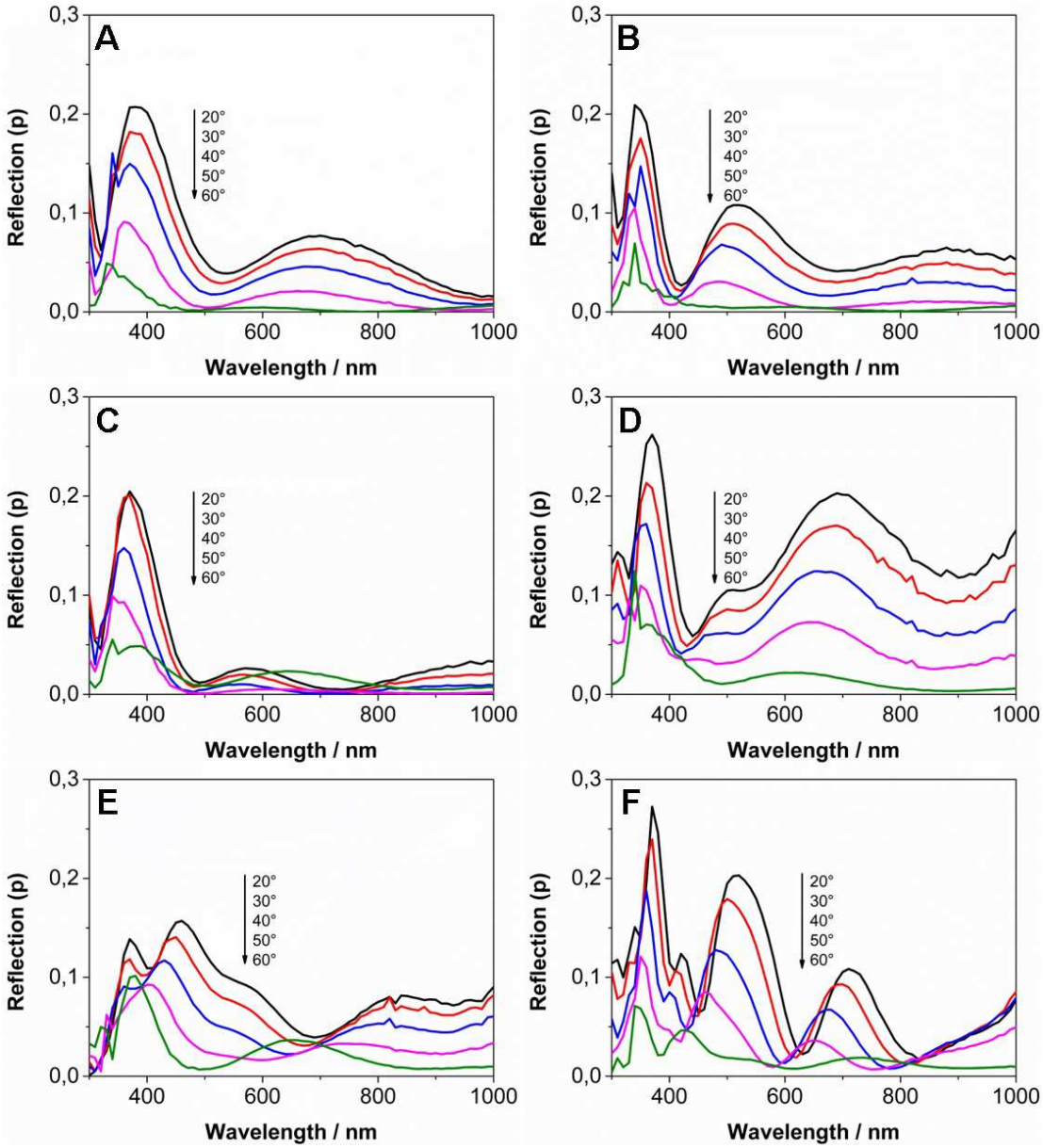

Figure 5.16: Reflection p-polarized on ITO substrate. Bare ITO (A), TiO_2 one layer (B), SiO_2 one layer (C), two layers SiO_2-TiO_2 (D), three layers SiO_2-TiO_2-SiO_2 (E), four layers SiO_2-TiO_2-SiO_2-TiO_2 (F). Reflection at 20° (black line), 30° (red line), 40° (blue line), 50° (magenta line), 60° (green line)

Table 5.1: Reflection of p-polarized light on stainless steel (SS). Comparison between four layers (SiO_2-TiO_2-SiO_2-TiO_2) and bare substrate. Data extrapolated from figure 5.15

Angle	λ (nm)	Reflection on 4 layers (%)	Reflection on bare SS (%)
20°	577	51.5	34.8
30°	559	49.2	34.3
40°	541	43.5	34.1
50°	526	38.5	33.2
60°	492	29.8	30.7

Table 5.2: Reflection of p-polarized light on ITO. Comparison between four layers (SiO_2-TiO_2-SiO_2-TiO_2) and bare substrate. Data extrapolated from figure 5.16

Angle	λ (nm)	Reflection on 4 layers (%)	Reflection on bare ITO (%)
20°	517	20.3	4.1
30°	500	17.8	3.6
40°	479	12.7	2.7
50°	462	8.5	1.4
60°	423	4.5	<1

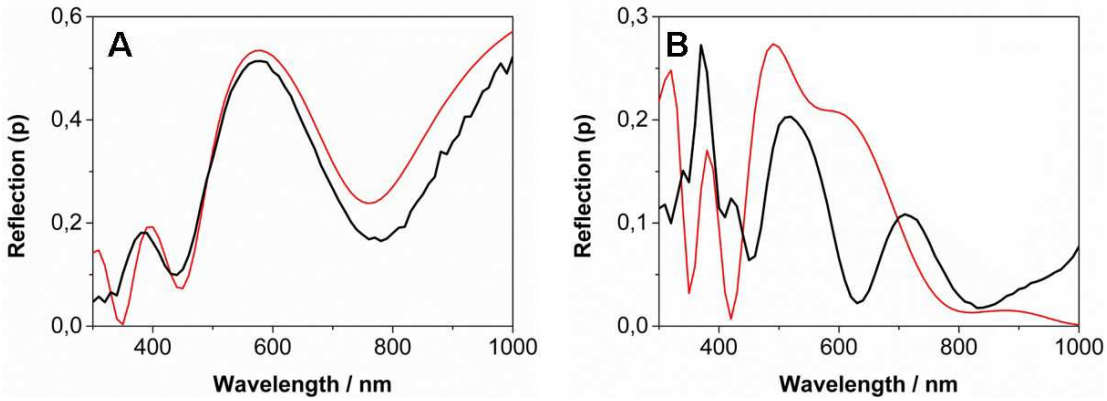

Figure 5.17: Four layers reflection fitting at 20° on stainless steel (A) and ITO (B). Real reflection (black line) and theoric reflection with fitted thickness (red line)

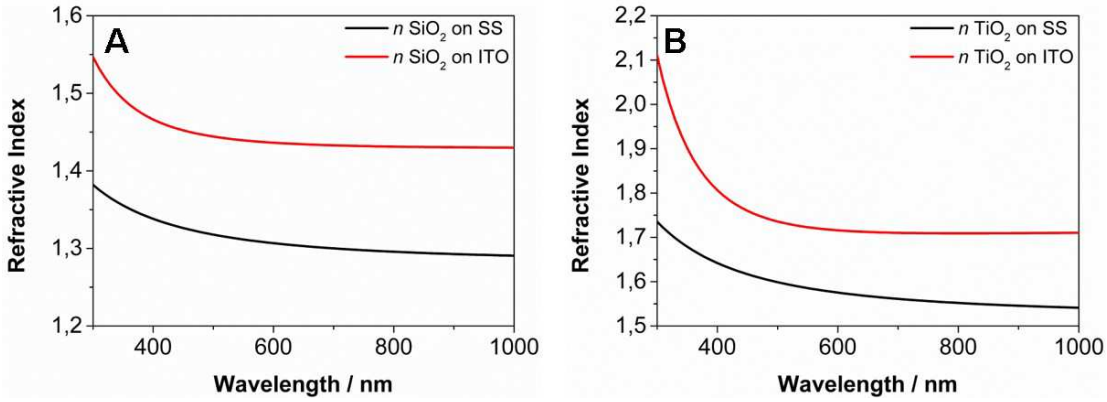

Figure 5.18: Dispersion of refractive index n for one layer of SiO_2 (A) and one layer of TiO_2 (B). On stainless steel (black line) and on ITO (red lilne)

- creating a stack model that contains the parameters found in the previous two points;
- generating the reflection data, keeping fixed the optical constant and fitting the thicknesses further.

The reflection data fitting for SiO_2-TiO_2-SiO_2-TiO_2 multilayer (two stacks) are shown in figure 5.17. As for stainless steel, the starting hypotheses are valid, *i.e.* the optical constants measured by the single layers are also preserved in the subsequent layers. As for ITO, the model fails to fit the real behavior (figure 5.17B).

In figure 5.18, the dispersion of the refractive index n is shown for the first time in literature. For silica (single layer) material, n reach a value of 1.43 on ITO and 1.29 on stainless steel. Titanium oxide has a refractive index of 1.71 when it is deposited on ITO and 1.54 when the deposition occurs on stainless steel. It is clear that the films have a different n depending on the working electrode used. The explanation of these results has to be find analyzing the composition of the films: n decreases when the number of OH-groups increases and increases with the density of the films. Both hypothesis could find explanation in electro-assisted deposition process. In fact, the number of OH^- ions that increases the pH near the electrode surface, depends on the working electrode used, *ceteris paribus*.

5.4 Conclusions

In this chapter the results of a study aimed to increase the thickness of a silica coating deposited by the sol-gel electrochemically assisted deposition are described and discussed. In the first section, the deposition of multiple layers was obtained by repeated extraction and re-immersion of the sample from the batch. It was demonstrated that the thickness increases linearly with the number of layers, which means that the film building process is not affected by the previously deposited layers, at least up to a certain thickness, and that the film is stable against re-dissolution in the sol when it is re-immersed. Furthermore, very good quality films were obtained.

Furthermore, we demonstrated the possibility to apply the EASA deposition method in consecutive steps in order to generate highly ordered and vertically aligned multilayered films up to a thickness of 400 nm. Compared to the Stöber solution growth, the present method offers the advantage of being faster but is restricted to film deposition onto conductive substrates. The mesoporous silica films and especially the interlayer regions remain permeable to reagents in solution, with mass transport properties as effective as in single layer films. The approach is compatible with the elaboration of functionalized materials, with mesopore channels bearing azido groups covalently attached to the silica walls, which can be derivatized over the whole film depth by click coupling, as exemplified for ferrocene groups. Once immobilized, these groups keep their electrochemical activity, exhibiting responses proportional to the amount of ferrocene in the material and film thickness.

The formation of multilayer of intercalated silica and titania was reached on ITO and stainless steel. The optimization of titania solution in order to obtain homogeneous layer and optical characterizations was performed; in particular, the

distribution of the refractive index was recorded for titania and silica materials on both substrates. A more reflective coating in a multilayer format was created, although the product can still be studied and optimized.

The reported results have a practical interest, as they give different methods for increasing the thickness of the deposited films without affecting their quality, opening perhaps to new application possibilities, but they also allow to better understand some of the mechanisms of the sol-gel electrochemically assisted deposition method.

Bibliography

[1] Brinker, C. J.; Hurd, A. J.; Schunk, P. R.; Frye, G. C.; Ashley, C. S. Review of Sol-Gel Thin Film Formation. J. Non-Cryst. Solids 1992, 424, 147-148

[2] Uhlmann D. R.; Ulrich D. R. Ultrastructure Processing of Advanced Materials; John Wiley & Sons Ltd: Chichester, U.K., 1992

[3] Innocenzi, P.; Abdirashid, M. O.; Guglielmi M. Structure and Properties of Sol-Gel Coatings from Methyltriethoxysilane and Tetraethoxysilane. J. Sol-Gel Sci. Techn. 1994, 3, 47-55

[4] Schmidt, H. Sol-Gel Optics II: Proceedings of SPIE; J. D. Mackenzie SPIE: Bellingham, WA, 1992

[5] Kozuka, H.; Kajimura, M.; Hirano, T.; Katayama K. Crack-Free, Thick Ceramic Coating Films via Non-Pepetitive Dip-Coating Using Polyvinylpyrrolidone as Stress-Relaxing Agent. J. Sol-Gel Sci. Techn. 2000, 19, 205-209

[6] Kozuka, H.; Takenaka, S.; Tokita, H.; Hirano, T.; Higashi, Y.; Hamatani, T. Stress and Cracks in Gel-Derived Ceramic Coatings and Thick Film Formation. J. Sol-Gel Sci. Techn. 2003, 26, 681-686

[7] Kozuka, H.; Kajimura, M. Single-Step Dip Coating of Crack-Free BaTiO3 Film > 1 μm Thick: Effect of Poly(Vinylpyrrolidone) on Critical Thickness. J. Am. Ceram. Soc. 2000, 83, 1056-1062

[8] Sims, R. R. A.; Holmes, A. S. Deposition of Thick Silica-Titania Sol-Gel Films on Si Substrates. J. Non-Cryst. Solids 1994, 170, 223-233

[9] Giordano G.; Durante C.; Gennaro A.; Guglielmi M. Electrochemical Deposition of Silica Sol-Gel Films on Stainless Steel. Preliminary Analysis of Key Variables. J. Sol-Gel Sci. Technol. 2015, 76, 233-240

[10] Giordano, G.; Durante, C.; Gennaro, A.; Guglielmi, M. Multilayer Deposition of Silica Sol-Gel Films by Electrochemical Assisted Techniques. J. Phys. Chem. C 2016, 120, 28820-24

[11] Menzel, N.; Ortel, E.; Kraehnert, R.; Strasser, P. Electrocatalysis using porous nanostructured materials. ChemPhysChem 2012, 13, 1385

[12] Guo, D.-J.; Ding, Y. Porous nanostructured metals for electrocatalysis. Electroanalysis 2012, 24, 2035

[13] Fang, Z.; Wang, Y.; Liu, C.; Chen, S.; Sang, W.; Wang, C.; Zeng, J. Rational design of metal nanoframes for catalysis and plasmonics. Small 2015, 11, 2593

[14] Peng, Y.; Su, H. Recent innovations of molecularly imprinted electrochemical sensors based on electropolymerization technique. Curr. Anal. Chem. 2015, 11, 307

[15] Walcarius, A. Mesoporous materials and electrochemistry. Chem. Soc. Rev. 2013, 42, 4098

[16] Li, G.-R.; Xu, H.; Lu, X.-F.; Feng, J.-X.; Tong, Y.-X.; Su, C.-Y. Electrochemical synthesis of nanostructured materials for electrochemical energy conversion and storage. Nanoscale 2013, 5, 4056

[17] Ye, Y.; Jo, C.; Jeong, I.; Lee, J. Functional mesoporous materials for energy applications: solar cells, fuel cells, and batteries. Nanoscale 2013, 5, 4584

[18] Ellis, B. L.; Knauth, P.; Djenizian, T. Three-Dimensional Self-Supported Metal Oxides for Advanced Energy Storage. Adv. Mater. 2014, 26, 3368

[19] Walcarius, A.; Minteer, S. D.; Wang, J.; Lin, Y.; Merkoci, A. Nanomaterials for bio-functionalized electrodes: recent trends. J. Mater. Chem. 2013, 1, 4878

[20] de Poulpiquet, A.; Ciaccafava, A.; Lojou, E. New trends in enzyme immobilization at nanostructured interfaces for efficient electrocatalysis in biofuel cells. Electrochim. Acta 2014, 126, 104

[21] Wang, J. Template electrodeposition of catalytic nanomotors. Faraday Discuss. 2013, 164, 9

[22] Walsh, F. C.; Ponce de Leon, C.; Bavykin, D. V.; Low, C. T. J.; Wang, S. C.; Larson, C. The formation of nanostructured surfaces by electrochemical techniques: a range of emerging surface finishes - Part 1: achieving nanostructured surfaces by electrochemical techniques. Trans. IMF 2015, 93, 209

[23] Jayakrishnan, D. S. in Corrosion Protection and Control Using Nanomaterials. Saji, V. S.; Cook, R. M. eds., Woodhead Publishing Limited, Cambridge, UK, 2012, 86-125

[24] Lee, W.; Park, S.-J. Porous anodic aluminum oxide: anodization and templated synthesis of functional nanostructures. Chem. Rev. 2014, 114, 7487

[25] Plowman, B. J.; Jones, L. A.; Bhargava, S. K. Building with bubbles: the formation of high surface area honeycomb-like films via hydrogen bubble templated electrodeposition. Chem. Commun. 2015, 51, 4331

[26] Davydov, A. D.; Volgin, V. M. Template electrodeposition of metals. Review. Russian J. Electrochem. 2016, 52, 806

[27] Plowman, B. J.; Bhargava, S. K.; O'Mullane, A. P. Electrochemical fabrication of metallic nanostructured electrodes for electroanalytical applications. Analyst 2011, 136, 5107

[28] Bartlett, P. N.; Cook, D. A.; George, M. W.; Hector, A. L.; Ke, J.; Levason, W.; Reid, G.; Smith, D. C.; Zhang, W. Phys. Electrodeposition from supercritical fluids. Chemi. Chem. Phys. 2014, 16, 9202

[29] Choi, K.-S.; Steinmiller, E. M. P. Electrochemical synthesis of lamellar structured ZnO films via electrochemical interfacial surfactant templating. Electrochim. Acta 2008, 53, 6953

[30] Mousty, C.; Walcarius, A. Electrochemically assisted deposition by local pH tuning: a versatile tool to generate ordered mesoporous silica thin films and layered double hydroxide materials. J. Solid State Electrochem. 2015, 19, 1905

[31] Etienne, M.; Guillemin, Y.; Grosso, D.; Walcarius, A. Electrochemical approaches for the fabrication and/or characterization of pure and hybrid templated mesoporous oxide thin films: a review. Anal. Bioanal. Chem. 2013, 405, 1497

[32] Walcarius, A. Mesoporous materials-based electrochemical sensors. Electroanalysis 2015, 27, 1303

[33] Walcarius, A.; Despas, C.; Trens, P.; Hudson, M. J.; Bessière, J. Voltammetric in situ investigation of an MCM-41-modified carbon paste electrode—a new sensor. J. Electroanal. Chem. 1998, 453, 249

[34] Walcarius, A.; L*ü*thi, N.; Blin, J.-L.; Su, B.-L.; Lamberts, L. Electrochemical evaluation of polysiloxane-immobilized amine ligands for the accumulation of copper (II) species. Electrochim. Acta 1999, 44, 4601

[35] Lee, U-H.; Kim, M.-H.; Kwon, Y.-U. Mesoporous thin films with accessible pores from surfaces. Bull. Korean Chem. Soc. 2006, 27, 808

[36] Yamauchi, Y.; Suzuki, N.; Radhakrishnan, L.; Wang, L. Breakthrough and future: nanoscale controls of compositions, morphologies, and mesochannel orientations toward advanced mesoporous materials. Chem. Rec. 2009, 9, 321

[37] Etienne, M.; Walcarius, A. Evaporation induced self-assembly of templated silica and organosilica thin films on various electrode surfaces. Electrochem. Commun. 2005, 7, 1449

[38] Etienne, M.; Sallard, S.; Schr*ö*der, M.; Guillemin, Y.; Mascotto, S.; Smarsly, B. M.; Walcarius, A. Electrochemical generation of thin silica films with hierarchical porosity. Chem. Mater. 2010, 22, 3426

[39] Sel, O.; Sallard, S.; Brezesinski, T.; Rathousky, J.; Dunphy, D. R.; Collord, A.; Smarsly, B. M. Periodically ordered meso and macroporous SiO_2 thin films and their induced electrochemical activity as a function of pore hierarchy. Adv. Funct. Mater. 2007, 17, 3241

[40] Urbanova, V.; Walcarius, A. Vertically-aligned mesoporous silica films. Z. Anorg. Allg. Chem. 2014, 640, 537

[41] Yan, F.; Lin, X.; Su, B. Vertically ordered silica mesochannel films: electrochemistry and analytical applications. Analyst 2016, 141, 3482

[42] Brinker, C. J.; Dunphy, D. R. Morphological control of surfactant-templated metal oxide films. Curr. Opin. Colloid Interface Sci. 2006, 11, 126

[43] Teng, Z.; Zheng, G.; Dou, Y.; Li, W.; Mou, C.-Y.; Zhang, X.; Asiri, A. M.; Zhao, D. Highly ordered mesoporous silica films with perpendicular mesochannels by a simple st*ö*ber-solution growth approach. Angew. Chem. Int. Ed. 2012, 51, 2173

[44] Walcarius, A.; Sibottier, E.; Etienne, M.; Ghanbaja, J. Electrochemically assisted self-assembly of mesoporous silica thin films. Nat. Mater. 2007, 6, 602-608

[45] Goux, A.; Etienne, M.; Aubert, E. Lecomte, C.; Ghanbaja, J.; Walcarius, A. Oriented Mesoporous Silica Films Obtained by Electro-Assisted Self-Assembly (EASA), Chem. Mater. 2009, 21, 731

[46] Ma, C.; Han, L.; Jiang, Z.; Huang, Z.; Feng, J.; Yao, Y.; Che, S. Growth of mesoporous silica film with vertical channels on substrate using gemini surfactants. Chem. Mater. 2011, 23, 3583

[47] Kao, K.-C.; Lin, C.-H.; Chen, T.-Y.; Liu, Y.-H.; Mou, C.-Y. A general method for growing large area mesoporous silica thin films on flat substrates with perpendicular nanochannels. J. Am. Chem. Soc. 2015, 137, 3779

[48] Li, W.; Ding, L.; Wang, Q.; Su, B. Differential pulse voltammetry detection of dopamine and ascorbic acid by permselective silica mesochannels vertically attached to the electrode surface. Analyst 2014, 139, 3926

[49] Zhou, Z.; Guo, W.; Xu, L.; Yang, Q.; Su, B. Two orders-of-magnitude enhancement in the electrochemiluminescence of Ru (bpy) 32^{+} by vertically ordered silica mesochannels. Anal. Chim. Acta 2015,886, 48.

[50] Serrano, M. B.; Despas, C.; Herzog, G.; Walcarius, A. Mesoporous silica thin films for molecular sieving and electrode surface protection against biofouling. Electrochem. Commun. 2015, 52, 34

[51] Yan, F.; Zheng, W.; Yao, L.; Su, B. Direct electrochemical analysis in complex samples using ITO electrodes modified with permselective membranes consisting of vertically ordered silica mesochannels and micelles. Chem. Commun. 2015, 51, 17736

[52] Lin, X.; Yang, Q.; Ding, L.; Su, B. Ultrathin silica membranes with highly ordered and perpendicular nanochannels for precise and fast molecular separation. ACS Nano 2015, 9, 11266

[53] Vilà, N.; André, E.; Ciganda, R.; Ruiz, J.; Astruc, D.; Walcarius, A. Molecular sieving with vertically aligned mesoporous silica films and electronic wiring through isolating nanochannels. Chem. Mater. 2016, 28, 2511

[54] Etienne, M.; Goux, A.; Sibottier, E.; Walcarius, A. Oriented mesoporous organosilica films on electrode: a new class of nanomaterials for sensing. J. Nanosci. Nanotechnol. 2009, 9, 2398

[55] Herzog, G.; Vodolazkaya, N. A.; Walcarius, A. Platinum ultramicroelectrodes modified with electrogenerated durfactant-templated mesoporous organosilica films: effect of film formation conditions on its performance in preconcentration electroanalysis. Electroanalysis 2013, 25, 2595

[56] Yan, F.; He, Y.; Ding, L.; Su, B. Highly ordered binary assembly of silica mesochannels and surfactant micelles for extraction and electrochemical analysis of trace nitroaromatic explosives and pesticides. Anal. Chem. 2015, 87, 4436

[57] Zheng, W.; Yan, F.; Su, B. Electrochemical determination of chloramphenicol in milk and honey using vertically ordered silica mesochannels and surfactant micelles as the extraction and anti-fouling element. J. Electroanal. Chem. 2016, 781, 383

[58] Fernández, I.; Sánchez, A.; Díez, P.; Martínez-Ruiz, P.; Di Pierro, P.; Porta, R.; Villalonga, R.; Pingarrón, J. M. Nanochannel-based electrochemical assay for transglutaminase activity. Chem. Commun., 2014, 50, 13356

[59] Saadaoui, M.; Fernández, I.; Sánchez, A.; Díez, P.; Campuzano, S.; Raouafi, N.; Pingarrón, J. M.; Villalonga, R. Mesoporous silica thin film mechanized with a DNAzyme-based molecular switch for electrochemical biosensing. Electrochem. Commun. 2015, 58, 57

[60] Rafiee, M.; Karimi, B.; Farrokhzadeh, S.; Vali, H. Hydroquinone functionalized oriented MCM-41 mesochannels at the electrode surface. Electrochim. Acta 2013, 94, 198-205

[61] Rafiee, M.; Karimi, B.; Arshi, S.; Vali, H.; Ethylenediamine-modified oriented MCM-41 at the electrode surface, cobalt adsorption ability and electrochemical performance. Dalton Trans. 2014, 43, 4901-4908

[62] Ding, L.; Li, W.; Sun, Q.; He, Y.; Su, B.; Gold nanoparticles confined in vertically aligned silica nanochannels and their electrocatalytic activity toward ascorbic acid. Chem. Eur. J. 2014, 20, 12777

[63] Guo, W.; Lin, X.; Yan, F.; Su, B. Vertically ordered silica mesochannel modified bipolar electrode for electrochemiluminescence imaging analysis. ChemElectroChem 2016, 3, 480

[64] Chen, M.; Burgess, I.; Lipkowski, J. Potential controlled surface aggregation of surfactants at electrode surfaces–A molecular view. Surf. Sci. 2009, 603, 1878

[65] Shacham, R.; Avnir, D.; Mandler, D. Electrodeposition of methylated sol-gel films on conducting surfaces. Adv. Mater. 1999, 11, 384

[66] Choi, K. S.; McFarland, E. W.; Stucky, G. D. Electrocatalytic properties of thin mesoporous platinum films synthesized utilizing potential-controlled surfactant assembly. Adv. Mater. 2003, 15, 2018

[67] Cheng, J.; Rathi, S. J.; Stradins, P.; Frey, G. L.; Collins, R. T.; Williams, S. K. R. Free standing silica thin films with highly ordered perpendicular nanopores. RSC Adv. 2014, 4, 7627

[68] Nasir, T.; Zhang, L.; Vilà, N.; Herzog, G.; Walcarius, A. Electrografting of 3-aminopropyltriethoxysilane on a glassy carbon electrode for the improved adhesion of vertically oriented mesoporous silica thin films. Langmuir 2016, 32, 4323

[69] Herzog, G.; Sibottier, E.; Etienne, M.; Walcarius, A. Electrochemically assisted self-assembly of ordered and functionalized mesoporous silica films: impact of the electrode geometry and size on film formation and properties. Faraday Discuss. 2013, 164, 259

[70] Vilà, N.; Ghanbaja, J.; Aubert, E.; Walcarius, A. Electrochemically assisted generation of highly ordered azide-functionalized mesoporous silica for oriented hybrid films. Angew. Chem. Int. Ed. 2014, 53 2945

[71] Vilà, N.; Ghanbaja, J.; Walcarius, A. Clickable bifunctional and vertically aligned mesoporous silica films. Adv. Mater. Interfaces 2016, 3, 1500440

[72] Giordano, G.; Vilà, N.; Aubert, E.; Ghambaja, J.; Walcarius, A. Multilayered, vertically-aligned and functionalized mesoporous silica films by sequential electrochemically assisted self-assembly. Electrochimica Acta 2017, 237, 227-236

[73] Etienne, M.; Cortot, J.; Walcarius, A. Preconcentration Electroanalysis at Surfactant-Templated Thiol-Functionalized Silica Thin Films. Electroanalysis 2007, 19, 129.

[74] Dourdain, S.; Colas, M.; Bardeau, J. F.; Gang, O.; Ocko, B.; Gibaud, A. Time-resolved in situ GISAXS experiment of evaporation-induced self-assembly of CTAB templated silica thin films under controlled humidity. Int. J. Nanosci. 2005, 4, 873

[75] Song, C.; Villemure, G. Electrode modification with spin-coated films of mesoporous molecular sieve silicas. Microporous Mesoporous Mater. 2001, 44-45, 679

[76] Etienne, M.; Quach, A.; Grosso, D.; Nicole, L.; Sanchez, C.; Walcarius, A. Molecular transport into mesostructured silica thin films: electrochemical monitoring and comparison between p 6 m, P63/mmc, and pm 3 n structures. Chem. Mater. 2007, 19, 844

[77] Birkin, P. R.; Silva-Martinez, S. Determination of heterogeneous electron transfer kinetics in the presence of ultrasound at microelectrodes employing sampled voltammetry. Anal. Chem 1997, 69, 2055

[78] Karman, C.; Vilà, N.; Walcarius, A. Amplified charge transfer for anionic redox probes through oriented mesoporous silica thin films. ChemElectroChem, 2016, 3, 263

[79] Laviron, E. General expression of the linear potential sweep voltammogram in the case of diffusionless electrochemical systems. J. Electroanal. Chem. 1979, 100, 263

[80] Vilà, N.; Walcarius, A. Electrochemical response of vertically-aligned, ferrocene-functionalized mesoporous silica films: effect of the supporting electrolyte. Electrochim. Acta 2015, 179, 304

[81] Yoldas, B.E.; O'Keeffe, T.W. Antireflective coatings applied from metal-organic derived liquid precursors. Applied Optics 1979, 18, 3133-3138

[82] Thomas, I.M. Optical coatings by the sol-gel process. Optics News 1986, 8, 18-22

[83] Thomas, I.M. Single-layer TiO_2 and multilayer TiO_2-SiO_2 optical coatings prepared from colloidal suspensions. Applied Optics 1987, 26, 4688-4691

[84] Thomas, I.M. Single layer Al_2O_3·Htextsubscript2O and multilayer Al_2O_3·Htextsubscript2O-SiO_2 optical coatings prepared from colloidal suspensions. Applied Optics 1989, 28, 4013-4016

[85] Lien, S.-Y.; Wuu, D.-S.; Yeh, W.-C.; Liu, J.-C. Tri-layer antireflection coatings (SiO_2/SiO_2-TiO_2/TiO_2) for silicon solar cells using a sol-gel technique. Solar Energy Materials & Solar Cells 2006, 90, 2710-2719

[86] Mazur, M.; Wojcieszak, D.; Domaradzki, R.; Kaczmarek, D.; Song, S.; Placido, F. TiO_2/SiO_2 multilayer as an antireflective and protective coating deposited by microwave assisted magnetron sputtering. Opto-Electronics Review 2013, 21, 233-238

[87] Xi, J.-Q.; Schubert, M.-F.; Kim, J.K.; Schubert, E.F.; Chen, M.; Lin, S.-Y.; Liu, W.; Smart, J.A. Optical thin-film materials with low refractive index for broadband elimination of Fresnel reflection. Nature 2007, 1, 176-179

[88] Liu, L.; Mandler, D. Electro-assist deposition of binary sol-gel films with graded structure. Electrochimica Acta 2013, 102, 212-218

[89] Curkovic, L.; Curkovic, H.O.; Salopek, S.; Renjo, M.M.; Segota, S. Enhancement of corrosion protection of AISI 304 stainless steel by nanostructured sol-gel TiO_2 films. Corrosion Science 2013, 77, 176-184

[90] Yakovlev, A.V.; Milichko, V.A.; Pidko, E.A.; Vinogradov, V.V.; Vinogradov, A.V. Inkjet printing of TiO_2/AlOOH heterostructures for the formation of interference color images with high optical visibility. Scientific Report 2016, 6, 37090

[91] Kallala, M.; Sanchez, C.; Cabane, B. Structures of inorganic polymers in sol-gel processes based on titanium oxide. Physical Review E 1993, 48, 3692-3704

[92] Li, M.; Yang, Y.-Q.; Liu, L.; Hu, J.-M.; Zhang, J.-Q. Electro-assisted preparation of dodecyltrimethoxysilane/TiO_2 composite films for corrosion protection of AA2024-T3 (aluminum alloy). Electrochimica Acta 2010, 55, 3008-3014

Chapter 6

Nanoparticles Imprinted Silica

This part of experiments was developed at The Hebrew University of Jerusalem, under the supervision of Daniel Mandler and in collaboration with Netta Bruchiel-Spanier. The results will be submitted to *Nanoscale*.

6.1 Introduction

Molecular imprinted polymer (MIP) has been attracting much interest in the scientific community for several years [1]. The goal is to create selective cavities in a 3D-polymeric network using a template-assisted synthesis. After template removal, exposed cavities can only attract the molecules with the same size and shape. In order to imprint the matrix, the most common practice is to mix the template with the polymer, ensuring the dispersion of the template. Clearly, the cross-linking of the polymer should not occur with the template. An additional requirement is that the polymer cross-linked has to preserve the shape after template removal and, furthermore, the binding sites should not be too flexible. The template removal is a critical point of the method and it usually obtained using solvents, acids or bases, or surfactants.

The method found several application in the field of sensors [2]. Ton *et al.* [3] developed a robust and sensitive sensing method for detection of UV-excited fluorescent analytes, reaching a sensitivity limit around 0.1 nM for enrofloxacin. MIP technique has also been widely used for bioapplications [4], such as chromatography [5], drug discovery [6] and cell culturing [7].

In 2005, Koenig and Chechik [8] developed a new approach based on MIP: Nanoparticles Imprinted Polymer (NIP). The idea was to incorporate gold nanoparticles thiol-protected into polystirene and, consequently, to remove Au NPs using I_2 aqueous solution. In 2013, Kraus-Ophir *et al.* [9] improved the technique

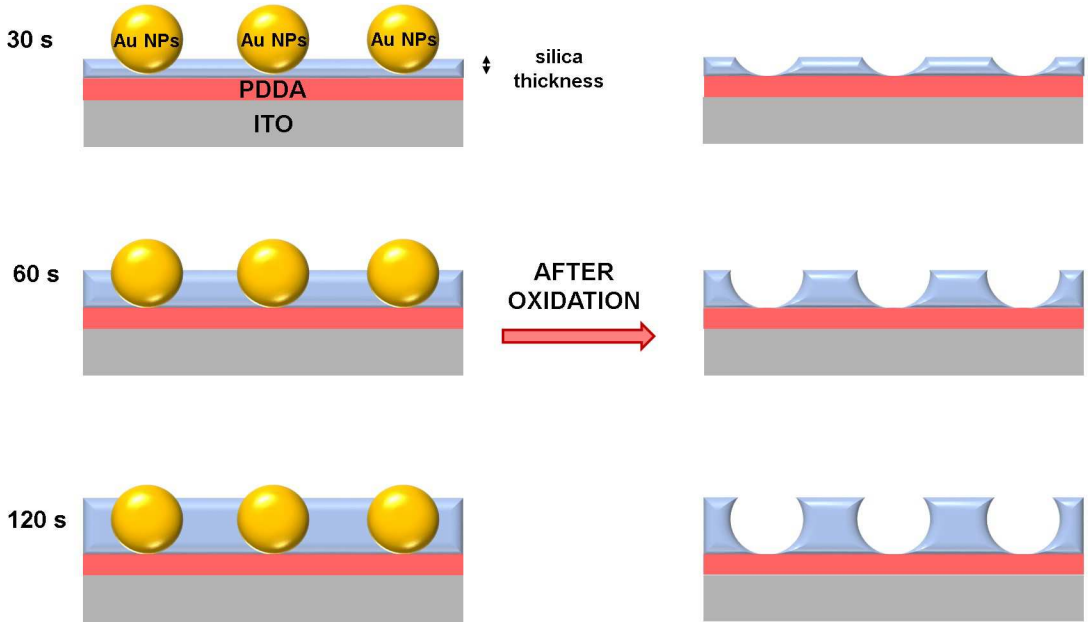

Figure 6.1: Schematic rapresentation of NIM oxidation step. Before and after oxidation of gold nanoparticles

embedding Au nanoparticles into PANI matrix via Langmuir-Blodgett (LB) approach [10]. Then, shell-selective and size recognition was demonstrated by the help of anodic oxidation of gold nanoparticles [11–13].

In this work, a silica matrix deposited via electrochemical assisted technique was used instead of polymer. The advantage is to create an imprinted matrix more robust and heat resistant. Moreover, as shown in the previous chapters, electro-assisted technique allows to tune the thickness of the film nanometer by nanometer. A monolayer of PDDA was deposited on ITO, then the samples were immersed in a Au NPs-citrate stabilized solution, obtained using Bastus's procedures [14]. Silica layers with different thickness were deposited at -1.1 V using TEOS as precursor. In order to remove Au NPs an anodic oxidation was conducted using KCl in aqueous solution, in this way the matrix does not undergo severe trauma due to heat or exposure to acids or bases. At the end, the re-uptake of gold nanoparticles was demonstrated re-immersing the samples into gold solution. A schematic rapresentation of the oxidation process was shown in figure 6.1.

6.2 Experimental

Materials and apparatus Tetraethylortosilicate (TEOS, >99%), potassium nitrate, nitric acid (32.5 %), ferricyanide, potassium chloride, ethanol, trisodium citrate, hydrochloric acid and PDDA (20 wt.% in H_2O) were purchased from Sigma Aldrich. Hydrogen tetrachloroaurate ($HAuCl_4$, 99.9%) was obtained from Strem Chemicals. One side coated indium tin oxide plates were purchased from Delta Technologies.

Electrochemical deposition and cyclic voltammetry were conducted with an Autolab PGSTAT10 potentiostat (ECO Chemie, Utrecht, The Netherlands) using a three electrode cell. Ag/AgCl (1 M KCl) was used as reference electrode and graphite rod was used as counter electrode.

Cyclic voltammetry solution consisted in H_2O (0.1 M KCl) with ferricyanide (2 mM).

PDDA monolayer formation Before PDDA monolayer deposition, ITO samples were washed in ethanol for 15 minutes, then they were washed in water for 5 minutes two times.

20 mg of PDDA (20 wt. % in water) were added to 180 ml of bidistelled water. ITO samples were immersed for 20 minutes into the solution. After removal, the samples were washed with water and in order to remove PDDA superfluous residue, the samples were gently stirred in water for 15 minutes (two times).

Au NPs synthesis Gold nanoparticles citrate-stabilized were obtained following Bastus's procedure [14]. 97 mg of trisodium citrate were added to 150 ml of water. The solution was stirred and boiling. 10 mg of $HAuCl_4$ in 1 ml of water were added to the boiling solution. The heating was turned off after 10 minutes. The solution was diluited 2:1, before any use. After silica deposition , the oxidation of gold nanoparticles was conducted applying a potential in the range 0 V to 1.3 V and using H_2O (0.1 M KCl) (scan rate: 50 mV/s).

Sol-gel synthesis and deposition 10 ml of H_2O (0.1 M KNO_3), 10 ml of ethanol and TEOS (100 mM) were mixed. Nitric acid was added drop by drop while stirring the solution until reach pH 3.0. The pre-hydrolysis was carried out stirring the solution for 1 h. The electrodeposition was conducted in a 20 mL glass vial at -1.1 V vs Ag/AgCl with different deposition time: 30, 60 and 120 seconds.

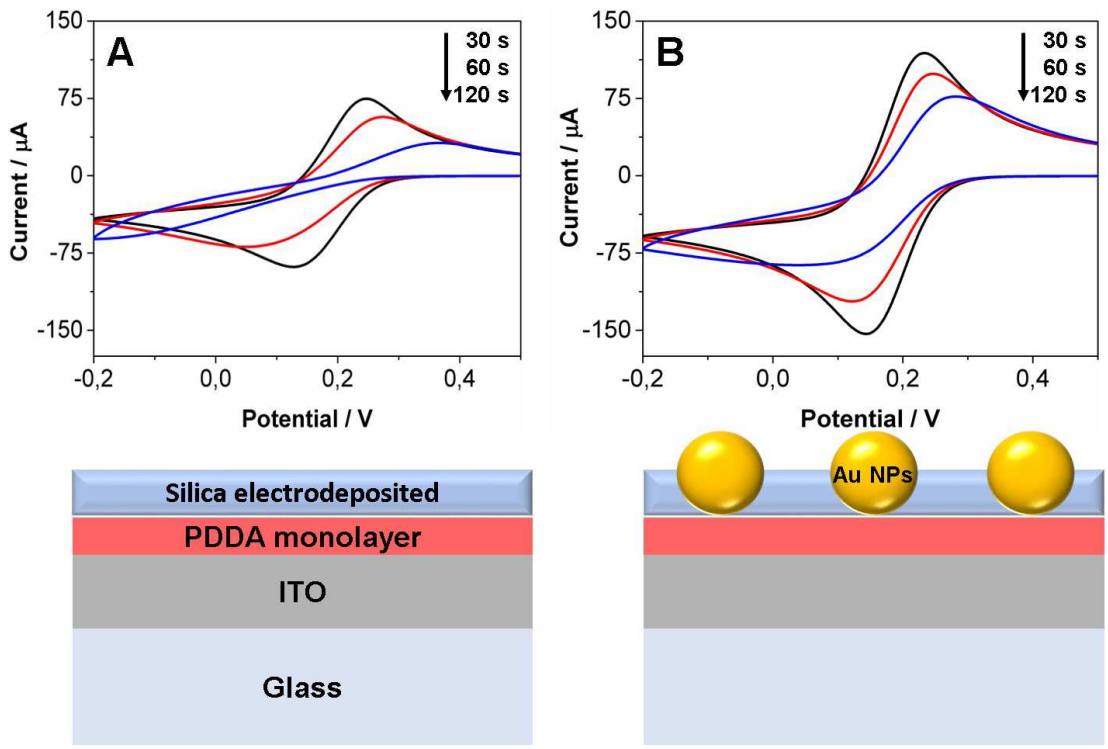

Figure 6.2: Cyclic voltammetry response of silica layers deposited for 30, 60 or 120 seconds: blank samples without Au NPs (A) and samples with Au NPs partially covered by the electrodeposition layer (B). Testing solution: ferricyanide (2 mM), H_2O 0.1 M KCl

6.3 Results and Discussion

After deposition of PDDA monolayer on ITO substrate, in order to create a blank sample, silica layer was deposited without gold nanoparticles.

Figure 6.2 shows the permeability properties of the films. Using ferricyanide as redox probe it is possible to compare the thickness of the films, studing the amount of redox probes that can reach the electrode surface. If the porosity of the films is the same, the signal decreases if the thickness increases. In fact, the figures 6.2A and 6.2B comfirm that increasing the deposition time the thickness increases and, consequently, a less amount of redox probe is oxidazed or reduced on the electrode surface. It is important to underline that 30 seconds of deposition generated a thickness less than 4 nanometers (TEM images not shown), for this reason it is more simple for ferricyanide molecules to reach the ITO substrate.

Moreover, one can observe that the potential of the oxidation peak increases

with the thickness of the film, for the same reason the potential of the reduction peak decreases, because the molecules have more difficulty to cross the coating. A further observation is that when gold nanoparticles are imprinted in silica matrix, the redox reactions of ferricyanide are promoted, in fact current intensity increases and the oxidation and reduction peaks occur at smaller potential. The explanation can be find taking into account that gold nanoparticles work like active nanoelectrode and they promote a smaller peak-to-peak separation [15].

After silica deposition on gold nanoparticles, an heat treatment at 60°C was necessary in order to stabilize the structure. Applying a potential from 0 V to 1.3 V with a scan rate of 50 mV/s, the oxidation of gold nanoparticles was promoted using an aqueous solution with 0.1 M of KCl. In figure 6.3 the oxidation peaks for 30, 60 and 120 seconds of deposition are shown ($Au^0 \rightarrow Au^{3+} + 3e^-$). In order to oxidize all the nanoparticles, more cycles are needed, in this way the silica template is ready for the re-uptake. The current generated is proportional to the amount of nanoparticles oxidized. As a matter of fact, when the thickness increases the amount of Au NPs exposed for the oxidation decreases. Considering that the nanoparticles size is around 8 nm, it is clear that it is simple to cover part of them if the thickness increases, due to the not perfect homogeneity of the coating. Moreover, the roughness of ITO is around 10 nm and some particles can remain entrapped and covered by the film. Furthermore, the first peak potential is at 0.814 V, 0.841 V and 0.875 V using 30 s, 60 s and 120 s deposition time, respectively. The shift is due to the major difficulty to extract the nanoparticles from the matrix (see figure 6.1 on page 110). Indeed, figure 6.3C (red line) shows that a certain amount of nanoparticles is also present in the second oxidation cycle.

The samples of figure 6.3 were left in gold nanoparticles solution diluited 2:1 with distilled water for 2 h in order to check the re-uptake properties of the silica matrix. Three blank samples were prepared without AuNPs imprinted as explained previously. The first oxidation peaks of blank samples (blue line), after re-uptake (red line) and after silica deposition (black line) for 30 s, 60 s and 120 s deposition time were compared in figure 6.4 on page 115. As expected, the re-uptake process is promoted if the thickness of the silica film decreases. The blank sample using 30 s deposition (figure 6.4A) shows a small re-uptake, because the silica layer is too thin (around 2 nm) and gold nanoparticles are electrostatically attracted from poly(diallyldimethylammonium chloride) PDDA, albeit it is much less than nanoparticle imprinted samples.

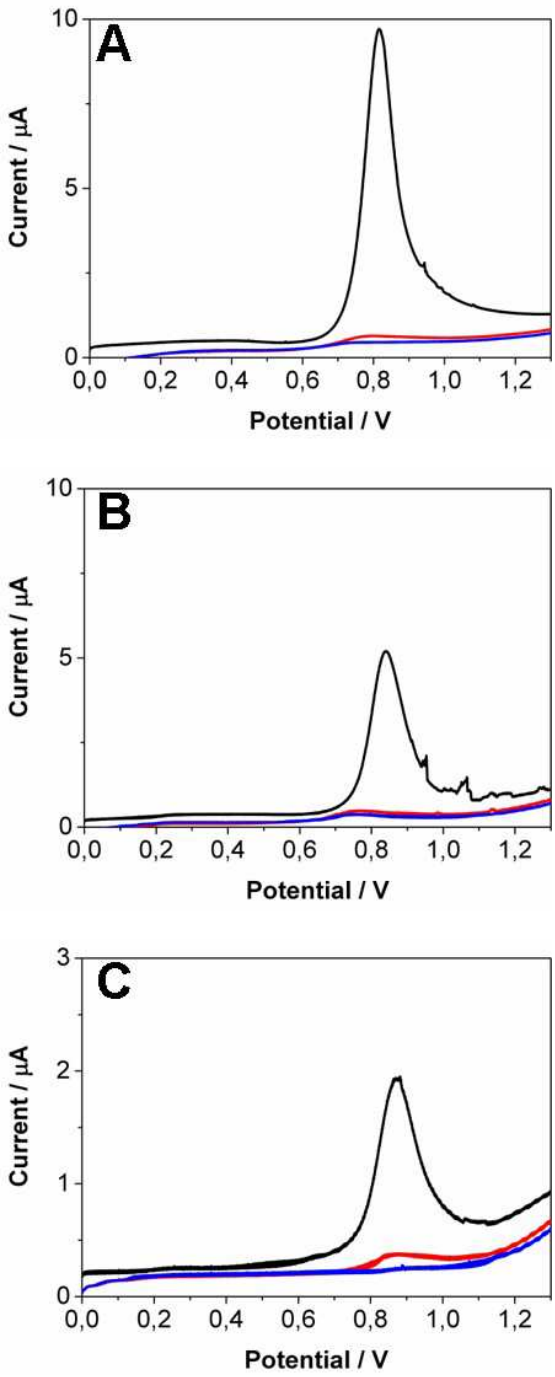

Figure 6.3: Oxidation peaks of Au NPs after silica deposition. First (black line), second (red line) and third (blue line) oxidation. 30 s (A), 60 s (B), 120 s (C) of deposition. Applied potential: from 0 V to 1.3 V. Oxidation solution: H_2O 0.1 M KCl. Scan rate: 50 mV/s

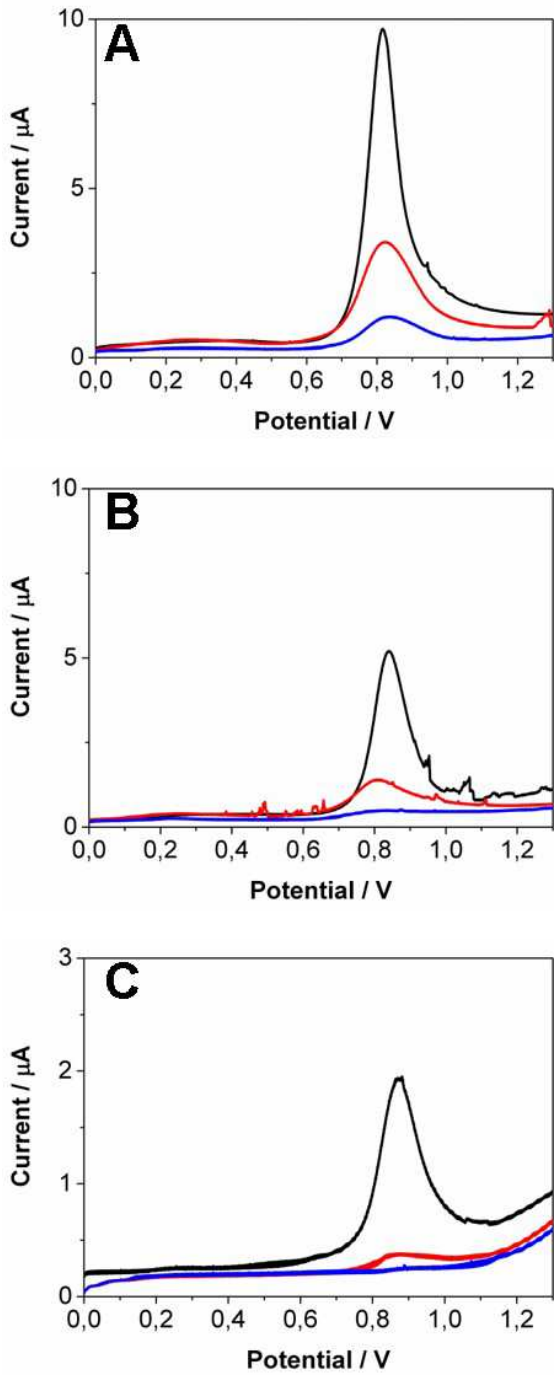

Figure 6.4: Oxidation peaks after re-uptake of Au NPs. First (black line), second (red line) and third (blue line) oxidation. 30 s (A), 60 s (B), 120 s (C) of deposition. Applied potential: from 0 V to 1.3 V. Oxidation solution: H_2O 0.1 M KCl. Scan rate: 50 mV/s

6.4 Conclusions

In conclusion, the Nanoparticle Imprinted Polymer (NIP) process was implemented using silica matrix deposited via electro-assisted deposition instead of polymer. The composite film ITO/PDDA/AuNPs+Silica was obtained in a three-steps process (deposition of PDDA, uptake of gold nanoparticles, electrodeposition of silica). A fine modulation of the thickness was achieved changing the deposition time. It was found that 60 seconds of deposition time is the right compromise in order to obtain the re-uptake of gold nanoparticles, in fact for 30 seconds of deposition the blank sample shows a small re-uptake, while using a deposition time equal to 120 s the thickness of the film is too thick and it cover the most nanoparticles, obstructing the extraction and voiding the re-uptake process.

Hence, we are currently designing better matrices with others sol-gel precursors that will interact by supramolecular chemistry with the nanoparticles rather than by electrostatic interactions. We believe that by this approach, the affinity of the matrix towards the nanoparticles can be significantly improved.

Bibliography

[1] Matsui, J.; Kato, T.; Takeuchi, T.; Suzuki, M.; Yokoyama, K.; Tamiya, E.; Karube, I. Molecular recognition in continuous polymer rods prepared by a molecular imprinting technique. Anal. Chem. 1993, 65, 2223-2224

[2] Uzun, L.; Turner, A.P.F. Molecularly-imprinted polymer sensors: realising their potential. Biosesors and Bioelectronics 2016, 76, 131-144

[3] Ton, X.-A.; Acha, V.; Haupt, K.; Bui, B.T.S. Direct fluorimetric sensing of UV-excited analytes in biological and environmental samples using molecularly imprinted polymer nanoparticles and fluorescence polarization. Biosens. Bioelectron. 2012, 36, 22-28

[4] Schirhagl, R. Bioapplications for molecularly imrpinted polymers. Anal. Chem. 2014, 86, 250-261

[5] Ellwanger, A.; Berggren, C.; Bayoudh, S.; Crecenzi, C.; Karlsson, L.; Owens, P.K.; Ensing, K.; Cormack, P.; Sherrington, D.; Sellergren; B. Evaluation of methods aimed at complete removal of template from molecularly imprinted polymers. Analyst 2001, 126, 784-792

[6] Yu, Y.; Ye, L.; Haupt, k.; Mosbach, K. Formation of a Class of Enzyme Inhibitors (Drugs), Including a Chiral Compound, by Using Imprinted Polymers or Biomolecules as Molecular-Scale Reaction Vessels. Angew. Chem., Int Ed. 2002, 41, 4459-4463

[7] DePorter, S.M.; Liu, I.; McNaughton, B.R. Programmed cell adhesion and growth on cell-imprinted polyacrylamide hydrogels. Soft Matter 2012, 8, 10403

[8] Koenig, S.; Chechik, V. Au nanoparticle-imprinted polymers. Chem. Commun. 2005, 4110-4112

[9] Nanoparticle-imprinted polymers for size-selective recognition of nanoparticles. Amger. Chem. Int. Ed. 2013, 52, 1-6

[10] Tanami, G.; Gutkin, V.; Mandler, D. Thin nanocomposite films of polyaniline/Au Nanoparticles by the Langmuir-Blodgett Technique. Langmuir 2010, 26, 4239-4245

[11] Bruchiel-Spanier, N.; Mandler, D. Nanoparticle-imprinted polymers: shell-selective recognition of Au nanoparticles by imprinting using the Langmuir-Blodgett method. Chem. Electro. Chem. 2015, 2, 795-802

[12] Hitrik, M.; Pisman, Y.; Wittstock, G.; Mandler, D. Speciation of nanoscale object by nanoparticle imprinted matrices. Nanoscale. DOI: 10.1039/c6nr01106c

[13] Yen-Fu, C.; Shin-Ru, T.; Yu-Jane, S.; Heng-Kwong, T. Shape recognition of nanoparticle-imprinting materials enhanced by depletants. J. Phys. Chem. C 2016, 120, 19871-19877

[14] Bastus, N.G.; Comenge, J.; Puntes, V. Kinetically controlled seeded growth synthesis of citrate-stabilized gold nanoparticles of up to 200 nm: size focusing versus Ostwald ripening. Langmuir 2011, 27, 11098-11105

[15] Cheng, W.; Dong, S.; Wang, E. Gold nanoparticles as fine tuners of electrochemical properties of the electrode/solution interface. Langmuir 2002, 18, 9947-9952

Chapter 7

Conclusions and Future Prospects

During the doctoral project, different aspects regarding electro-assisted deposition of sol-gel thin films were thoroughly examined. Below, the main results are listed and briefly explained.

- taking into account the literature, the role of the key variables was studied, confirming the trends found in other research groups and stressing the importance of some new parameters. In particular, applied potential, deposition time, starting solution, oxygen, electrolyte, temperature and the shape of the substrate were analyzed, comparing the thickness of the films [1];

- using specific solution, the thickness is difficult to control and it grows exponentially with the deposition time. Fort this reason, a new technique was developed in order to solve this issue. A pulsed potential was applied instead of a continuos potential. In this way, two new variables were introduced: the "ON" and the "OFF" time. By means of intermitted duty-cycles, the diffusion of hydroxide ions near the electrode surface was tuned, in order to obtain variable thicknesses [2];

- the mechanism of growth of silica film on the electrode surface is unknown. Recording the chronoamperometric curves during the deposition, it was observed that the behaviour is very similar to the growth of electrodeposited metals. Taking into account that silica is an ion conductor, the nucleation theory was applied using the same equation, but fitting the parameters. Changing the applied potential and the precursor concentration, the 3D-growth of silica was theorized [3];

- in order to increase the thickness of amorphous silica, a new technique was developed. Thanks to the re-immmersion of the substrate into the solution

and applying again the potential, a multilayer was obtained. Ten different layers were deposited on the same substrate, reaching a total thickness of ca. 1 μm without cracks [2]. Combined with the electrodeposition, multilayer technique unlocked new research branches later explored;

- thanks to multilayer deposition, the thickness of vertically-aligned hexagonally-packed mesoporous silica channels was increased up to 400 nm. The pores (diameter of ca. 2 nm) are interconnected from one layer to the other. Moreover, the nanochannels preserved their vertical orientation. Furthermore, the silica matrix was functionalized with azido groups, in order to attach ferrocene molecules by click chemistry, that can react with the ITO substrates via electron hopping [4];

- silica and titania were intercalated each other creating a multilayer with four layers. Reading the literature, the deposition of titania presented several issues. Tuning the starting solution, an homogeneous layer of titania was obtained. After deposition, the reflection of p-polarized light of the multilayer was analyzed, demonstrating that the intercalation was successfully obtained. Indeed, the reflection increased when SiO_2-TiO_2-SiO_2-TiO_2 structure was deposited on the electrode. Moreover, for the first time in literature, the dispersion of the refractive index of single layer of silica and titania was measured by ellipsometer using both stainless steel and ITO substrates [5];

- finally, Nanoparticles Imprinted Polymer (NIP) method was advanced using silica matrix instead of polymeric one. PDDA monolayer was deposited on ITO substrate in order to electrostatically catch gold nanoparticles citrate-stabilized (AuNPs-cit). Then, the deposition of silica was obtained using TEOS as precursor and the thickness of the film was tuned changing the deposition time, reaching three different thicknesses of ca. 2, 4 and 8 nm. After anodic oxidation of AuNPs-cit, the silica imprinted matrix was able to re-uptake gold nanoparticles with the same size of the templanting one [6].

In the light of what is written in this thesis, the electro-assisted deposition of sol-gel films results to be a versatile and powerful tool that can be used for the deposition of very thin films with tunable thickness and properties or for the formation of new materials and nanocomposites.

In conclusion, albeit some theoretical aspects should be carefully examinated, the method is ready to meet a scale-up process for the industrialization of products, such as complex surface coating or functionalized thin films for specific

applications (*e.g.* sensors, functional electrode for electrocatalysis, optical coatings). In this sense, an important aspect to consider is the model of thickness growth. Unfortunately, according to the literature available today, it is not possible to generalize and predict the growth of thickness, because it depends on the substrate and on the starting solution. A last aspect to consider for a successful industrial scale-up is the deterioration of the solution with the deposition time; surely, it could be useful to use buffers to adjust the pH of the bulk of the solution and, therefore, to increase its duration.

Bibliography

[1] Giordano G.; Durante C.; Gennaro A.; Guglielmi M. Electrochemical Deposition of Silica Sol-Gel Films on Stainless Steel. Preliminary Analysis of Key Variables. J. Sol-Gel Sci. Technol. 2015, 76, 233-240

[2] Giordano, G.; Durante, C.; Gennaro, A.; Guglielmi, M. Multilayer Deposition of Silica Sol-Gel Films by Electrochemical Assisted Techniques. J. Phys. Chem. C 2016, 120, 28820-24

[3] Giordano, G.; Durante, C.; Gennaro, A.; Guglielmi, M. Electrochemical 3D-growth of amorphous silica gel. J. Electroanal. Chem. 2017, 784, 153-158

[4] Giordano, G.; Vilà, N.; Aubert, E.; Ghambaja, J.; Walcarius, A. Multilayered, vertically-aligned and functionalized mesoporous silica films by sequential electrochemically assisted self-assembly. Electrochimica Acta 2017, 237, 227-236

[5] Giordano, G.; Durante, C.; Michieli, N.; Gennaro, A.; Martucci, A.; Guglielmi, M. SiO2-TiO2 Multilayer via Electrochemical Deposition: Characterization of Reflection and Refractive Index. J. Sol-Gel Sci. Technol. 2018, (*submitted*)

[6] Bruchiel-Spanier, N.; Giordano, G.; Vakahi, A.; Guglielmi, M.; Mandler, D. The Influence of Different Sol-gel Matrices on the Detection Ability of Gold Nanoparticles using Nanoparticles Imprinted matrices, (*in submission*)

List of Acronyms

DOE	Design of Experiments
CV	Cyclic Voltammetry
CA	Chronoamperometry
XRD	X-ray Diffraction
GIXD	Grazing Incidence X-ray Diffraction
SEM	Scanning Electron Microscope
ESEM	Enviromental Scanning Electron Microscope
FE-SEM	Field Emission Scanning Electron Microscope
TEM	Transmission Electron Microscope
FIB	Focused Ion Beam
AFM	Atomic Force Microscope
TEOS	Tetraethyl Orthosilicate
SCE	Saturated Calomel Electrode
Eet	Estimated Electrodeposited Thickness
EASA	Electro-Assisted Self-Assembly
ITO	Indium Tin Oxide
EHT	Electron High Tension
MIP	Molecular Imprinted Polymers

NIP Molecular Imprinted Polymers

NIM Molecular Imprinted Matrices